Universidade de Évora

PHYSIOLOGICAL CHARACTERIZATION OF A THERMOPHILIC *Bacillus* STRAIN (*B. licheniformis* CCMI 1034) ISOLATED FROM FOOD WASTE TREATMENT BIOREACTORS

Maria Teresa Saraiva Lopes da Silva

(Mestre)

Dissertação para obtenção do Grau de Doutor em Química

Orientador: Doutor José Carlos Pereira Roseiro

Co-orientador: Doutor José Maria Santos Arteiro

Esta tese não inclui as críticas e as sugestões feitas pelo júri

Dezembro de 2004

To my husband Alberto,

my children Tomás and Matilde

and my parents Maria José and Manuel

Abstract

A physiological characterization of a thermophilic strain from the genus *Bacillus* (*Bacillus licheniformis* CCMI 1034) isolated from Lammas industry bioreactors (a food waste treatment company in the UK) was carried out aiming at the improvement of the biodegradation process efficiency.

In a first step, a phenotypic characterization of the seventeen *Bacillus* strains isolated from Lammas bioreactors was carried out, using fatty acid and enzymatic activity profiles, in order to evaluate the biotechnological usefulness of these micro-organisms. *Bacillus licheniformis* strains exhibited the most significant enzyme production. Numerical analyses (principal component and hierarchical analyses) revealed that *Bacillus licheniformis* strains were homogeneous regarding their fatty acid profiles whilst *B. subtilis* and *Bacillus pumilus* strains showed some variation between strains concerning this phenotypic characteristic. However, the enzymatic activities numerical analyses indicated that the three *Bacillus* species were more homogeneous regarding this phenotypic characteristic.

The physiological characterization of a selected strain was further studied based on microbial responses to changes of growth conditions. This study was carried out in a bench continuous stirrer tank reactor (CSTR) which was firstly characterized through the study of the effect of the impeller configuration, aeration rate and stirring rate on the gas-liquid mass transfer coefficient k_La, under Lammas bioreactors working temperatures

(45-60 °C). It was found that the most appropriate impeller combination was a Rushton impeller (four blades) mounted below an axial Pitched-blade (three blades) impeller.

The physiological characterization of the selected *Bacillus* strain was then carried out by adding pulses of glucose and lactose (carbon sources frequently found in industrial growth media and food waste streams) to *B. licheniformis* CCMI 1034 glucose limited steady-state continuous cultures (D=0.27 h^{-1}). The responses of the batch sections were monitored by measuring optical density, substrate consumption, carbon dioxide production, oxygen uptake and flow cytometric analyses were carried out in order to understand the physiology and the dynamics of the subpopulations during the sequential utilization of substrates, a common situation in waste streams. Glucose pulse specific growth rate and the biomass yield were 0.45 h^{-1} and 0.26 g biomass·(g glucose)$^{-1}$ respectively, whilst lactose pulse specific growth rate and the biomass yield were 0.009 h^{-1} and 0.05 g biomass·(g lactose) $^{-1}$ respectively. These results, together with the cell physiological state information suggest that, conversely the growth on glucose, the growth on lactose induced the storage materials synthesis which allowed a high proportion of polarised cytoplasmic membrane (healthy) cells, nine hours after the lactose exhaustion.

The ability of *B. licheniformis* cells to form biofilm was studied in order to improve biomass separation from the treated wastewater, usually the limiting step of the biodegradation process. For this purpose, different growth conditions (e.g. carbon and nitrogen limiting fermentations, wherein the dilution rate and the stirring rate changed)

were operated in order to obtain the immobilization of healthy cells, thus metabolically active. Glucose limited steady-state continuous cultures growing between D= 0.64 h^{-1} and D= 0.87 h^{-1}, at 1000 rpm, led to a thin and smooth biofilm formation which allowed the presence of a high proportion of polarised cytoplasmic membrane cells, therefore metabolically active. Above the dilution rate of 0.87 h^{-1}, a thick biofilm was formed and the number of polarised cytoplasmic membrane cells decreased, with a parallel increase of depolarised cytoplasmic membrane cells. The increase of the stirring rate to 1750 rpm hindered *B. licheniformis* CCMI 1034 cell attachment and the rods were dispersed in the broth. The carbon conversion efficiency calculated in this case indicated that an extracellular polymer could be produced at higher dilution rates (D≥ 1.24 h^{-1}). *B. licheniformis* CCMI 1034 growth under nitrogen limitation at 1000 rpm induced floc formation which increased in size with dilution rate. The flocs became thicker with the increase of the stirring rate to 1750 rpm.

In all studies of microbial response to environmental changes, multi-parameter flow cytometry coupled with fluorescent stains were used to monitor the physiological response of the culture, at the individual cell level. The use of this rapid and real time analysis of individual microbial cells enhances the knowledge of how different physiological sub-populations develop throughout the course of a bioprocess further demonstrating the inherent complex physiological heterogeneity of microbial cultures. The results were discussed in terms of devising a better control system based on measurements made at the individual cell level for optimization of bioprocess performance.

RESUMO

Caracterizou-se fisiologicamente uma estirpe termófila do género *Bacillus* (*Bacillus licheniformis* CCMI 1043) isolada dos bioreactores da empresa Lammas Resourc Ltd (uma empresa de processamento de desperdícios alimentares, localizada no Reino Unido) com o objectivo de se aumentar a eficiência do processo de biodegradação.

Numa primeira fase, as dezassete estirpes *Bacillus* isoladas dos bioreactores Lammas foram caracterizadas fenotipicamente através dos seus perfis de ácidos gordos e das suas actividades enzimáticas , com o objectivo de se avaliar a utilidade destes microrganismos sob o ponto de vista biotecnológico. A espécie *Bacillus licheniformis* revelou a produção de enzimas mais significativa. Análises numéricas (componentes principais e hierárquica) revelaram que as estirpes da espécie *B. licheniformis* são homogéneas relativamente aos seus perfis de ácidos gordos, enquanto que as estipes das espécies *B. subtilis* e *B. pumilus* apresentaram alguma variação entre si relativamente a esta característica fenotípica. Contudo, a análise numérica das actividades enzimáticas mostrou que as três espécies de *Bacillus* são mais homogéneas relativamente a esta característica fenotípica.

A caracterização fisiológica da estirpe seleccionada foi estudada posteriormente com base nas respostas do microrganismo a alterações das condições de crescimento. Uma parte deste estudo foi realizado num fermentador de bancada perfeitamente agitado, préviamente caracterizado através do estudo do efeito da configuração de turbinas, da taxa de arejamento e da velocidade de agitação no coeficiente de transferência de massa

gás-líquido k_La, realizado a temperaturas de trabalho dos bioreactores Lammas (45-60 °C). A combinação da turbina Rushton (quatro pás) colocada por baixo da turbina "Pitched-blade" (três pás) foi considerada a mais adequada.

A caracterização fisiológica da estirpe seleccionada foi depois realizada através da adição de pulsos de glucose e lactose (fontes de carbono geralmente presentes nos meios de cultura industriais e efluentes de indústrias alimentares) a culturas contínuas de *B. licheniformis* CCMI 1034 limitadas pela glucose, em estado estacionário (D= 0,27 h^{-1}). As respostas da cultura de *B. licheniformis* CCMI 1034 a estes pulsos foram monitorizadas através de medições de densidade óptica, produção de dióxido de carbono e consumo de oxigénio, consumo de susbtrato e análises de citometria de fluxo multi-paramétrica, com o objectivo de se compreender a fisiologia e a dinâmica das subpopulações daquele microrganismo, durante a utilização sequencial destes substratos, uma situação frequente nos efluentes industriais. A taxa específica de crescimento e o rendimento em biomassa do pulso de glucose foram 0,45 h^{-1} e 0,26 g biomassa·(g glucose)$^{-1}$ respectivamente, enquanto que a taxa específica de crescimento e o rendimento em biomassa do pulso de lactose foram 0,009 h^{-1} e 0,05 g biomassa·(g lactose)$^{-1}$ respectivamente. Estes resultados, em conjugação com a informação do estado fisiológico das células sugerem que, contrariamente ao crescimento do microrganismo em glucose, o crescimento em lactose induziu a síntese de materiais de reserva que permitiram a existência de uma elevada proporção de células com a membrana citoplasmática polarizada (células saudáveis) nove horas após a exaustão da lactose.

A capacidade das células de *B. licheniformis* de formarem biofilme foi posteriormente estudada com o objectivo de se optimizar o processo de separação da biomassa do efluente tratado, uma vez que este é geralmente o passo limitante dos processos de tratamento biológico dos efluentes. Deste modo, diferentes condições de crescimento (i.e., fermentações limitadas por carbono e azoto, em que a taxa de diluição e a velocidade de agitação foram alteradas) foram impostas a culturas contínuas de *B. licheniformis*, com o objectivo de se obter a imobilização de células saudáveis, portanto metabolicamente activas. Culturas contínuas limitadas pelo carbono, crescendo à taxa de diluição entre D=0,64 h^{-1}e D=0,87 h^{-1}, à velocidade de agitação de 1000 rpm, levaram à formação de um biofilme fino e liso, composto por uma elevada proporção de células metabolicamente activas. Acima da taxa de diluição de D=0,87 h^{-1}, observou-se a formação de um biofilme espesso e liso, e a proporção de células com a membrana citoplasmática polarizada diminuiu, o que foi acompanhado por um aumento da proporção de células com a membrana citoplasmática despolarizada. O aumento da velocidade de agitação para 1750 rpm impediu a ligação entre as células de *B. licheniformis*, pelo que o crescimento do microrganismo foi disperso. A eficiência da conversão do carbono calculada nestas condições indicou que um polímero extracelular poderia ser produzido a altas taxas de diluição ($D \geq 1,24\ h^{-1}$). O crescimento de *B. licheniformis* sob limitação de azoto operado a 1000 rpm, induziu a formação de flocos, que aumentaram de dimensão com o aumento da taxa de diluição. O aumento da velocidade de agitação para 1750 rpm conduziu ao aumento de espessura dos flocos.

Em todos os estudos de resposta do microrganismo a variações ambientais, a citometria de fluxo multi-paramétrica em associação com corantes fluorescentes foi utilizada para monitorizar a resposta fisiológica da cultura, ao nível da célula individual. A utilização desta análise célula a célula, rápida e em tempo real, permite o conhecimento da evolução de subpopulações em diferentes estados fisiológicos, ao longo de um bioprocesso, revelando desta forma a complexa heterogeneidade fisiológica inerente às culturas microbianas. Os resultados foram discutidos na perspectiva de se obter um sistema de controlo eficaz dos bioprocessos, baseado em medições realizadas ao nível da célula individual, o que permite aumentar a eficiência dos bioprocessos.

The Story

This is the story of someone who loves each day of her work.

All began six years ago. Matilde was born in April 1996 and I had restarted working at INETI in September after a six months maternity leave at home. Before, I followed a boring routine in the Lab, making me feel professionally lost, with no aims in my job.

The idea of doing a Master of Science degree (Msc) at Instituto Superior Técnico in Biotechnology came a few months later. Then I attended the first year of a taught course at the University. Subjects as Molecular Biology or Fermentation Technology, among others, were amazing discoveries for me, compared with the arid Chemical Engineering graduation at the same place a few years before. The Msc thesis consisted in fungal continuous cultures and Carlos Roseiro, my supervisor, introduced me this tool that I would always use in the future. It was a hard and difficult task to control the untamed microbial growth, and sometimes I was so tired that I almost regretted doing such a work. Matilde was 2 and Tomas 7. Sometimes I felt guilty for leaving my family and spending hours at the bench. However, I always had a strong support and help from my husband Alberto, who has always encouraged my work and trusted me. Without him, I could not have done what I did. My parents and my brothers also encouraged me to go on and looked after the children all day, sometimes until late.

At last, after an exhausted work, we could control the fungus growth and were able to cultivate it in the bioreactor! This was my first scientific achievement. I remembered how

proud I felt when I saw the data published a few months later in "Enzyme and Microbial Technology".

Having finished the Msc, I could not stop working; I had experienced the feeling of accomplishing an objective in Science, which is unforgettable. Fortunately our Laboratory (Industrial Microbiology Laboratory) was a partner in the European Project QLK3-1999-00004 "Enhanced, intelligent processing of food and related wastes using thermophilic populations" (the "Thermophilic" Project) and I was member of the team. Francisco Gírio allowed me to set up the bioreactor in his laboratory so I started there my "thermophilic" fermentations. I had long and useful conversations with Luis Duarte and Helena Albergaria, with whom I have learnt so much.

I applied for a PhD grant to Fundação para a Ciência e a Tecnologia in order to get further financial support for my PhD programme, designed within the scope of the "Thermophilic" Project. A laboratorial part would be carried out in England, at the University of Birmingham, under the supervision of Dr Christopher Kent, the coordinator of the "Thermophilic" Project. This project also allowed my participation in several scientific meetings in other countries (Check Republic and Poland) where I met other researchers also involved in the Project. These meetings allowed the exchange of scientific ideas and quite often new ideas for further projects arose.

Alberto applied for a pos-doc grant at the same University, and both of us got research grants. Then the great adventure started: all the family moved to Birmingham for eight months, four months each summer (2002 and 2003).

We started working in Flow Cytometry with Dr. Chris Hewitt, Alberto's post-doc supervisor. I will always remember the day he came to teach us the basis of Flow Cytometry: "you have got two children, so you are reproducible, but other people have no children: viable but non culturable cells..."

So we became fond of the new and powerful technique which made us work night and day without stopping. James speaking loudly, the sweet Ann, the good Larry were our fellows in those long nights of hard work. Hazel was our good angel, as she provided the best conditions possible for our work. Elaine had always a smile and a word of encouragement for everybody. David French, the competent and skilled David helped us to overcome several technical problems that arose during the development of our work.

Nevertheless, we were able to visit almost all green England with the children. For them, it was an unforgettable experience. We lived in a detached house with a communal garden, where our children met other children with different cultures and made lots of friends. I will always remember those times with nostalgia.

Coming back from England, the thesis would be submitted to the University of Évora where Prof Arteiro was the internal supervisor of the work. I have always felt a warm and a friendly welcome from the people of this University, with whom I hope to maintain scientific contacts in the future.

During the thesis writing, Professor Sebastião Alves and Professor Jorge Vasconcelos from Instituto Superior Técnico (Lisbon) gave a strong support in the k_La Chapter. The comments of Pablo Pereira (LMI, INETI) were very useful in Chapter 2.

When I look back, I realise that many people have taught, helped, encouraged and supported me during the long way I have been going through. I could not mention all of

them in this little Story, as the list would be too long. However, I want to mention the optimistic and encouraging presence of my friend and supervisor (Msc and PhD) Carlos Roseiro throughout this long way, who taught me that the self belief of a scientist in his own work is the key for the successful research.

I want to express my gratitude to all these people. Without each of them, I could not have done what I did. I could not love my family, my work and my life in the way I do.

Lisbon, 31st December 2004

Teresa Lopes da Silva

Chapter 5 Impact of growth conditions on *Bacillus licheniformis* CCMI 1034 morphology and physiology

Abbreviations

Roman Symbols		Units
a	Interfacial area	m^{-1}
ADP	Adenosine diphosphate	
ATP	Adenosine triphosphate	
BOX	Bis-(1,3-diethylthiobarbituric acid)trimethine oxonol	
$[C^+]_0$	Concentration of C^+ ions outside the cytoplasmic membrane	g l^{-1}
$[C^+]_i$	Concentration of C^+ ions inside the cytoplasmic membrane	g l^{-1}
C*	Oxygen concentration in the liquid in equilibrium with the gas phase	kg m^{-3}
CCCP	Carbonylcyanide m-chlorophenylhydrazone	
C_i	Initial oxygen concentration in the liquid	Kg m^{-3}
COD	Chemical oxygen demand	mg l^{-1}
C_L	Oxygen concentration in the liquid phase	Kg m^{-3}
$\mathcal{D}$	Diffusion coefficient	m^2 s^{-1}
DO	Dissolved oxygen concentration	%
D	Dilution rate	h^{-1}
D	Impeller diameter	m
$DiBAC_4$	Bis-(1,3-diethylthiobarbituric acid)trimethine oxonol	
$DiOC_2(3)$	3,3'-Diethyloxacarbocyanine iodide	
$DiOC_6(3)$	3,3'-Dihexylcarbocyanine, iodide	
DX	Cell productivity	(g cells) l^{-1} h^{-1}
EB	Ethidium bromide	
ECP	Extracellular polymers	
F	Air flow rate	l h^{-1}
F	Faraday constant	F = 96 485.309 29 C mol^{-1}
FALS	Forward angle light scatter	
FAMEs	Fatty acid methyl esters	
Fl	Gas flow number	dimensionless
GM	Growth medium	
HCA	Hierarchical cluster analysis	
k_L	Liquid film mass transfer coefficient	m h^{-1}
k_La	Gas-liquid mass transfer coefficient	h^{-1}
m	Maintenance coefficient	mmol glucose (g cells)$^{-1}$ h^{-1}
M	Torque	N m
MP (or $\Delta\psi$)	Membrane potential	V

N	Impeller speed	rpm
NADH	Nicotinamide adenine dinucleotide, reduced form	
NAD(P)H	Nicotinamide adenine dinucleotide phosphate, reduced form	
N_p	Power number	dimensionless
OD	Optical density	
OTR	Oxygen transfer rate	Kg m^{-3} h^{-1}
P	Power (unaerated)	W
P	Product concentration	g l^{-1}
P/V	Specific power input	KW m^{-3}
PB3	Pitched blade turbine with three blades	
PC1	First principal component	
PC2	Second principal component	
PCA	Principal component analysis	
P_g	Power (aerated)	W
PI	Propidium iodide	
Q_g	Gas flow rate	m^3 s^{-1}
q_{CO2}	Specific carbon dioxide production rate	mmol carbon dioxide (g cells)$^{-1}$ h^{-1}
q_{O2}	Specific oxygen uptake rate	mmol oxygen (g cells)$^{-1}$ h^{-1}
q_p	Specific product formation c rate	mmol product (g cells)$^{-1}$ h^{-1}
q_s	Specific glucose uptake rate	mmol substrate (g cells)$^{-1}$ h^{-1}
R	Gas constant	R= 8.3144 J mol^{-1} K^{-1}
RALS	Right angle light scatter	
Re	Reynolds number	dimensionless
RQ	Respiratory quotient	mmol carbon dioxide (mmol oxygen)$^{-1}$
RT4	Rushton turbine with four blades	
S	Glucose concentration	mmol l^{-1}
S_R	Residual glucose concentration	mmol l^{-1}
STD	Standard deviation	
T	Temperature	K
TEM	Transmission electron micrograph	
V	Culture volume	l
X	Biomass concentration	g l^{-1}
Y^{max}	Theoretical biomass yield	g biomass (mol substrate)$^{-1}$
Yx/s	Biomass yield	g biomass (g substrate)$^{-1}$

Greek and greek /roman symbols		Units
ρ_L	Liquid density	Kg m^{-3}
ΔP	Proton-motive force	V
ΔpH	Proton gradient	V
Δψ	Membrane potential	V
μ	Specific growth rate	h^{-1}
μ	Viscosity	Pa s

Fatty Acid Nomenclature

i-14:0	12-Methyl tridecanoic acid
14:0	Tetradecanoic acid
i-15:0	13-Methyl tetradecanoic acid
a-15:0	12-Methyl tetradecanoic acid
15:0	Pentadecanoic acid
i-16:0	14-Methyl pentadecanoic acid
16:0	Hexadecanoic acid
i-17:0	15-Methyl hexadecanoic acid
a-17:0	15-Methy lpentadecanoic acid
17:0	Heptadecanoic acid
17:1	Heptadecenoic acid
18:0	Octadecanoic acid
18:2ω6	cis-9,12-Octadecadecenoic acid
18:3ω6	6,9,12-Octadecatrienoic acid

Figure List

Table List

CHAPTER 1

Introduction

1.1 General background

The European food processing industry produces vast volumes of aqueous wastes, many of which contain suspended solids and dissolved organic materials. The current approach for handling such waste streams include off-site disposal, physico-chemical or thermal (incineration) processes. Off-site is by far the most commonly used method where wastes are hauled to private or public disposal facilities. As more and more regulations in Europe are prohibiting land disposal of wastes, more facilities are considering on-site treatment of their high strength wastes. Physical and chemical treatment processes tend to be expensive and are prone to generating large quantities of chemical sludge, which can be very costly for off-site disposal. Incineration provides a total destruction alternative at high cost and strong public opposition (Rozich and Bordacs, 2002).

Among the biological processes available, anaerobic thermophilic processes produce much less sludge and are typically less costly than aerobic processes to operate, vastly

because energy costs for aeration are eliminated, and methane production provides a valuable fuel source. However, anaerobic treatment processes are known to produce low quality effluent and can be somewhat difficult to operate if imbalances arise between organic acids producers and the methanogenic organisms (Lapara, 2000).

On the other hand, aerobic thermophilic processes offer several advantages over mesophilic or anaerobic systems. Many engineers therefore started to design and install thermophilic aerobic treatment processes for the treatment of industrial wastes containing elevated concentrations of soluble, readily degradable organics. The performance advantages of thermophilic aerobic include:

- Ability to destroy pathogens micro-organisms due to the high working temperatures.
- Lower waste sludge production – Thermophilic aerobic systems have characteristically lower biomass yields, which results in lower sludge production. The low biomass yield is a consequence of high maintenance requirement which include all cell energy requirements for functions other than growth such as mobility, repair and resynthesis of macromolecules and creating concentration gradients. Pure cultures of thermophilic aerobes have demonstrated high maintenance requirements (Lapara, 2000). Indeed some commercial systems are engineered which virtually eliminates waste organic sludge production.
- Enhanced chemical oxygen demand (COD) removal – The high temperatures facilitates the biodegradation of organic components that are more soluble at high temperatures and more efficiently converts up to 99 % of the soluble organics to carbon dioxide and water. Therefore, thermophilic aerobic units have been observed to perform higher levels of COD removal than mesophilic systems.

• Enhanced biodegradability capability – Thermophilic aerobic systems have the biokinetic capability of aerobic systems and are much more kinetically robust than anaerobic systems, by exhibiting high biodegradation rates, which reduce the necessary detention time for treatment, and thus for capital cost for facility construction.

• High loading capacity – The high biodegradation rates of the thermophilic aerobic treatment systems may improve the process stability by allowing rapid recovery from upset conditions. For this reason, these systems are able to handle very high loading rates, in comparison with mesophilic aerobic or anaerobic treatment systems.

However, experience has shown that aerobic thermophilic treatment systems have a number of requirements such as aeration system, solids separation, foam control and heating.

• Oxygen transfer – Although it is commonly believed that at higher temperatures the oxygen transfer rate (OTR) decreases due to lower oxygen solubility, this is not entirely true, since OTR depends not only on the solubility of the gas but also on the volumetric mass transfer coefficient k_La. The diffusion coefficient for gases in liquid increases with temperature due to a smaller boundary layer of the liquid at higher temperatures, so the oxygen transfer rate at thermophilic conditions should be the same or even higher than within the mesophilic temperature range (Surucu et al, 1975; Krahe et al, 1996).

However, higher COD loading requires the design of more efficient aeration systems. To respond to the high oxygen transfer requirements of the process, aggressive aeration systems are used (e.g., jet aeration) and reactor water depths are increased above conventional applications.

• Solid separation – Thermophilic bioprocesses almost has poor bacterial settling characteristics resulting from dispersed growing micro-organisms. Therefore biomass can not be separated using gravity settling and biomass yields are very low. Hence the system requires more aggressive methods of solid separation. Ultracentrifugation, dissolved air flotation and rotary drum thickeners have been proven to be effective in providing high capture efficiency of the thermophilic biomass.

• Foaming – Both high biomass concentration in the bioreactor and high temperature lead to foaming incidents that can be controlled by adding antifoam agents or designing mechanical foam breakers.

• Heat and energy balance – Due to the thermophilic nature of the process, a component of the design has to focus on reactor heating characteristics so that appropriate considerations for insulating and/or cooling the biological reactor are addressed.

Although aerobic wastewater treatment systems have these requirements, the extremely high kinetics rates coupled with the resistance to shock loads and low residual sludge production make it an attractive process to treat high strength industrial waste streams.

Brock (1986) defined thermophilic micro-organisms as those which proliferate at temperatures greater than 55-60 °C. This classification, used by many microbiologists, has some practical significance because these temperatures are almost exclusively related to geothermal activity. From a biological waste treatment point of view however, common terminology includes any process operating at temperatures of 45 °C or higher as thermophilic. This definition distinguishes these high temperatures from transitional

systems, such as conventional anaerobic sludge digestion operated at 35-40 °C (Lapara and Alleman, 1999).

1.2 Process description

This work was carried out within the scope of the European Project QLK3-1999-00004 "Enhanced, intelligent processing of food and related wastes using thermophilic populations". The overall aim of the Project was the development of protocols for the transformation of complex waste streams using thermophilic populations. It was also intended to use advanced microbiological and process analysis and control to assist operation and evaluation of a thermophilic bioprocess for the pathogen-free treatment of food industry and related wastes.

A waste treatment contracting company, Lammas Resources Ltd (United Kingdom), one of the partners of the Project consortium, processed organic waste (restaurant and commercial food preparation wastes, cheese, whey and other dairy products, fish processing waste, fruit and vegetable processing waste, animal manure, waste water treatment plant sludges, abattoir wastes, etc.) into nutritious pathogen-free pig feed in an aerobic thermophilic digestion. Digestion took place in a sequence of two bioreactors, maintained at 45 °C and 60 °C respectively. The bioreactors were equipped with mixers and aerators to provide an environment conducive to the rapid growth of micro-organisms, which converted the organic residue materials to single cell protein. The end

product was a material which had a commercial value as livestock feed/additives, organic fertilizer and soil conditioner.

The mixed thermophilic population used in the process had the ability to degrade complex wastes streams, and for this reason, Lammas Resources Ltd was the supplier of the thermophilic micro-organisms population used in the microbial physiology studies within the scope of the Project.

The biology of thermophilic aerobic waste treatment reactors differs from conventional activated sludge microflora in that nitrifying bacterium, floc-forming organisms, or protozoa not present. The genus *Bacillus* have been found in thermophilic aerobic waste treatment bioreactors and solid-waste composting as a major component of the thermophilic microbial community (Lapara and Alleman, 1999; Surucu and al, 1975; Strom, 1995). In fact, *Bacillus* strains were the dominant micro-organisms isolated from Lammas bioreactors. Bacteria of the genus *Bacillus* are aerobic, endospore-forming, gram-positive rods and are one of the most diverse and commercially useful groups of micro-organisms. Representatives of this genus are widely distributed in soil, air and water where they are involved in a range of chemical transformations that rival those of Pseudomonas and Actinomycetes. The ability of certain strains to tolerate high or low temperature and high or low pH make them a particularly important source of commercial enzymes. The metabolic diversity of *Bacillus* spp., together with low reported incidence of pathogenicity has led to representatives of this group being used in a wide range of industrial processes (Harwood, 1989).

1.3 Biological system and advanced microbiological techniques used in this work

1.3.1 Continuous culture

In the present work, continuous culture system was used in the bioreactor experiments. The essential feature of this technique is that when microbial growth in continuous culture takes place under steady-state conditions, the growth occurs indefinitely at a constant rate and in a constant environment. Such factors as pH, nutrients concentration, metabolic products and oxygen, which inevitably change during the growth cycle of a batch culture, are all maintained constant in a steady-state continuous culture. Moreover, they may be independently controlled by the operator. These features of the continuous culture technique make it a valuable research tool (Herbert et al, 1956). However, the continuous addition of feed streams over several weeks greatly increases the probability of contamination. This drawback is partially overcome when thermophilic micro-organisms are cultivated in this system, since the risk of contamination of thermophilic continuous cultures is lower, so long-term, steady-state experiments investigating physiological response to culture perturbations are possible (Rinker and Kelly, 1999).

During the steady-state, the dynamics of the growing population are not highlighted (Fiechter, 1981). To understand the physiology of the micro-organism, changes can be made in their growth environment (e.g., media formulation, specific growth rate, stirring rate, etc.), disturbing the steady-state equilibrium. A transient state results where the population characteristics change or oscillate before finally reaching a new steady sate. Instead of a step change the steady-state can also be disturbed by short time alterations of

one of these parameters (pulse). Both methods are useful for studying the impact of changes in environmental growth conditions on microbial physiology (Rinker and Kelly, 1999).

1.3.2 Flow cytometry

During the course of any bioprocess, it is vital to monitor cell proliferation and viability. Accurate estimates of viable biomass concentration are essential so that decisions on process control can be made to optimize the bioprocess or to develop new strategies. This allows products to be harvested at optimum concentrations and the activation of inducible systems to be initiated at the correct time, so that maximum product yields can be obtained.

Classical microbiological techniques routinely used for cell proliferation and viability may give erroneous information. Manual cell counts, dilution plates, optical density and dry cell weight give an indication of reproductive growth, but provide no information on cell physiological data. Manual cell counts are tedious to perform, and, for statistical accuracy, rely on the equal distribution of cells within the counting chamber, a virtually impossible situation. Dilution plating results can take up to 12 h to obtain, too late for changes in process control to have any significant effect. Due to differences in cell nutrient requirement and the potential for long lag phases, the success of this technique depends on growth media. As a result, significant differences in reproductive viable cell counts have been reported (Nebe-von Caron et al, 2000). Traditional staining techniques

used with microscopy suffer from the same problems associated with manual cell counts. Besides, it is the user who makes the decision on whether a cell has taken up the stain and hence, on its physiological state. This leads to inconsistencies between time spaced samples when different personnel have made the measurement. Dry cell weight data is usually available a considerable time after the sample is taken, again too late for alterations to be made to process control. Additionally, such measurements made during the early stages of a fermentation, when biomass concentrations are low, are known to be inaccurate. Optical density measurements rarely take into account changes in cell size or background medium composition. Importantly, these bulk measurements (optical density and dry cell weight) bring about just a single value for the whole cell population (i.e., each cell is treated as an average micro-organism) thus assuming that the microbial population is homogeneous with respect to its physiological state (Hewitt and Nebe-von Caron, 2004). However this has been shown not to be the case (Hewitt, et al, 1999a and b; Hewitt and Nebe-Von-Caron, 2001; Onyaka et al, 2003; Reis et al, 2005).

Flow cytometric analysis allows the differentiation of stages far beyond the classical definition of viability which is usually defined by the demonstration of growth. The fact that complex cellular functions, other than growth that are not detected by classical microbiological techniques but can now be detected by flow cytometry, led to a shift in the interpretation of the term "viability", thus generated the term of "viable but non-culturable cells" and allowed the assessment of microbial population heterogeneity. Hence, the conception of homogeneous microbial population is unfounded. Therefore, current mathematical methods based on the concept of homogeneous microbial

populations that are used to predict fermentation performance during cultivation process on scale-up often yield erroneous data (Hewitt and Nebe-von Caron, 2001).

A high fraction of dead or dormant cells (stressed, injured or otherwise so-called "viable but non-culturable" that remain undetected by growth based methods) present in any part of a bioprocess will be detrimental on the synthesis of a desired product or on biodegradation process efficiency; it is therefore crucial to have accurate information on the physiological states of individual cell within a population (Hewitt and Nebe-von-Caron, 2004). Flow cytometry offers the possibility for this type of specific and detailed analysis of cell populations. The power of this technique lays both in the wide range of cellular parameters that can be determined and in the ability to obtain information on how these parameters are distributed in the cell population. Measurements that reveal the distribution of these parameters in cell populations are important for biotechnology because they better describe the population than the average values obtained from traditional techniques (Rieseberg et al, 2001, Amour et al, 2002).

A flow cytometry system consists of five main operating units (Figure 1.1). A light source (usually a laser), flow cell, optical filter units for specific wavelength detection over a broad spectral range, photodiodes or photomultiplier tubes for sensitive detection of the signals of interest, and a data processing and operating unit. A cell suspension is injected into the flow cell where the cells pass one after another across a laser beam that is orthogonal to the flow. This is achieved by hydrodynamic focusing of the sample stream, wherein the sample stream is injected into the sheath stream inside the flow cell (Figure 1.2). The velocities of both fluids are in the range of laminar flow. Since the sheath flow is faster than the sample flow, the sample stream is reduced in its cross-

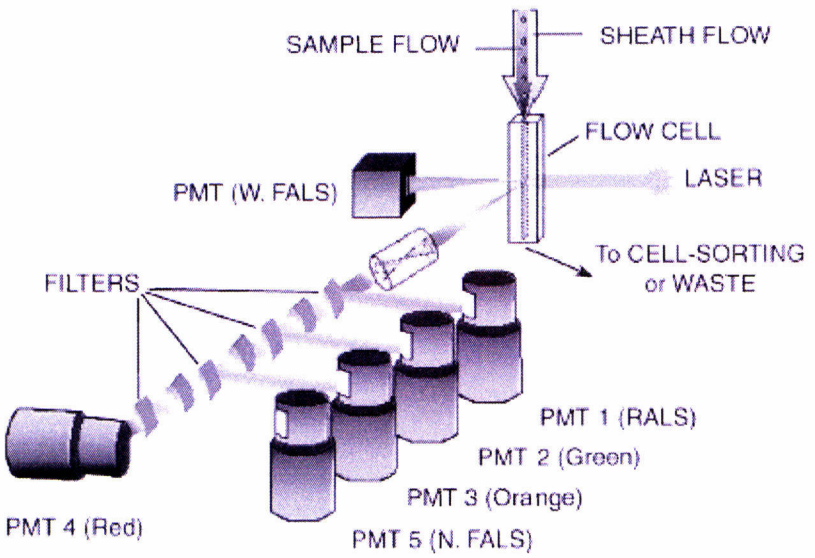

Figure 1.1 Schematic diagram of standard flow cytometry equipment. Cells pass individually through the center of a Laser beam and scattered light is detected at two angles. Forward angle light scatter (FALS) is measured in the plane of the beam and right angle light scatter (RALS) is measured at 90° angle by photomultipliers tubes (PMT) (Hewitt and Nebe-von -Caron, 2004).

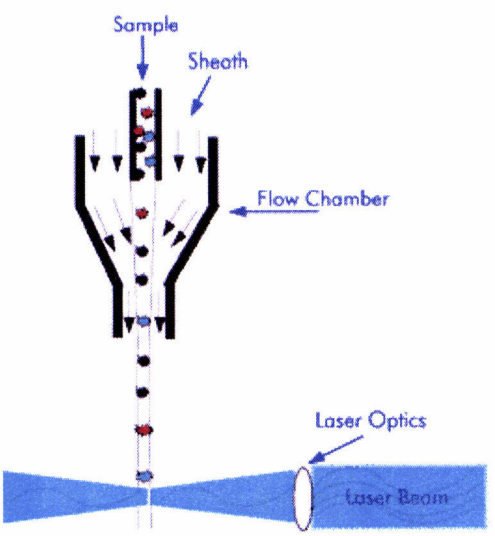

Figure 1.2 Schematic diagram of a flow cell.

sectional area and therefore the cells are isolated in this focused stream. Using this technology it is possible to detect more than 50,000 cells in minutes (thus enabling the collection of data from tens of thousands of cells per sample rather quickly), and large amounts of data are produced. When the laser beam impacts a cell, the excitation light is scattered in two planes: forward angle light scatter (FALS) is measured in the plane of the beam and right angle light scatter (RALS) is measured at 90° to the beam. Intracellular compounds that possess an intrinsic fluorescence (e.g. NAD(P)H), or are stained with specific fluorescence dyes, allow certain cell components to be selectively assayed. The resulting fluorescence light is processed through the photomultiplier to the data system and the resulting data are analyzed by the cytometer software. The scattering and fluorescence signals can be combined in various ways that allowed all subpopulations to be observed. In addition, flow cytometers can be combined with sorting units that offer the possibility of separating of selected subpopulations. Most sorters are based on a sorting unit that breaks the cell stream into droplets. Before the droplets are formed, the cells are electrically charged. The resulting droplets are deflected into a collection vessel by passage through an electric field. The separated subpopulations or individual cells can be isolated in to microliters plates or grown on agar for further analysis and investigation (Nebe-von-Caron et al, 2000; Rieseberg et al, 2001).

Flow cytometry has been used for the "at-line" study during the course of bacterial fermentations, as this technique provides statistically reliable information about individual cell physiology. This technique has been used to monitor the composition and population dynamics of waste water microbial communities (Wallner et al, 1995)..

1.3.2.1. Light scatter

Light scatter measurements require no sample preparation or reagent additions. Practically, both yeast and bacteria can be detected on the basis of their intrinsic light scattering properties in the forward (FALS) and the right angle direction (RALS). The correlation between cell morphology and light scatter depends on the optical system configuration and can be used to estimate biomass concentration. However, changes in refractive index for example due to the presence of inclusion bodies can affect this relationship (Allman at al, 1992; Hewitt and Nebe-Von-Caron, 2004). Whilst forward angle light scatter (FALS) gives relative information on cell size, right angle light scatter (RALS) provides information on cell granularity. Light scatter can be used to discriminate between a range of organisms in a mixed population based on their light scattering characteristics (Allman at al, 1992) and was also used to distinguish yeast cells from contaminating cells (Hewitt and Nebe-Von-Caron, 2004). The differentiation of bacterial endospores from vegetative cells using changes in the intrinsic light scattering properties alone has also been carried out (Comas-Riu and Vives-Rego, 2002; Reis et al, 2005).

1.3.2.2. Fluorescence monitoring

Most applications of flow cytometry are based on fluorescence monitoring. The measurable cell parameters can be characterized as intrinsic or extrinsic, depending on

their need for reagents. While no pretreatment is required for the assay of intrinsic fluorescence (e. g., NAD(P)H), studies of specific cell components with fluorescent dyes (extrinsic fluorescence) requires a staining procedure performed before the cells are analyzed.

The following sections describe the use of stains for the cell viability parameters detection such as membrane potential and membrane integrity.

1.3.2.2.1. Membrane potential

All microbial cells are bounded by the cytoplasmic membrane, which allows the cell to communicate selectively with its immediate environment (Appendix 1). Passive and active transport systems across the membrane generate an electrochemical gradient. In metabolically active bacteria with intact cytoplasmic membranes, there is, typically, a difference of electrical potential across the membrane between 100 and 200 mV with the interior electrically negative charged with respect to the exterior. A reduction in the magnitude of membrane potential (MP) is referred to as electrical depolarization. Several classes of chemical compounds, specifically ionophores, can also alter MP without affecting permeability to propidium iodide (PI) and similar dyes (Novo et al, 2000) (Appendix 1).

MP is an early indicator of cell damage that can affect cell viability and can be measured directly using implanted microelectrodes. However, this method becomes increasingly difficult as the technique is applied to smaller cells. MP can be measured by flow

cytometry using lipophilic dyes such as cyanines or oxonols. Due to their lipophilicity, these compounds are able to pass freely through the lipid portion of the membrane, provided that the concentration of the indicator is substantially lower than the concentrations of the ions which establish the potential, the concentration gradient of the indicator is determined by the potential difference across the membrane. Dyes which behave in this faction are often referred to as distributional probes and are translocated across membranes by an electrophoretic mechanism (Shapiro, 2000; Haughland, 2002).

The concentration gradient of a lipophilic cation C^+ across an intact cytoplasmic membrane is determined by the transmembrane potential difference according to the Nernst equation:

$$[C^+]_i/[C^+]_o = e^{(-F\Delta\Psi/RT)}$$

where $[C^+]_i$ is the concentration of C^+ ions inside the cytoplasmic membrane, $[C^+]_o$ is the concentration of C^+ ions outside the cytoplasmic membrane, $\Delta\Psi$ is the membrane potential, R is the gas constant, T is the temperature in Kelvin degrees and F is the Faraday constant. Once cells equilibrate with an indicator cation, electrical depolarization of the cells will cause release of indicator from cells into the medium, while polarization will make cells take up additional indicator from the medium (Figure 1.3 a). The distribution mechanism of an anionic probe across the membrane is the opposite (Figure 1.3 b). The indicator distribution will not adequately represent the new value of $\Delta\psi$ until equilibrium has again been reached; this process requires periods ranging from seconds to several minutes. Thus while distributional probes may be suitable for detection

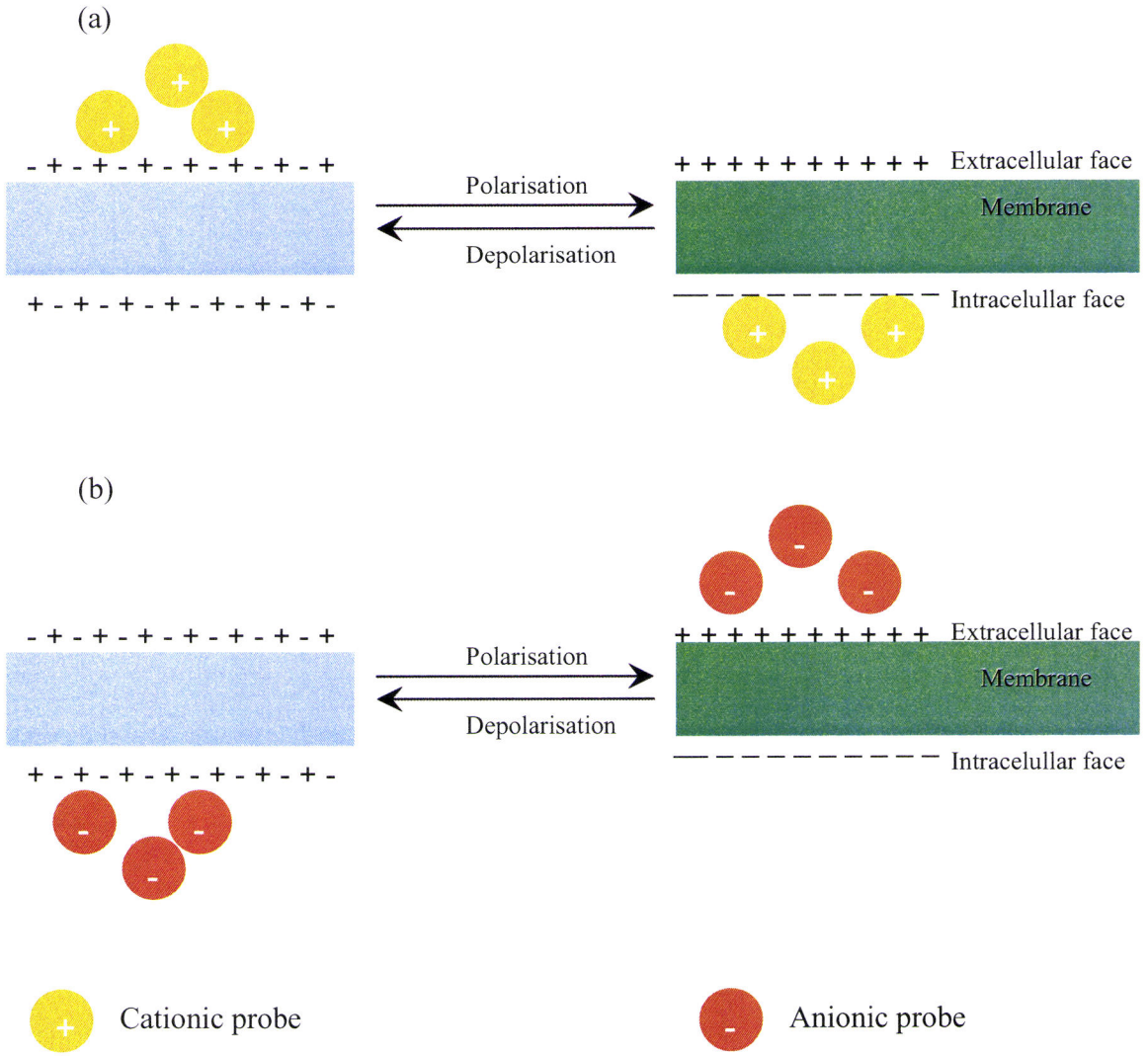

Figure 1.3 Response mechanisms of distributional probes.

(a) Cationic probes slow mechanism. Once the equilibrium between cells and the cation C^+ has been reached, the cation will accumulate intracellularly if the membrane is polarized, as in this case the inner membrane is negatively charged.

(b) Anionic probes slow mechanism. Once the equilibrium between cells and the anion A^- has been reached, the anion will accumulate intracellularly if the membrane is depolarized, as in this case the inner membrane is less negatively charged (Adaptation from Haughland, 2002).

of slow changes in $\Delta\psi$, such as changes in average membrane potentials of nonexcitable cells caused by respiratory activity, ion-channel permeability and drug binding, they cannot be used during the propagation of action potentials in tissues such as nerve and muscle. In this case, fast-response probes must be used (Haugland, 2002). Cyanine dyes have been among the most widely used distributional probes and are a family of membrane potential sensitive lipophilic cations. These have been used to determined membrane potential in a diversity of cells and vesicles including cultured mammalian cells, lymphocytes, red blood cells, yeast and bacteria (Mason et al, 1995). Cyanine lipophilic cationic probes like 3,3'-Dihexylcarbocyanine iodide [$DiOC_6(3)$] (Figure 1.4) that accumulates proactively are preferential for reflecting cytoplasmic membrane in Gram positive cells because such cells only generate a sufficiently large membrane potential to exclude anionic fluorescent stains such as Bis-(1,3-dibutylbarbituric acid) trimethine oxonol (Bis-oxonal, $DiBAC_4$, BOX) when metabolizing rapidly during exponential growth (Hewitt and Nebe-von Caron, 2004).

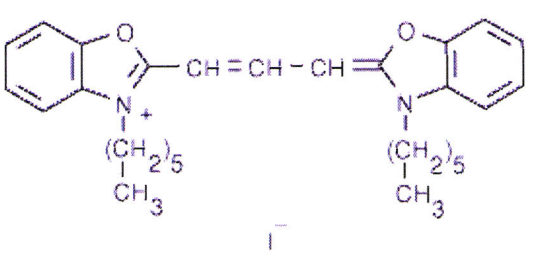

Figure 1.4 $DiOC_6(3)$ structure.

1.3.2.2.2 Membrane integrity

MP reduces to zero if the membrane ruptures, i.e., develops holes large enough to permit large inorganic ions to cross freely, as may occur when cells are killed for instance by heating. Under these circumstances the damage is irreversible and the cytoplasmic membrane becomes permeable to dyes such as propidium iodide (PI) (Figure 1.5) which is generally excluded from viable cells. This stain binds to DNA by intercalating between the bases with little or no sequence preference and with a stoichiometry of one dye molecule per 4-5 base pairs of DNA. PI is commonly used for identifying dead cells in a population (Haughland, 2002).

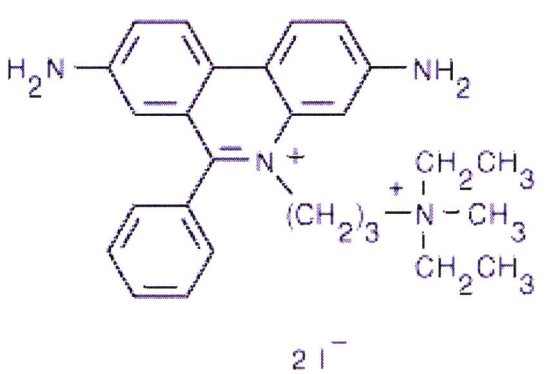

Figure 1.5 Propidium iodide structure.

1.3.2.2.3 Membrane potential and membrane integrity dyes mixtures

The presence of an intact polarized cytoplasmic membrane and active pumps define a fully energized cell. It is thought that when a cell is stressed energetically, the active transport systems will cease, the cytoplasmic membrane will depolarize and permeabilisation will occur, indicating cell death (Hewitt, 2001).

Using various mixtures of membrane potential and membrane integrity fluorescent dyes, it is possible to resolve individual microbial cells physiological state beyond culturability based on the presence or absence of an intact polarized cytoplasmic membrane and transport across it, enabling assessment of population heterogeneity (Onyeaka et al. 2003, Davey and Winson 2003, Shapiro 2000). Hewitt et al (1999b) were able to differentiate stressed *E. coli* cells by 3-colour analysis using combinations of Bis-(1,3-dibutylbarbituric acid trimethine oxanol (BOX), ethidium bromide (EB) and PI. Using this combination, four subpopulations of cells could be distinguished, corresponding to (A) healthy cells; no staining; (B) vital cells (non-pumping) uptake of EB; (C) intact cells (non-pumping, depolarized cytoplasmic membranes) uptake of EB/BOX; and (D) dead cells (permeabilised cytoplasmic membranes) uptake of BOX/EB/PI. This type of measurements characterizes the presence or absence of an intact polarized cytoplasmic membrane and the active dye extrusion system across it.

When selecting a combination of fluorescent stains to use together in a mixture, there are several factors that need to be considered. These include the facts that 1) the stains must be excited efficiently by the light sources available, 2) the emission wavelengths should

not overlap and 3) the cellular targets of the constituents of the mixture should be different (Davey and al, 1999).

1.4 References

Allman, R., Hann, A.C., Manchee, R. and Lloyd, D. 1992. Characterization of bacteria by multiparameter flow cytometry. J. Appl. Bacteriol. 73, 438-444.

Amor, K. B., Breeuwer, P., Verbaarschot, P., Rombouts, F., Akkermans, A.D.L., Vos, W.M and Abee, T. 2002. Multiparametric flow cytometry and cell sorting for the assessment of viable, injured, and dead bifidobacterium cells during bile salt stress. Appl. Environ. Microbiol. 68, 5209-5216.

Brock T.D. 1996. Introduction: An overview of the thermophiles. In Thermophiles: General, Molecular, and applied microbiology, ed. T.D. Brock, John Wiley and Sons, New York, NY, U.S.A.

Comas-Riu, J. and Vives-Rego, J. 2002. Cytometric monitoring of growth, sporogenesis and spore cell sorting in *Paenibacillus polymyxa* (formerly *Bacillus polymyxa*). J. Appl. Microbiol. 92, 475-481.

Davey, H.M. and Winson M.K., (2003). Using flow cytometry to quantify microbial heterogeneity. Curr. Issues Mol. Biol. 1, 9-15.

Fiechter, A. 1981. Batch and continuous culture of microbial, plant and animal cells. In Biotechnology: Microbial Fundamentals. H.-J Rehm and G. Reed eds. Vol I, Verlag Chemie, Weinheim, 453-505.

Harwood, C.R. 1989. Introduction to the biotechnology of *Bacillus*. In: *Bacillus*, ed. Colin R. Harwood, New York.

Haughland, R.P. 2002. Handbook of Fluoresecent Probes and Research Products, Molecular Probes, ninth edition.

Herbert, D., Elsworth, R., and Telling, R.C. 1956. The continuous culture of bacteria: a theoretical and experimental study. J. Gen. Microbiol. 14, 601-622.

Hewitt, C.J., Nebe-Von Caron, G., Nienow, A.W. and McFarlane, C. 1999a. The use of multi-parameter flow cytometry to compare the physiological response of *Escherichia coli* W3110 to glucose limitation during batch, fed-batch and continuous culture cultivations. J. Biotechnol. 75, 251-264.

Hewitt, C.J., Nebe-Von Caron, G., Nienow, A.W. and McFarlane, C. 1999b. Use of multi-staining flow cytometry to characterize the physiological state of *Escherichia coli* W3110 in high cell density fed-batch cultures. J. Biotechnol. 63, 705-711.

Hewitt C. J., and Nebe-von-Caron G. 2001. An industrial application of multi-parameter flow cytometry: Assessment of cell physiological state and its application to the study of microbial fermentations. Cytometry 44, 179-187.

Hewitt C. J. and Nebe-von-Caron G. 2004. Advances in Biochemical Engineering/Biotechnology. In: Enfors S. O., Springer (Eds.), The application of multi-parameter flow cytometry to monitor individual microbial cell physiological state. Special volume 89, pp 197 – 223.

Krahe, M. Antranikian, G. and Märkl, H. 1996 . Fermentation of extremophilic micro-organism. FEMS Microbiol. Rev. 18, 271-285.

Lapara, T.M. and Alleman, J.E. 1999. Thermophilic aerobic biological wastewater treatment. Wat. Res. 33, 895-904.

Lapara, T.M., Konopka, A., Nakatsu, C.H., Alleman, J.E. 2000. Thermophilic aerobic wastewater treatment in continuous-flow bioreactors. J. Environm. Eng. 126, 739-744.

Nebe-von-Caron G., Stephens P. J., Hewitt C. J., Powell J. R. and Badley R. A. 2000. Analysis of bacterial function by multi-color and single cell sorting. J. Microbiol. Meth. 42, 97-114.

Novo, D., Perlmutter, N.G., Hunt, R.H., and Shapiro, H.M. 2000. Multiparameter flow cytometry analysis of antibiotic effects on membrane potential, membrane permeability and bacterial counts of *Staphylococcus aureus* and *Micrococcus luteus*. Antimicrob. Agents CH 44, 827-833.

Onyeaka H., Nienow A. W., and Hewitt C. J. 2003. Further studies related to the scale-up of high cell density *Escherichia coli* fed-batch fermentations: the additional effect of a changing micro-environment when using aqueous ammonia to control pH. Biotechnol. Bioeng. 84, 474 – 484.

Reis, A., Lopes da Silva, T., Kent, C.A., Kosseva, M., Roseiro, J.C. and Hewitt, C.J. 2005. Monitoring populations dynamics of thermophilic *Bacillus licheniformis* CCMI 1034 in continuous cultures using multi-parameter flow cytometry. J. Biotechnol. 115, 199-210.

Rieseberg, M., Kasper, C., Reardon, K.F., Scheper, T. 2001. Flow cytometry in biotechnology. Appl. Microbiol. Biotechnol. 56, 350-260.

Rinker, K.D., Han C.J. and Kelly, R.M. 1999. Continuous culture as a tool for investigation for growth physiology of heterotrophic hyperthermophiles and extreme thermoacidophiles. J. Appl. Microbiol. Symp. Suppl, 85, 118S-127S.

Rozich, A.F. and Bordacs, K. 2002. Use of thermophilic biological aerobic technology for industrial waste treatment. Wat. Sci. Technol. 46, 83-89.

Shapiro, H.M. 2000. Membrane potential estimation by flow cytometry. Methods 21, 271-279.

Strom, P.F. 1985. Identification of thermophilic bacteria in solid-waste composting. Appl. Environ. Microbiol. 50, 906-913.

Surucu, G.A., Engelbrecht, R.S. and Chian, E.S.K. 1975. Thermophilic microbial treatment strength wastewates with simultaneous recovery of single cell protein. Biotechnol. Bioeng. 17, 1639-1662.

Wallner, G., Erhart, R. and Amann, R. 1995. Flow cytometry analysis of activated sludge with rRNA-target probes. Appl. Environ. Microbiol. 61, 1859-1866.

CHAPTER 2

Phenotypic characterization of *Bacillus* strains isolated from the Lammas Industry bioreactors

2.1 Introduction

Phenotypic characterization of *Bacillus* species have been carried out using cellular fatty acid profiles (Kaneda, 1963; Kämpfer, 1994), biochemical tests (Logan and Berkleley, 1984; Priest and Alexander, 1988; Priest et al, 1988), antibiotic sensitivity, bacteriocin sensitivity, and esterase patterns (Baillie and Walker; 1968; Sharp et al, 1980). These characterizations have contributed for the assessment of the biotechnological usefulness of the genus.

Bacteria grown under controlled conditions exhibit constant, unique whole fatty acids profiles which can be used to differentiate even very closely related organism. Genera and species are distinguishable by qualitative differences (the presence or absence of particular fatty acids) or quantitative differences in acid abundances. Strains within the same species show minor quantitative differences in fatty acids profiles (Miller and Berger, 1985). It has been well established that the total fatty acid composition of a

micro-organism is an important taxonomic character and that fatty acid data can be analyzed quantitatively to provide useful taxonomic information at the species level and, in some cases, as the subspecies level (Mukwaya and Welsh, 1989).

Gas-liquid chromatography of bacterial cellular fatty acid methyl esters (FAMEs), a rapid and simple method has been extensively used as a primary or an adjunctive mean for identification of many micro-organisms (Marumo and Aoki, 1990; Gilarová et al, 1994; Lopes da Silva et al, 1998).

The presence of iso- and anteiso methyl-branched fatty acids as major constituents of cell membranes, was first reported in the genus *Bacillus* by Saito (1960) and Kaneda (1963). Kämpfer (1994) grouped *Bacillus* strains into seven clusters, although heterogeneity in fatty acid profiles within some species was found.

Enzymatic patterns for lactic acid bacteria were used to evaluate their biochemical and technological properties (Bianch-Salvadori, 1995) using the apiZYM test strips. This system is a rapid and semi quantitative biochemical micromethod designed for the research of enzymatic activities.

The aim of this study was the evaluation of the potential biotechnological usefulness of the *Bacillus* strains isolated from the Lammas bioreactors through the assessment of cellular fatty acid and enzyme productions by the *Bacillus* strains. For this purpose, FAMEs analyses as well as apiZYM enzyme strips tests were carried out. As a complement, numerical analyses of the fatty acid and enzymatic activities quantitative data were carried out to differentiate the *Bacillus* species isolated from the Lammas bioreactors and a comparison of the results obtained from both methods (FAMEs and

apiZYM) was made, in order to evaluate the homogeneity of these phenotypic characteristics within the *Bacillus* species.

2.2. Materials and Methods

2.2.1 Organisms

The following 17 *Bacillus* species [1]isolated from Lammas bioreactors and deposited in the Industrial Micro-organisms Culture Collection (CCMI) were studied: *Bacillus licheniformis* CCMI 1030, *B. licheniformis* CCMI 1031, *B. licheniformis* CCMI 1032, *B. licheniformis* CCMI 1033, *B. licheniformis* CCMI 1034, *B. licheniformis* CCMI 1035, *B. licheniformis* CCMI 1036, *B. licheniformis* CCMI 1037, *B. pumilus* CCMI 1038, *B. pumilus* CCMI 1039, *B. pumilus* CCMI 1040, *B. subtilis* CCMI 1041, *B. subtilis* CCMI 1042, *B. subtilis* CCMI 1043, *B. subtilis* CCMI 1044, *B. subtilis* CCMI 1045, *B. subtilis* CCMI 1046. Reference strains of each species were also included [*B. licheniformis* ATCC 21667 (CCMI 232), *B. pumilus* NCIB 9369 (CCMI 692) and *B. subtilis* ATCC 9372 (CCMI 255)]. The micro-organisms were maintained in glass beads, using glycerol as cryoprotectant, at -72 °C.

[1] The *Bacillus* species isolated from the Lammas bioreactors were previously identified using Polimerase Chain Reaction (PCR) and Randomly Amplified Polymorphe DNA (RAPD) techniques at 30 ° C, within the scope of the Project "Enhanced, intelligent processing of food and related wastes using thermophilic populations" QLK3-1999-00004.

2.2.2 Fatty acid analysis

Bacillus strains slants were obtained by growth on nutrient agar at 30 °C for 24 hours. Two milliliters of each cell suspension were transferred into 1-litre baffled-Erlenmeyers flasks containing 200 ml of growth medium: $(NH_4)_2SO_4$, 2.00 g l^{-1}, KH_2PO_4, 1.33 g l^{-1}, $CaCl_2.2H_2O$, 0.13 g l^{-1}, $MgSO_4.7H_2O$ 0.33 g l^{-1}, yeast extract, 13.30 g l^{-1} and trace elements solution 3 ml l^{-1} (Vishniac and Santer, 1975). Glucose (55 g l^{-1}) was sterilized separately. The initial pH of the medium was 7.0. Cultures were grown on an orbital shaker incubator at 30 °C, set at 150 rpm, for 24 hours. Biomass was separated from the culture medium by centrifugation in a ultracentrifuge Avanti J-25 I Beckman (Fullerton, California) at 8000 rpm (11900 g), for 20 minutes at 4 °C, washed with sodium chloride solution (0.85 % w/v), freeze-dried and ground.

Fatty acids extraction and preparation of methyl esters were carried out according to Lepage and Roy (1986). Freeze-dried samples of *Bacillus* strains (100 mg) were transmethylated with 5 ml of methanol/acetyl chloride (95:5 v/v). The mixture was sealed in a light-protected Teflon-lined vial under nitrogen atmosphere and heated at 80 °C for 1 hour. The vial contents were then cooled, diluted with 1 ml water and extracted with 2 ml of n-heptane. The heptane layer was dried over Na_2SO_4, evaporated to dryness under nitrogen atmosphere and redissolved in heptane, which contained the methyl esters. The methyl esters were then analyzed by gas-liquid chromatography, on a Varian (Palo Alto, USA) 3800 gas-liquid chromatograph (USA), equipped with a flame ionization detector. Separation was carried out on a 0.32 mm × 30 m fused silica capillary column (film 0.32

µm) Supelcowax 10 (Supelco, Bellafonte PA, USA) with helium as carrier gas at a flow rate of 1.3 $ml.min^{-1}$. The column temperature was programmed at an initial temperature of 200 °C for 10 min, then increased at 4 °C min^{-1} to 240 ° C and held there for 16 min. Injector and detector temperatures were 250 and 280 °C respectively and split ratio was 1:100. Peak identification was carried out using known standards (Nu-Chek-Prep, Elysian, USA). From each duplicate sample two independent derivatizations were prepared. Two injections were made for each derivate, thus each fatty acid analysis was the peak area average of eight injections.

2.2.3 Constitutive enzyme production using ApiZYM test strips

ApiZYM (bioMérieux sa, Marcy-l'Etoile, France) allows the systematic study of nineteen enzymatic reactions. The strips contain the substrates which were incubated with the suspension of the micro-organisms. The metabolic end products during the incubation period were detected through colored reactions revealed by the reagents addition.

The micro-organisms referred in section 2.2.1 were grown for 24 hours on nutrient agar plates at 30 °C. Suspensions of cells were prepared in suspension medium to give the turbidity of 5-6 McFarland scale and 65 µl was added to each microtube of the API galleries. The strips were incubated at 37 °C for 4 hours before reading. The specific reagents (ZYM A and ZYM B from the API system) were added to each microtube, to become colored in case of a positive test. The intensity of colors (from 1 to 5) allowed differentiation between positive (3-5) and negative (1-2) enzymatic reactions.

2.2.4 Numerical analyses

The quantitative data obtained from the fatty acid profiles and enzymatic activities were used as the basis of numerical analyses. Peak area values for each fatty acid were calculated as percentages of the total peak area. Principal component analysis (PCA) and hierarchical clusters analysis (HCA) (Appendix 2) were used to calculate similarities between the fatty acid profiles and the quantitative data from the enzymatic reactions of the 20 strains, using the SCAN Software for Chemometric Analysis (Minitab Inc, State College, USA). In all cases, projections of more than the first two principal components provide no additional information on the relationship between species so only plots of the first two principal components are presented.

2.3 Results and discussion

2.3.1 Fatty acid analysis

Table 2.1 shows the fatty acid profiles for the 20 *Bacillus* strains that were analyzed by gas-liquid chromatography. All strains were characterized by the predominance of branched fatty acids (i14:0, i15:0, a15:0, i16:0, i17:0 and a17:0) ranging from 63.9 % to 89.5 % of the total peak area for the 20 *Bacillus* strains and a15:0 was the major fatty

Table 2.1- Fatty acid composition of the 20 *Bacillus* strains. The reference strains are in bold.
STD – Standard deviation

Bacillus strains	% of total fatty acid content (mean ± STD)													
	i-14:0	14:0	i-15:0	a-15:0	15:0	i-16:0	16:0	i-17:0	a-17:0	17:0	17:1	18:0	18:2ω6	18:3ω3
1.*B.lichenformis*	**1.20±**	**0.54±**	**14.98±**	**30.60±**	-	**8.93±**	**12.88±**	**12.57±**	**17.29±**	-	-	**1.96±**	-	-
CCMI 232	**0.04**	**0.02**	**0.19**	**0.17**		**0.08**	**0.28**	**0.15**	**0.58**			**0.15**		
2. *B.lichenformis*	0.94 ±	0.44±	15.24 ±	33.65±	0.36±	6.32±	9.75±	10.08±	18.28±	-	-	0.91±	-	-
CCMI 1030	0.07	0.03	1.11	2.64	1.71	1.02	0.44	0.44	0.77			0.08		
3 *B.licheniformis*	1.04±	0.28±	13.50±	34.80±	0.35±	7.72±	7.95±	9.92±	20.10±	0.34±	-	0.99±0.	0.76±	-
CCMI 103*1*	0.11	0.00	1.35	1.73	0.02	0.97	0.97	0.59	1.90	0.00		16	0.48	
4 *B.lichenformis*	0.96±	0.31±	13.45±	35.60±	0.35±	7.85±	7.11±	9.69±	21.72±	0.61±	-	0.82±	0.90±	-
CCMI 1032	0.09	0.09	1.30	2.39	0.03	0.75	1.06	0.23	2.37	0.44		0.07	0.66	
5 *B.lichenformis*	1.42±	0.39±	15.6±	28.94±	0.49±	10.09±	9.97±	11.35±	17.27±	0.51±	-	1.22±	-	-
CCMI 103*3*	0.79	0.00	0.37	0.89	0.02	0.20	1.06	0.37	0.49	0.02		0.06		
6 *B.lichenformis*	1.70±	0.38±	12.87±	27.21±	0.51±	11.02±	9.43±	10.60±	15.98±	-	-	1.07±	-	-
CCMI 103*4*	0.54	0.04	1.55	3.19	0.07	1.15	1.00	1.04	1.73			0.11		
7 *B.lichenformis*	1.28±	0.41±	15.55±	29.51±	0.43±	9.07±	11.22±	11.64±	16.79±	0.39±	0.64±	1.22±	-	-
CCMI 1035	0.11	0.15	0.72	1.17	0.12	0.72	0.31	0.34	0.50	0.15	0.32	0.14		
8 *B.lichenformis*	0.85±	0.42±	16.9±	31.46±	0.31±	5.48±	10.80±	12.30±	18.38±	-	-	0.86±	0.93±	-
CCMI 1036	0.06	0.02	0.77	1.49	0.01	0.18	2.92	2.07	0.54			0.03	0.23	
9 *B.lichenformis*	1.78±	-	14.31±	31.02±	0.62±	13.10±	9.12±	11.04±	16.75±	0.48±	0.65±	1.29±	-	-
CCMI 1037	0.05		0.62	0.72	0.32	0.19	0.20	0.42	0.54	0.02	0.24	0.11		
10 *B. pumilus*	**1.29±**	**1.47±**	**12.68±**	**35.82±**	-	**5.17±**	**16.33±**	**9.66±**	**16.24±**	-	-	**1.05±**	-	-
CCMI 692	**0.12**	**0.12**	**0.66**	**1.69**		**0.06**	**0.42**	**0.85**	**1.18**			**0.19**		
11 *B. pumilus*	1.68±	1.81±0.	13.98±	33.29±	0.50±	5.05±	18.36±	9.14±	14.18±	0.30±	1.01±	1.47+	0.87±	-
CCMI 103*8*	0.08	06	0.77	1.88	0.02	0.13	0.56	0.24	0.35	0.00	0.21	0.21	0.09	
12 *B. pumilus*	1.87±	1.88±	12.53±	34.88±	0.51±	5.34±	19.05±	8.51±	14.52±	0.27±	1.26±	1.19±	-	-
CCMI 1039	0.27	0.23	0.41	0.87	0.01	0.31	1.19	0.74	1.22	0.03	0.12	0.15		
13 *B. pumilus*	2.68±	2.70±	10.66±	28.35±	0.63±	5.35±	22.14±	6.52±	10.22±	2.09±	2.78±	1.55±	2.85±	
CCMI 1040	0.36	2.26	0.96	2.52	0.07	0.42	1.88	0.68	1.12	0.28	0.05	0.32	0.62	
14 *B. subtilis*	**1.52±**	**0.95±**	**4.68±**	**42.28±**	-	**6.12±**	**13.52±**	**6.93±**	**18.05±**	-	-	**4.63±**	-	-
CCMI 255	**0.16**	**0.08**	**0.29**	**2.60**		**0.08**	**0.30**	**0.52**	**1.18**			**0.73**		
15 *B. subtilis*	6.43±	3.22±	5.44±	36.41±	-	6.28±	10.72±	6.11±	17.11±	0.63±	-	2.59±	0.64±	-
CCMI 1041	4.39	1.52	2.38	4.23		1.44	1.68	1.96	3.42	0.46		1.13	0.60	
16 *B. subtilis*	2.50±	1.35±	3.71±	37.59±	-	5.47±	11.02±	5.63±	16.29±	2.23±	-	3.07+	1.60±	
CCMI 1042	1.00	0.60	0.41	3.42		0.56	0.89	0.09	1.62	1.13		0.39	0.61	
17 *B. subtilis*	1.62±	0.73±	4.02±	41.61±	-	5.97±	10.68±	6.07±	17.98±	-	-	2.95±	0.94±	1.52+
CCMI 1043	0.24	0.12	0.18	1.66		0.36	0.44	0.19	0.72			0.22	0.92	0.38
18 *B. subtilis*	1.46±	0.66±	4.10±	42.75±	-	6.04±	11.48±	6.28±	19.14±	-	-	2.93±	2.15±	1.24±
CCMI 1044	0.47	0.16	0.31	1.66		0.27	0.75	0.27	0.74			0.20	1.21	0.44
19 *B. subtilis*	2.34±	1.08±	4.45±	40.13±	-	5.82±	10.67±	6.01±	17.31±	-	-	3.3±	1.19±	-
CCMI 1045	0.83	0.24	0.52	2.48		0.27	0.47	0.33	0.84			0.33	0.69	
20 *B. subtilis*	1.57±	0.89±	4.01±	40.09±	-	5.77±	10.73±	5.99±	17.0+	-	-	3.25-	1.92±	-
CCMI 1046	0.26	0.12	0.34	3.10		0.48	0.48	0.56	1.56			0.29	1.08	

i-14:0, 12-methyl tridecanoic acid; 14:0 tetradecanoic acid; i-15:0, 13-methyl tetradecanoic acid; a-15:0, 12-methyl tetradecanoic acid; 15:0, pentadecanoic acid; i-16:0, 14-methyl pentadecanoic acid; 16:0, hexadecanoic acid; i-17:0, 15-methylhexadecanoic acid; a-17:0, 15-methylpentadecanoic acid; 17:0, heptadecanoic acid; 17:1, heptadecenoic acid; 18:0, octadecanoic acid; 18:2ω6, cis-9,12-octadecadecenoic acid; 18:3ω6, 6,9,12-octadecatrienoic acid.

Table 2.2 – i15:0/a15:0 and i17:0/17:0 ratios and the proportions of branched and saturated fatty acids for the *Bacillus* species (mean±STD)

Species	Ratio i15:0 / a15:0	Ratio i17:0 / a17:0	Σ branched fatty acids (%)	Σ saturated fatty acids (%)
B.licheniformis	0.47 ± 0.06	0.62 ± 0.10	85.32 ± 2.89	11.94 ± 1.86
B.pumilus	0.38 ± 0.03	0.63 ± 0.03	74.9 0± 7.54	23.3 2± 4.26
B.subtilis	0.10 ± 0.00	0.35 ± 0.01	76.60 ± 3.01	16.18 ± 1.79

acid in all strains. Table 2.2 displays the i15:0/a15:0 and i17:0/17:0 ratios and the proportions of branched and saturated fatty acids for the *Bacillus* species. The three *Bacillus* species were characterized by different ratios and proportions of the major fatty acids. *B. subtilis* strains showed the lowest i15:0/a15:0 and i17:0/a17:0 ratios (0.10 and 0.35 respectively). *B. licheniformis* strains exhibited the highest proportion of branched fatty acids (85.32 %) and the lowest proportion of saturated fatty acids (11.94 %) whilst *B. pumilus* strains displayed the highest proportion of saturated fatty acids, due to the highest percentage of 16:0 produced by this species (16.3 % – 22.1 %). The i15:0/a15:0 ratio calculated for these *Bacillus* species are not in accordance with those reported by Kämpfer (1994) who assigned 7 groups of *Bacillus* species mainly based on the ratio of i15:0/a15:0. This could be due to the different growth conditions which led to different fatty acid profiles.

The projection of the two PCA axes named PC1 and PC2 (Figure 2.1) described 67.2% (37.7 % + 29.9 %) of the total variance. The clusters were defined based on the presence of fatty acids in a set of strains and the distance between them. Three different groups (A,

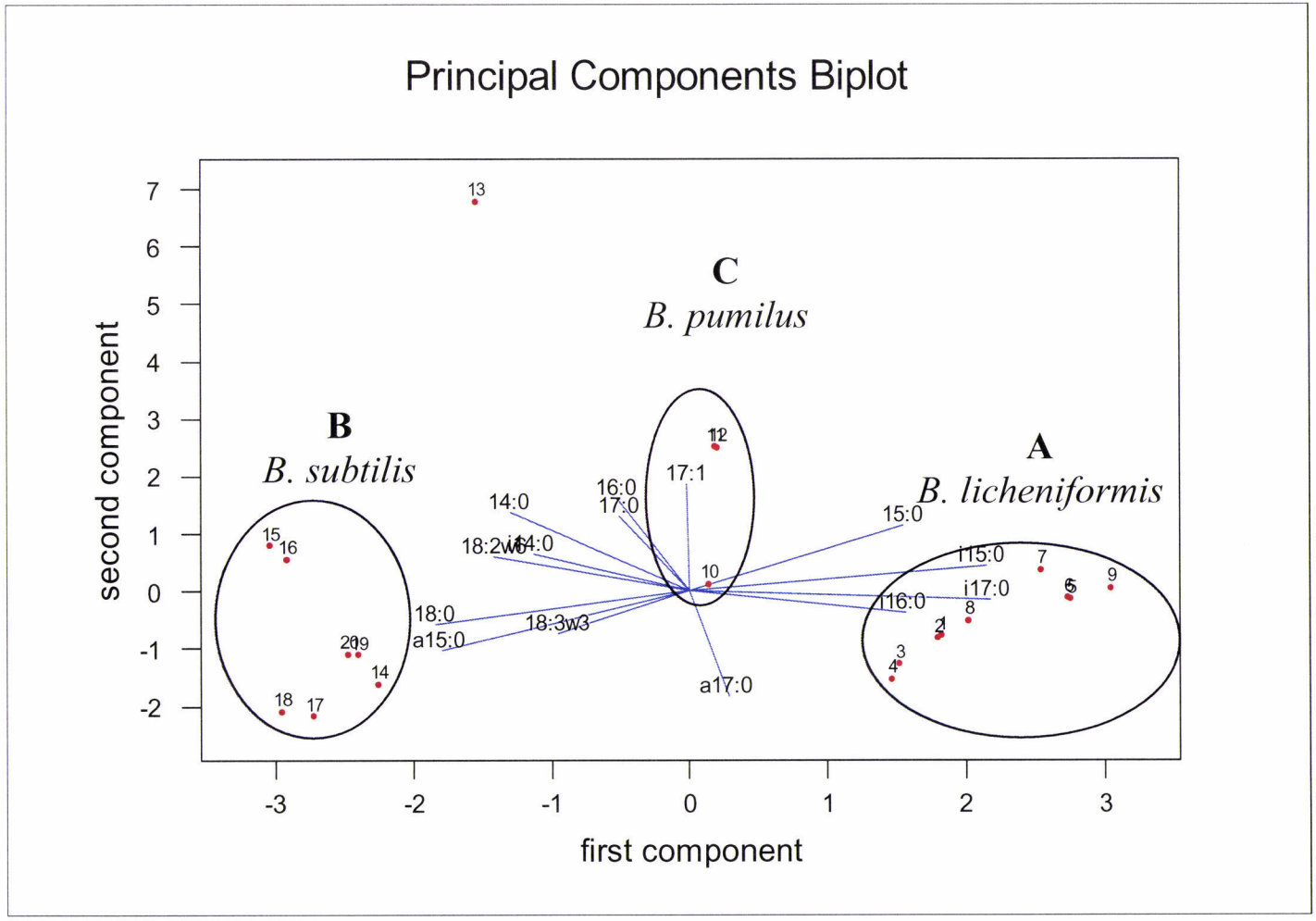

Figure 2.1 – Fatty acids PC1-PC2 plot of all *Bacillus* strains. The variables (fatty acid profiles) are also projected in the same plot (blue lines ending with the fatty acid designation). Strain 1 corresponds to *B. licheniformis* CCMI 232; 2- *B. licheniformis* CCMI 1030; 3- *B. licheniformis* CCMI 1031: 4- *B. licheniformis* CCMI 1032; 5 – *B. licheniformis* CCMI 1033; 6- *B. licheniformis* CCMI 1034; 7 – *B. licheniformis* CCMI 1035; 8 – *B. licheniformis* CCMI 1036; 9 – *B. licheniformis* CCMI 1037; 10 – *B. pumilus* CCMI 692; 11– *B. pumilus* CCMI 1038; 12- *B. pumilus* CCMI 1039; 13- *B. pumilus* CCMI 1040; 14- *B. subtilis* CCMI 225; 15- *B. subtilis* CCMI 1041; 16- *B. subtilis* CCMI 1042; 17- *B. subtilis* CCMI 1043; 18- *B. subtilis* CCMI 1044; 19- *B. subtilis* CCMI 1045; 20- *B. subtilis* CCMI 1046.

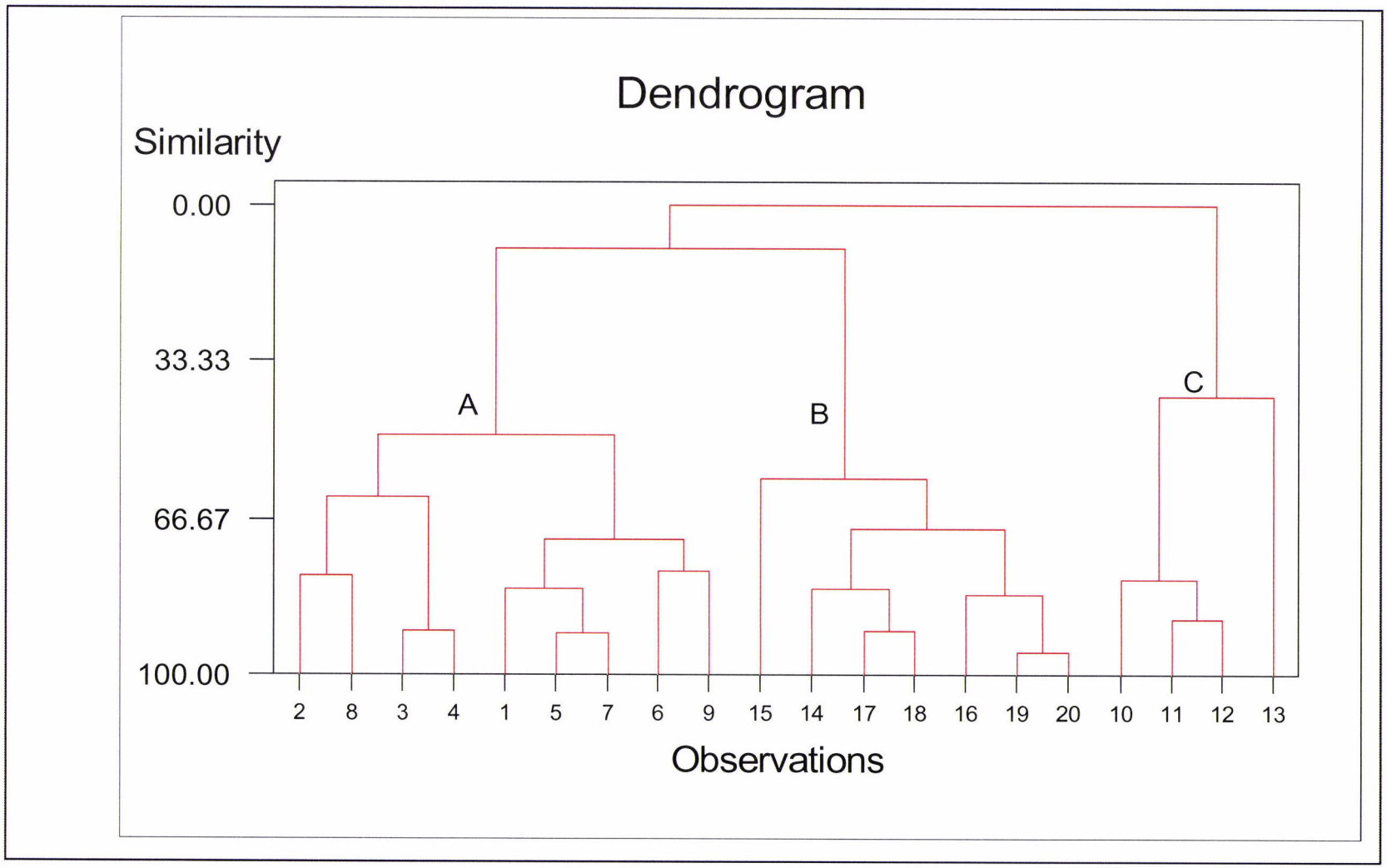

Figure 2.2 - Dendogram of all *Bacillus* strains generated by HCA of the fatty acid profiles showing the three *Bacillus* species The strains numbers are the same as in Figure 2.1.

B and C) could be defined, corresponding to the three *Bacillus* species isolated from Lammas bioreactors. All *B. licheniformis* strains were close and were included in cluster A (Figure 2.1). In fact, this species has been reported as genomically and physiologically homogeneous (Priest et al, 1988a; Kämpfer et al, 1992 and Kämpfer, 1994). From the variables projection (blue lines ending with the fatty acid designation), it can be seen that the strains included in this cluster were characterized by the highest content of i15:0, i16:0 and i17:0 within all the *Bacillus* strains. Cluster B included all *B. subtilis* strains which were characterized by the highest relative amount of a15:0 and 18:0 within all *Bacillus* strains. Strain 15 and 16 (*B. subtilis* CCMI 1041 and *B. subtilis* CCMI 1042, respectively) were slightly apart from the remaining *B. subtilis* strains due to their high proportions of i14:0 and 14:0, but still stayed in the same cluster because displayed high proportions of the fatty acids which characterized this cluster (a15:0 and 18:0). These differences in fatty acid profiles within the *B. subtilis* strains are in accordance with Kämpfer (1994). In a numerical study of fatty acid patterns of 313 *Bacillus* strains, this author reported that although most *B. subtilis* strains were similar in their fatty acids profiles, some strains showed considerable variability and were divided into two subgroups.

Cluster C included strains 10, 11 and 12 (the reference strain *B. pumilus* CCMI 692, *B. pumilus* CCMI 1038, *B. pumilus* CCMI 1039 respectively). The variables projection showed that strain 11 and 12 were characterized by higher proportions of 17:1 comparing with the other *Bacillus* strains. It was also possible to see that strain 13 (*B. pumilus* CCMI 1040) exhibited a different fatty profile from the other *B. pumilus* strains, showing a higher relative amount of 17:0 and the highest content of 16:0 within all *Bacillus* species. As a result, it was located at a distance from the remaining *B. pumilus* strains.

Heterogeneity in fatty acid profiles for *B. pumilus* strains has been reported by Kämpfer (1994) and Väisänen and Salkinoja-Salonen (1989). In a study of the evaluation of the usefulness of fatty acid analysis for *Bacillus* species differentiation, the latter noted two fatty acid biotypes for this species.

Examination of the quantitative fatty acid profiles data by HCA revealed that the 20 *Bacillus* strains could be assigned in three main different groups, A, B and C (Figure 2.2). Group A (*B. licheniformis* strains) and group B (*B. subtilis* strains) showed a level of similarity of 8.89 % between them and were not related to group C (*B. pumilus* strains) (0 % similarity). In fact, Kämpfer (1994) in its study used a numerical analysis of *Bacillus* species fatty acid profiles based on a similarity coefficient, and found that B. *licheniformis* and *B. subtilis* species were related and included in the same cluster, whilst *B. pumilus* was grouped together with other *Bacillus* species. Group C was defined at the similarity level of 40.57 %, whilst groups A and B were defined at the level of similarity of 52.29 % and 56.53 % respectively. Within the species groups, subgroups of strains were found at least at the similarity level of 59.59%. Strains 15 and 16 were not as close as they were in the PCA plot (Figure 2.1). In fact, strain 15 displayed a level of similarity of 56.53 % with the remaining *B. subtilis* strains (including strain 16) which displayed a higher level of similarity between them (68.69 %).

Clearly group C (*B. pumilus* species) displayed the lowest level of similarity between the strains. Strain 13 showed a level of similarity of 40.47 % with other *B. pumilus* strains, which displayed a higher level of similarity between them (80.46 %), indicating that in fact the fatty acid profile of this strain was slightly different from the remaining *B. pumilus* strains. This result was in agreement with the PCA results (Figure 2.1), where

strain 13 was placed far from the *B. pumilus* cluster. Therefore, both numerical analyses highlighted the variability of fatty acid profiles within *B. pumilus* strains.

Wauthoz et al (1995) analyzed cellular fatty acids of 160 strains of *Bacillus*, lactic acid bacteria, Enterobacteriaceae and *Staphylococcus* and the best results of discrimination between species was obtained for the heterogeneous genus *Bacillus*, for which 12 species (23 strains) could be separated into 6 clusters at a similarity level of 79 %. However, *B. licheniformis*, *B. pumilus* and *B. subtilis* strains were grouped in the same cluster. In the present work, these species could be separated at a similarity level at least of 40.57%.

PCA and HCA of *Bacillus* strains fatty acid profiles could differentiate the three B*acillus* species, although some subgroups found within the species were not the same in both numerical analyses.

2.3.2 apiZYM test strips

Table 2.3 shows the constitutive enzyme production by the *Bacillus* strains detected using the apiZYM system. From these results it was observed that each species showed a typical enzymatic pattern. Most *Bacillus* strains displayed positive reaction (reaction intensity color higher than level 3) to esterase C4 (column C), esterase lipase C8 (column D), acid phosphatase (column K) and naphthol-AS-BI-phosphohydrolase (column L). *B. licheniformis* and *B. pumilus* species showed the widest enzyme production (eight enzymes) whilst *B. subtilis* only showed positive reactions to four enzymes. Beyond the

Table 2.3 – Constitutive enzyme production by the *Bacillus* strains detected using the apiZYM system. Enzyme production was assessed on a scale 0 to 5, 0 indicating no enzyme production, and 5 high enzyme production. The substrate is indicated in brackets after the corresponding enzyme.
(**A**) Control, (**B**) Alkaline phosphatase (2-naphthyl phosphate), (**C**) Esterase(C4) (2-naphthyl butyrate), (**D**) Esterase lipase (C8) (2-naphthyl caprylate), (**E**) Lipase (2-naphthyl myristate) (C14), (**F**) Leucine arylamidase (L-leucyl-2-naphthylamide), (**G**) Valine arylamidase (L-valyl-2- naphthylamide), (**H**) Cystine arylamidase (L-cyctyl-2-naphthylamide), (**I**) Trypsin (N-benzoyl-DL-arginine-2-naphthylamide), (**J**) α-chymotrypsin (N-glutaryl-phenylalanine-2-naphthylamide), (**K**) Acid phosphatase (2-naphthyl phosphate), (**L**) Naphthol-AS-BI-phosphohydrolase (Naphthol-AS-BI-phosphate), (**M**) α-galactosidase (6-Br-2-naphthyl-αD-galactopyranoside), (**N**) β-galactosidase (2-naphthyl-βD-galactopyranoside), (**O**) β-glucuronidase (Naphtol-AS-BI-βD-glucuronide), (**P**) α-glucosidase (2-naphthyl-αD-glucopyranosidase), (**Q**) β-glucosidase (6-Br-2-naphthyl-βD-glucopyranoside), (**R**) N-acetil-β-glucosaminidase (1-Naphthyl-N-acetyl-βD-glucosaminide), (**S**) α-mannosidase(6-Br-2-naphthyl-αD-mannopyranoside, (**T**) α-fucosidase (2-naphthyl-αL-fucopyranoside).
Yellow columns - positive reactions of *Bacillus licheniformis* strains; blue columns – positive reactions of *Bacillus pumilus* strains; Red columns – positive reactions of *Bacillus* subtilis strains.

	Enzyme detected in microtube reaction																		
Strain	A	B	C	D	E	F	G	H	I	J	K	L	M	N	O	P	Q	R	S	T
1 *B.lichenformis* CCMI 232	**0**	**0**	**5**	**5**	**0**	**5**	**0**	**0**	**0**	**3**	**3**	**3**	**0**	**1**	**0**	**5**	**0**	**0**	**0**	**0**
2 *B.lichenformis* CCMI 1030	0	0	5	5	0	5	0	0	0	3	3	5	1	3	0	5	0	0	0	0
3 *B.licheniformis* CCMI 1031	0	0	4	5	0	5	0	0	0	3	3	3	0	1	1	5	0	0	0	0
4 *B.lichenformis* CCMI 1032	0	0	4	4	0	3	0	1	1	3	3	3	0	3	0	5	0	0	0	0
5 *B.lichenformis* CCMI 1033	0	0	5	5	0	5	0	0	0	3	3	5	0	3	0	5	0	0	0	0
6 *B.lichenformis* CCMI 1034	0	0	5	5	0	3	0	0	1	2	3	4	0	3	0	5	0	0	0	0
7 *B.lichenformis* CCMI 1035	0	0	4	5	0	4	0	0	0	4	3	3	2	3	0	5	0	0	0	0
8 *B.lichenformis* CCMI 1036	0	0	4	4	0	4	0	0	0	3	3	2	0	3	0	5	0	0	0	0
9 *B.lichenformis* CCMI 1037	0	0	5	5	0	4	0	0	0	2	3	5	0	3	0	5	0	0	0	0
10 *B. pumilus* CCMI 692	**0**	**4**	**5**	**0**	**0**	**3**	**0**	**0**	**0**	**5**	**2**	**3**	**0**	**0**	**0**	**1**	**5**	**1**	**0**	**0**
11 *B. pumilus* CCMI 1038	0	5	5	5	0	3	0	0	0	3	3	3	0	0	0	0	5	0	0	0
12 *B. pumilus* CCMI 1039	0	5	3	3	0	3	0	0	0	3	3	3	0	0	0	0	5	0	0	0
13 *B. pumilus* CCMI 1040	0	4	4	5	0	3	0	0	0	5	2	2	0	0	0	0	4	0	0	0
14 *B. subtilis* CCMI 255	**0**	**0**	**4**	**5**	**0**	**0**	**0**	**0**	**0**	**0**	**2**	**4**	**0**	**0**	**0**	**0**	**0**	**0**	**0**	**0**
15 *B. subtilis* CCMI 1041	0	0	4	5	0	0	0	0	0	0	3	3	0	0	0	0	0	0	0	0
16 *B. subtilis* CCMI 1042	0	0	5	5	0	0	0	0	0	0	2	2	0	0	0	0	0	0	0	0
17 *B. subtilis* CCMI 1043	0	3	4	5	0	2	0	0	0	1	3	3	0	0	0	0	0	0	0	0
18 *B. subtilis* CCMI 1044	0	0	3	4	0	0	0	0	0	0	2	3	0	0	0	0	0	0	0	0
19 *B. subtilis* CCMI 1045	0	0	4	5	0	0	0	0	0	0	3	3	0	0	0	0	0	0	0	0
20 *B. subtilis* CCMI 1046	0	1	4	5	0	0	0	0	0	0	3	3	0	0	0	0	0	0	0	0

four enzymes that were produced by all strains, most *B. licheniformis* strains showed positive reaction to leucine arylamidase (column F), α- chymotrypsin (column J), β-galactosidase (column N) and α-glucosidase (column P). The reactions of maximum intensity (colour reaction higher than 4) were to esterase C4 (column C), esterase lipase C8 (column D) and α-glucosidase (column P). *B. pumilus* strains showed positive reactions to four enzymes [alkaline phosphatase (column B), leucine arylamidase (column F), α-chymotrypsin (column J), and β-glucosidase (column Q)] beyond the four enzymes that were produced by all *Bacillus* strains. The reactions of maximum intensity were alkaline phosphatase (column B) and β-glucosidase (column Q). Most *B. subtilis* strains displayed only positive reactions to four enzymes, those which were produced by all *Bacillus* strains. The maximum intensity reaction was to esterase lipase C8 (column D). *B. subtilis* CCMI 1043 (strain 17) was the only *B. subtilis* strain displaying a positive reaction (level 3) to alkaline phosphatase (column B).

The projection of PC1 and PC2 (Figure 2.3) described 50 % (31.1 + 18.9 %) of the total variance. The clusters were defined based on enzymatic activities detected in a group of strains and the distance between them. Three groups of *Bacillus* strains could be differentiated, corresponding to the *B. licheniformis* strains (cluster A), *B. subtilis* strains (cluster B) and *B. pumilus* strains (cluster C). From the variables projection (the enzymes), it can be seen that *B. licheniformis* strains were mainly characterized by the production of β-galactosidase (variable N) and glucosidase (variable P) which were not produced by the other species. It was observed that although the variables C, K and L (corresponding to esterase C4, acid phosphatase and naphtol-AS-BI-phosphohydrolase respectively) also produced by the other species, directed towards cluster A, indicating

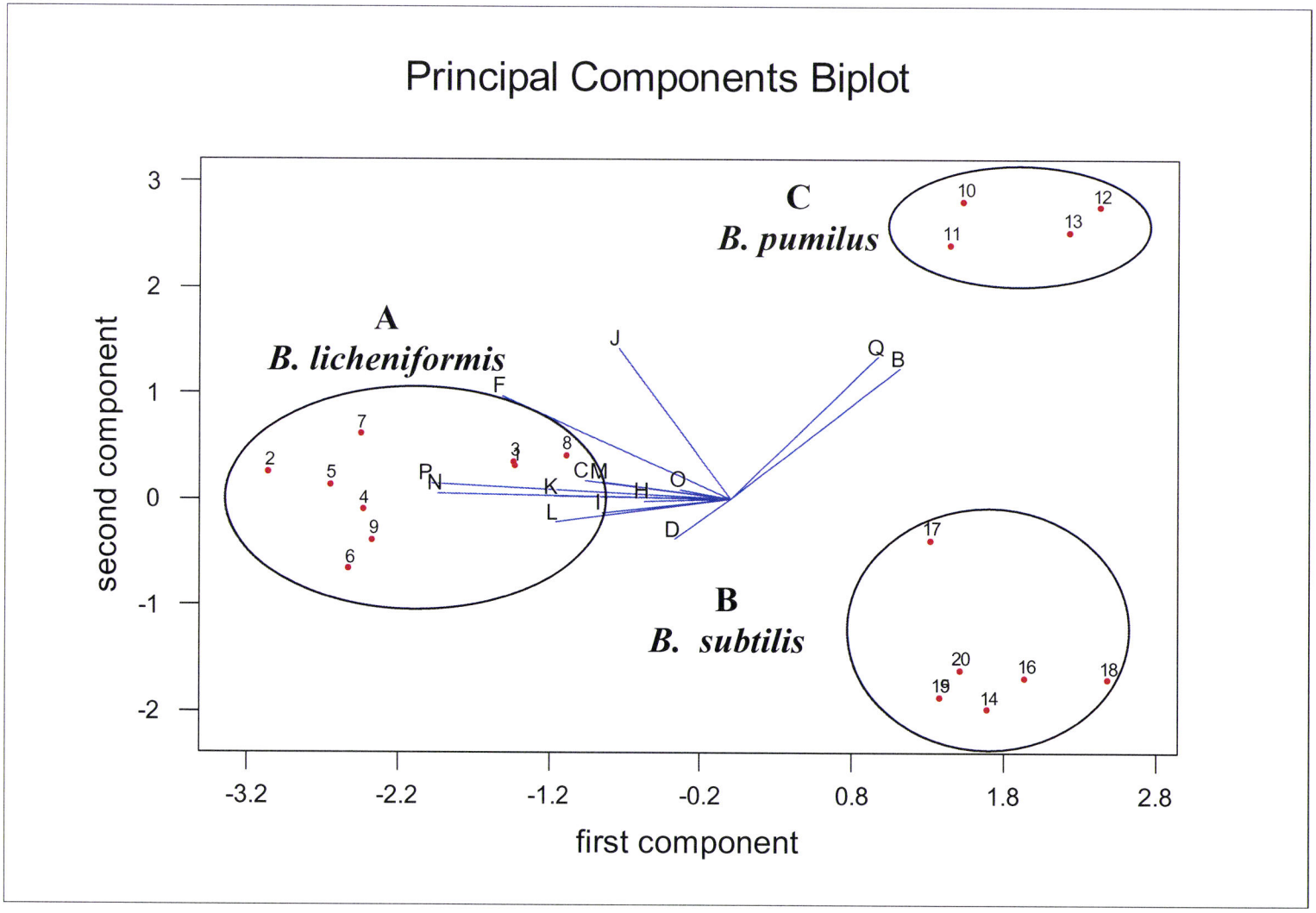

Fugure 2.3 – Enzymatic activities PC1-PC2 plot of all *Bacillus* strains. The variables (enzymes) are also projected in the same plot (blue lines ending with letters – the variables). Strain 1 corresponds to *B. licheniformis* CCMI 232; 2- *B. licheniformis* CCMI 1030; 3- *B. licheniformis* CCMI 1031: 4- *B. licheniformis* CCMI 1032; 5 – *B. licheniformis* CCMI 1033; 6- *B. licheniformis* CCMI 1034; 7 – *B. icheniformis* CCMI 1035; 8 – *B. licheniformis* CCMI 1036; 9 – *B. licheniformis* CCMI 1037; 10 – *B. pumilus* CCMI 692; 11– *B. pumilus* CCMI 1038; 12- *B. pumilus* CCMI 1039; 13- *B. pumilus* CCMI 1040; 14- *B. subtilis* CCMI 225; 15- *B. subtilis* CCMI 1041; 16- *B. subtilis* CCMI 1042; 17- *B. subtilis* CCMI 1043; 18- *B. subtilis* CCMI 1044; 19- *B. subtilis* CCMI 1045; 20- *B. subtilis* CCMI 1046.. The letters correspond to the enzymes designated in Table 2.3.

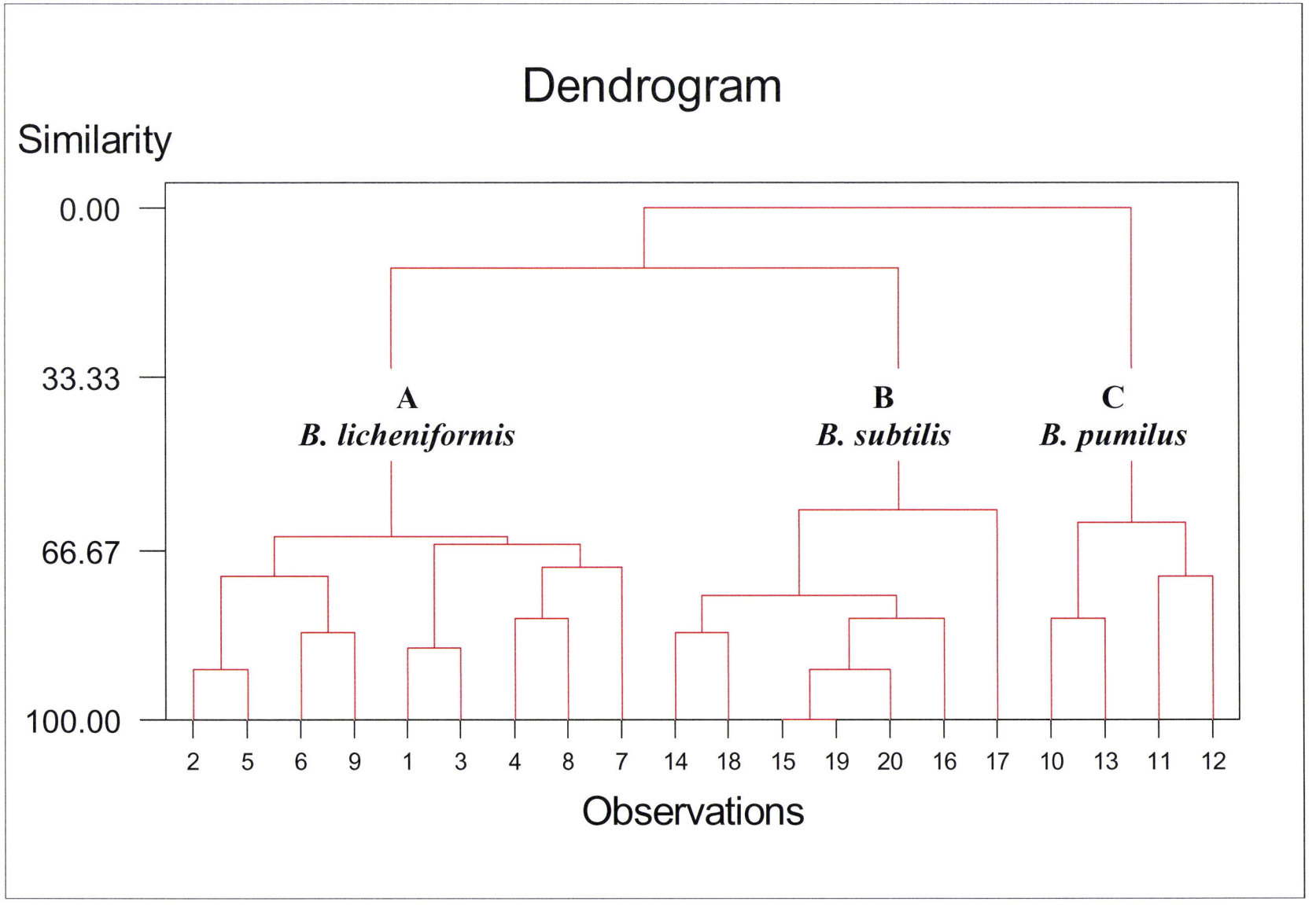

Figure 2.4 - Dendogram generated by HCA of *Bacillus* strains enzymatic activities showing the three *Bacillus* species. The strains numbers are the same as in Figure 2.3.

that the intensity of these enzymatic reactions were stronger in *B. licheniformis* species than in the others. From these results, *B. licheniformis* was considered the species displaying the highest enzymatic production. All strains from cluster B belonged to *B. subtilis* species. These strains produced the enzymes that were detected in the other species, so in this case no typical enzymatic pattern was found for cluster B. However, strain 17 (*B. subtilis* CCMI 1043) was placed slightly distant from the remaining *B. subtilis* strains and close to *B. pumilus* strains cluster because that bacteria produced phosphatase alkaline (variable B) which was not produced by the other *B. subtilis* strains but was produced by *B. pumilus* strains. *B. pumilus* species were characterized by strong reactions to alkaline phosphatase (variable B) and β-glucosidase (variable Q).

Conversely to the fatty acid PCA (Figure 2.1), strain 13 was close to the other *B. pumilus* strains and was included in the same cluster, indicating a higher level of homogeneity within this species, for this phenotypic characteristic.

Examination of the enzymatic activity data by HCA revealed that the 20 *Bacillus* strains could be assigned in three groups, A, B and C, corresponding to *B. licheniformis* strains, *B. subtilis* strains and *B. pumilus* strains respectively (Figure 2.4). Group A and group B showed a similarity of 11.56 % between them and were not related with the group C (0% similarity). Similar relation between the species was found in the fatty acid profiles data (section 2.3.1) although in the present case *B. subtilis* and *B. licheniformis* species displayed a higher level of similarity between them. Group A was defined at the similarity level of 64.12 %, whilst groups B and C were defined at the similarity level of 58.97 % and 61.46 % respectively. Subgroups of strains were formed at the level of similarity at least of 58.97 %. Strain 17 (*B. subtilis* CCMI 1043) showed a level of

similarity of 58.97 % with the remaining *B. subtilis* strains which displayed a level of similarity of 75.63% between them. This result indicated that this strain had an enzymatic activity profile slightly different from the other *B. subtilis* strains, which has been previously shown in the enzymatic activities PCA (Figure 2.3). All species showed a higher level of similarity between the strains, including *B. pumilus* strains, comparing with the fatty acid HCA (Figure 2.2), indicating that the *Bacillus* species were more homogeneous regarding their enzymatic activities than their fatty acid profiles, which showed some variability between the strains, particularly *B. pumilus* species.

Logan and Berkeley (1984) using API systems (50 CHB, 20E and apiZYM tests) and a small number of morphological and supplementary characters, studied a collection of 600 *Bacillus* isolates and produced a system for ready and rapid identification of *Bacillus* strains. A *B. subtilis* group was assigned, where *B. pumilus* and *B. licheniformis* were included. These species were readily separated, despite appreciable within-species variation. Priest et al (1988) in a study of three hundred and sixty-eight *Bacillus* strains based on numerical analysis of phenotypic features could also differentiate *B. licheniformis*, *B. pumilus* and *B. subtilis* strains.

In this work, numerical analyses of the quantitative data obtained by FAMEs and apiZYM analyses was a successful tool for a rapid physiological characterization and differentiation of *Bacillus* species isolated from Lammas bioreactors.

PCA and HAC of enzymatic activities indicated that all *Bacillus* species were more homogeneous regarding these phenotypic characteristic than the fatty acid profiles.

2.4 References

Baillie, A. and Walker, P.D. 1968. Enzymes of thermophilic aerobic sporeforming bacteria. J. Appl. Bact. 31, 114-119.

Bianchi-Salvadori, B. Camaschella, O. and Cislaghi, S. 1995. Rapid enzymatic method for biotyping and control of lactic acid bacteria used in the production of yogurt and some cheeses. Int. J. Food. Microbiol. 27, 253-261.

Gilarová, R., Voldrich, M., Demnerová, K., Cerovsky, M. and Dobiás, K. 1994. Cellular fatty acids analysis in the identification of lactic acid bacteria. Int. J. Food Microbiol. 24, 315-319.

Kämpfer, T., Bark, K., Busse, H. J., Auling, G. and Dott, W. 1992. Numerical and chemotaxonomy of polyphosphate accumulating *Acinobacter* strains with high polyphosphate: AMP phosphotransferse (PPAT) activity. System. Appl. Microbiol. 15, 409-419.

Kämpfer, P. 1994. Limits and possibilities of total fatty acid analysis for classification and identification of *Bacillus* species. System. Appl. Microbiol. 17, 86-98.

Kaneda, T. 1963. Biosynthesis of branched chain fatty acids. I. Isolation and identification of fatty acids from *Bacillus subtilis* (ATCC 7059). J. Biol. Chem. 238, 1222-1228.

Lepage, G. and Roy, C.C. 1986. Direct transesterification of all classes of lipids in a one-step reaction. J. Lipid Res., 27, 114-119.

Logan, N.A. and Berkeley, R.C. 1984. Identification of *Bacillus* strains using the API System. J. Gen. Microbiol. 130, 1871-1882.

Logan, N.A. and Berkeley, C.W. 1984. Identification of strains using the API systems. J. Gen. Microbiol. 130, 1871-1882.

Lopes da Silva, T., Sousa, E., Pereira, P., Ferrão, A. and Roseiro, J.C. 1998. Cellular fatty acid profiles for the differentiation of *Penicillium* species. FEMS Microbiol. Lett. 164, 303-310.

Marumo, K and Aoki, Y. 1990. Discriminant analysis of cellular fatty acids of *Candida* species, *Torulopsis glabrata*, and *Cryptococcus neoformans* determined by gas-liquid chromatography. J. Clin. Microbiol. 28, 1509-1513.

Millar, L. and Berger, T. 1985. Bacteria identification by gas chromatography of whole cell fatty acids. Hewlett-Packard Application Note 228-41. Hewlett-Packard Co., Avondale, Pa.

Mukwaya, G.M. and Welch, D.F. 1989. Subgrouping of *Psedomonas cepacia* by cellular fatty acid composition. J. Clin. Microbiol. 27, 2640-2646.

Priest, F.G., Goodfellow, M. and Todd, C. 1988. A Numerical classification of the genus *Bacillus*. J. Gen. Microbiol. 134, 1847-1882.

Priest, F.G. and Alexander, B. 1988. A frequency matrix for probabilistic identification of some bacilli. J. Gen. Microbiol. 134, 3011-3018.

Saito, K. 1960. Chromatographic studies on bacterial fatty acids. J. Biochem. 47, 699-719.

Sharp, R.J., Bown, K.J. and Atkinson, A. 1980. Phenotypic and genotypic characterization of some thermophilic species of *Bacillus*. J. Gen. Microbiol. 117, 201-210.

Väisäen, O., Salkinoja-Salonen, M. 1989. Use of phage typing and fatty acid analysis for the identification of bacilli from food packaging paper and board machines. System. Appl. Microbiol. 12, 103-111.

Wauthoz, P., Lioui, M. and Decallonne, J. 1995. Gas chromatographic analysis of cellular fatty acids in the identification of foodborne bacteria. J. Food Protect. 58, 1234-1240.

Vishniac, W. and Santer, M. 1957. The Thiobacilli. Bacteriol. Rev. 21, 95-213.

CHAPTER 3

Effect of impeller configuration, aeration and stirring rate on the gas-liquid mass transfer coefficient k_La, under Lammas bioreactors thermophilic conditions

3.1 Introduction

Bioprocesses are often carried out in aqueous medium where the solubility of oxygen is very low and the rate of oxygen utilization by micro-organisms is high. Hence oxygen transfer is often a rate limiting step during the development of the bioprocesses (Krahe et al, 1996; Nienow, 2003). Oxygen transfer rate (OTR) as well as carbon dioxide transfer rate, the gaseous product of metabolism are governed by aeration and stirring conditions which is associated with the power input. Power considerations are quite important and care has to be taken right at an early stage of the process development (Arjunwadkar et al, 1998a).

The standard single-impeller stirred tanks are often criticized for the uneven distribution of shear and energy dissipation which is known to be harmful, especially to the micro-organisms in the bioreactors. For the equivalent power dissipation, impeller speeds will be lower in the case of multiple-impeller systems resulting in lower generation of shear.

Thus, multiple-impeller systems are preferential where shear sensitivity to micro-organisms is an important criteria for design (Gogate et al, 2000). Moreover, the gas-liquid contact is favored by the higher residence time distribution of the gas phase as compared with a single impeller system of the same volume (Arjunkwadkar et al., 1998b).

The types of impellers in the case of multiple-impeller systems have been restricted to Rushton turbines, pitched-blade turbines (downflow or upflow) or various combinations arising from these.

It is commonly believed that at higher temperatures the oxygen transfer rate (OTR) will decrease due to lower oxygen solubility. This is not true since the OTR depends not only on the solubility of the gas but also on the volumetric mass transfer coefficient k_La as shown by equation 1:

$$OTR = k_La\,(C^* - C_L) \qquad (1)$$

where OTR is the oxygen transfer rate, k_La is the gas-liquid mass transfer coefficient for oxygen, k_L is the liquid film mass transfer coefficient, a is the interfacial area of gas-liquid interface, C* is the oxygen concentration in the liquid in equilibrium with the gas phase and C_L is the dissolved oxygen concentration in the liquid phase.

Higbie (1935) postulated the penetration theory, which described the relationship between the liquid film mass transfer coefficient (k_L) and the diffusion coefficient of the gas in water ($\mathcal{D}$) (equation 2):

$$k_L \propto \mathcal{D} \qquad (2)$$

Since the diffusion coefficient for gases in liquids increases with temperature (Perry and Green, 1984), the mass transfer resistance due to the boundary layer of the liquid is smaller at higher temperatures. Krahe et al (1996) demonstrated that the oxygen availability in the medium is the same or even better at elevated temperatures. The temperature effect on the liquid film mass transfer coefficient k_L was also studied by Suresh et al. (1988), who found that the variation of diffusivity was brought about by the change of temperature (18 °C ~ 163 °C). The authors claimed that the variation of diffusivity affects the value of k_L, the effect being larger than those due to the changes in viscosity, surface tension and density.

The oxygen requirement in aerobic processes is vital. The shortage of this nutrient affects drastically the bioprocess efficiency. Although the OTR under thermophilic temperatures range should be the same or even higher than within mesophilic temperatures range, the high chemical oxygen demand (COD) loads found in waste streams requires special attention. Optimization of agitation and aeration conditions in an industrial scale bioreactor is not feasible and is usually done on laboratory scale. The aim of this work was to study the effect of single and dual impeller configurations, the aeration and the stirring rate on the gas-liquid mass transfer coefficient, at the working temperature range of Lammas bioreactors (45-60 °C), using a bench fermenter. The optimal configuration was then used in further continuous cultures experiments carried out in this fermenter.

3.2 Materials and Methods

3.2.1 Power measurements

A particular agitator dissipates power at a rate that is dependent on its type. Each type is characterized by the power number, N_P, which is a dimensionless quantity. Power (P) and power numbers are related to impeller size D and speed N by the equation

$$P = N_P \cdot \rho_L \cdot N^3 \cdot D^5 \qquad (3)$$

where ρ_L is the liquid density. Power is also related to torque M by the relationship

$$P = 2\pi \cdot N \cdot M \qquad (4)$$

The torque, the power and the speed are determined by the motor, drive, gear box and other characteristics, and on large scale fermenters their cost may be significant. The power number in turbulent flow does not depend on the Reynolds number, Re, the ratio of inertial to viscous forces, defined for Newtonian fluids as

$$Re = \frac{\rho_L \cdot N \cdot D^2}{\mu} \qquad (5)$$

where μ is the viscosity.

The pumping capacity of an impeller is characterized by its flow number, Fl, which is also a dimensionless quantity and is related to the gas flow rate Q_g, impeller size D and speed N by the equation

$$Fl = \frac{Q_g}{ND^3} \tag{6}$$

All experiments were carried out in a LSL (Life Science Laboratories, Ltd, UK) cylindro-conical 2L stirred-tank bioreactor. The vessel was fitted with two equally spaced baffles. Liquid height was 125.97 mm and liquid volume was 770 ml (Figure 3.1), equipped with two different impeller types: Three blade 45 ° "elephant ear" pitched impeller pumping down (PB3) with diameter equal to 50.53 mm, and a conventional four blade Rushton impeller (RT4) with diameter equal to 44.35 mm (Figure 3.2). Heating was supplied through the water jacket of the vessel. Different impeller combinations employed in this study were PB3-RT4, RT4-PB3, RT4-RT4, RT and PB3 where the first impeller indicates the lower impeller and the second is the top impeller. The distance between the impellers was chosen so that each impeller generated its own circulation pattern which occurs when the distance between the impellers is approximately 1.2·(impellers diameters average) (Doran, 1999). The gas flow rate and impeller speed varied in the range 1-3 vvm and the speed rate was studied at 1000 and 1500 rpm. The gas was sparged through a pipe sparger. For power input calculations, the torque exerted by the impellers was measured using a VISCO-MIX (Coesfeld Messtechnik GmbH, Dortmund, Germany) and the

friction losses were taken care of by measuring the power consumption for air only.

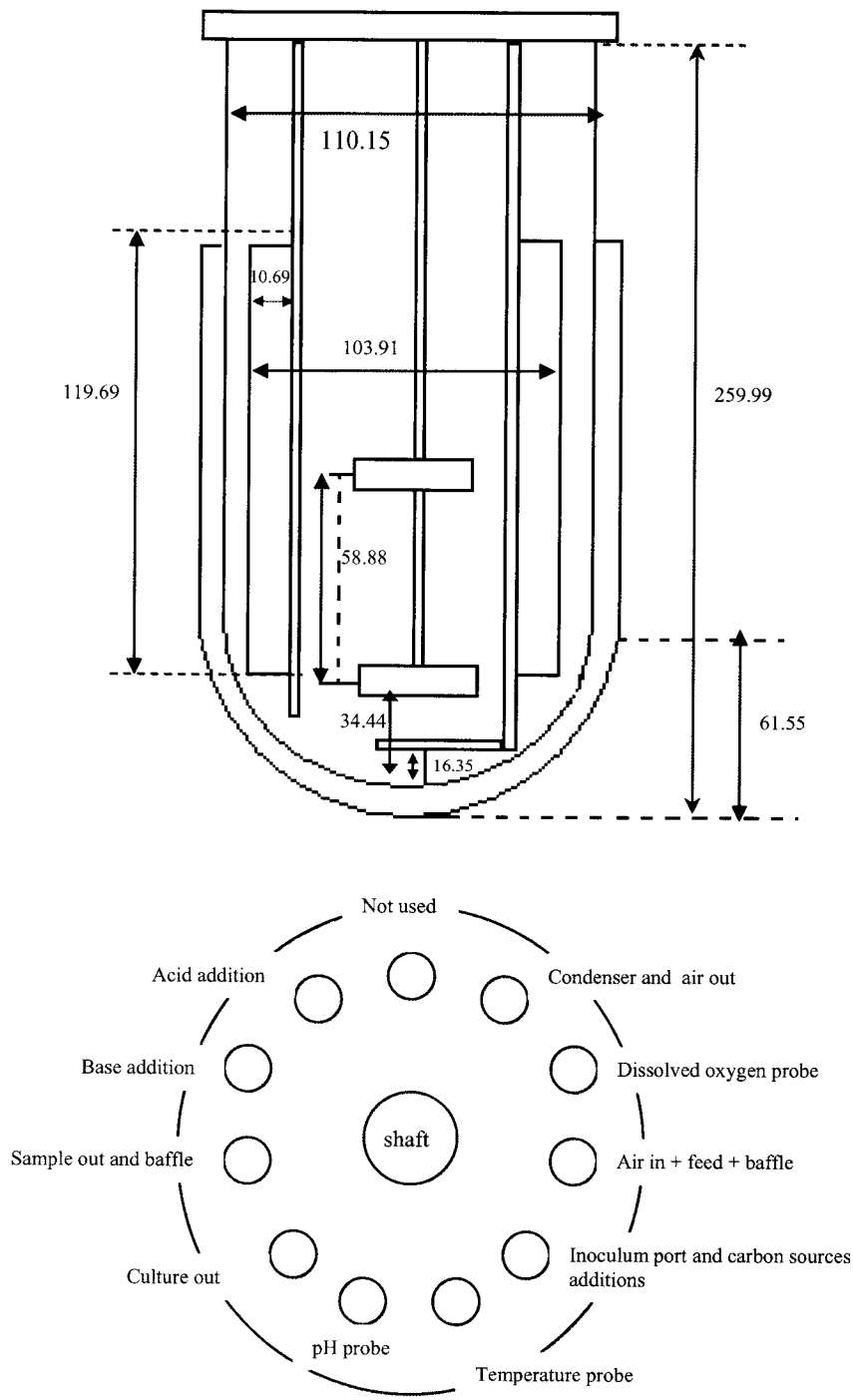

Figure 3.1 The LSL 2L vessel (dimensions in mm) and its top plate with the probe insertions points.

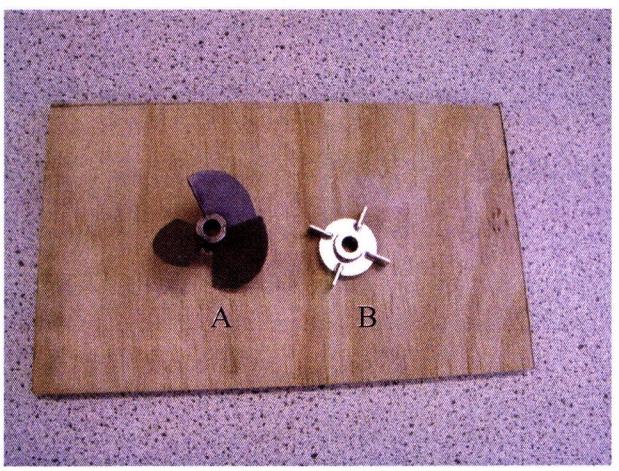

Figure 3.2 Three blade 45 ° elephant ear pitched impeller pumping down PB3 (A) and Rushton turbine four blade RT4 (B).

3.3.2 k_La measurements

The oxygen concentration in the liquid phase was measured using a polarographic probe (Ingold, USA). The gas-liquid mass transfer coefficient (k_La) was calculated by measuring the rate of oxygen transfer in nitrogen purged tap water (Sobotka et al, 1982). A typical response curve for oxygen concentration against time is shown in Figure 3.3. The k_La was calculated from the oxygen balance equation in transient state:

$$\frac{dC_L}{dt} = k_La\ (C^*\text{-}C_L) \qquad (7)$$

where C* is the oxygen saturation concentration and C_L is the dissolved oxygen concentration in the liquid. Separation of variables leads to the following equation:

$$\frac{dC_L}{(C^*-C_L)} = k_La \,.\, dt \qquad (8)$$

Assuming k_La constant with time, the integration of Equation (8) between the starting time of air sparging t=0 and t, corresponding to the initial dissolved oxygen concentration C_i and the dissolved oxygen concentration at time t, C_L, respectively, gives:

$$\int_{C_i}^{C_L} \frac{dC_L}{C^* - C_L} = k_La \int_0^t dt \qquad (9)$$

The resulting equation is:

$$\ln\left(\frac{C^* - C}{C^* - C_i}\right) = -k_La.\, t \qquad (10)$$

According to Equation (10), the slope of the straight line representing the left-hand member against time is equal to $-k_La$. The k_La was measured for all the different impeller configurations. For each impeller configuration, 4 temperatures were tested and, for each temperature, 3 volumetric flow rates (1vvm, 2vvm and 3 vvm) were tested at stirring rate values of 1000 and 1500 rpm. In order to obtain accurate experimental data, triplicate measurements were carried out and standard deviations were calculated. The data acquisition was made using LABVIEW software (Vernier Software & Technology, Beaverton, USA).

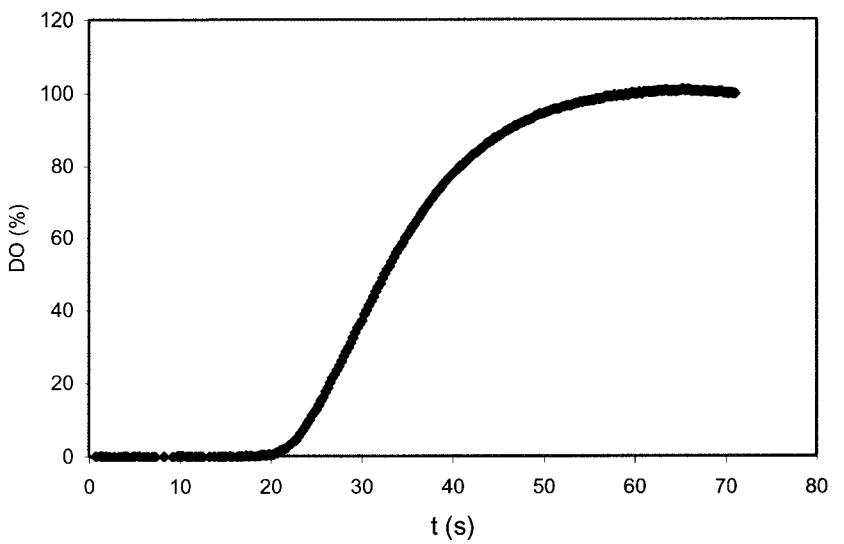

Figure 3.3 Response curve for oxygen concentration against time.

3.3 Results and Discussion

3.2.1 Impeller characterization

Power number Np is independent of Reynolds number (Re) in turbulent flow which means that Np should be constant for $Re>10^4$. Figure 3.4 shows the correlation between power number Np and Reynolds number Re for the RT4 and PB3 impellers without sparging. It can be seen that Np for the RT4 and PB3 impellers is approximately constant

between Re=12 000 and Re=30 000. Above Re=30 000 both impellers N_P decreased, indicating that surface aeration was occurring. Surface aeration takes place whenever gas is engulfed in the upper part of the vessel by the liquid and it depends on the stirring speed. At high stirring rates, the gas is entrained into the liquid after the liquid surface has been broken. As a result, the density falls leading to a decrease of the unaerated power P and N_P ((Sverak and Hrubý, 1981; Lee and Foster, 1990). In aerobic processes, the surface aeration is an additional oxygen supply (Vasconcelos, 1993)

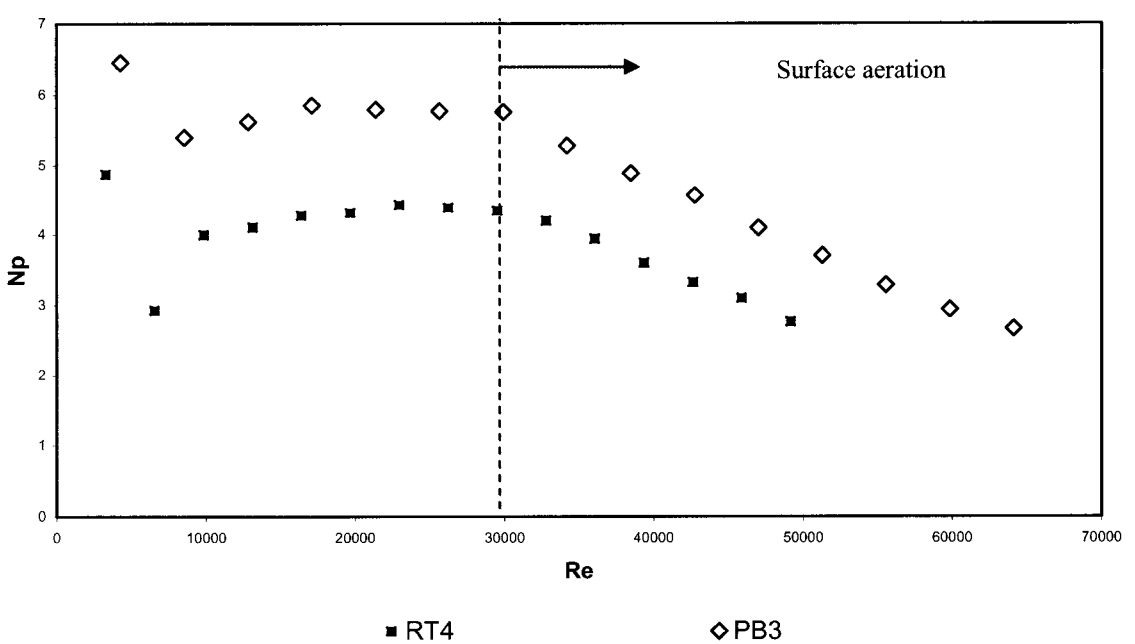

Figure 3.4 Correlation between power number for RT4 and PB3 impellers without sparging.

3.3.2 Power consumption

Single and dual impeller systems were used. Analysis of the dissipated power in the presence of gas is usually carried out in terms of the power ratio P_g/P vs gas flow number Fl (either at constant gas flow rate Q_g or at constant speed N). Thus the relative power inputs P_g/P were measured for each configuration and plotted against Fl. Figure 3.5 shows the characteristic behavior of such diagram for different combinations (at constant Q_g). It is well known that the impellers work in different regimes, so cavities formed behind the impeller blades are different because of different quantities of gas received. Flooding occurs when the stirrer speed is too low to handle the gas supply and it is characterized by the ceasing of gas recirculation in the region below the impeller. The loaded regime is usually defined by the conditions in which the gas is dispersed throughout the liquid in the whole vessel. Finally, the complete dispersion is characterized by gross gas recirculation patterns established in the contactor, thus enhancing the quality of the mixing process (Bouaifi and Roustan, 2001; Markopoulos et al, 2002). It can be seen from Figure 3.5 that the gas flow number is high for lower impellers speed, which causes flooding and loading, where the relative power input is also lower for the PB3, RT4-PB3 and PB3-RT4 configurations. As the impeller speed increases, the operational regime changes to dispersion or re-circulation. Therefore, the bubbles are dragged in the down flow region of the agitator.

RT4 and RT4-RT4 configurations displayed the largest fall in the P_g/P ratio for low Q_g/ND^3 values, as a result of a power drawn reduction when the impeller was gassed. The

single impeller configuration (RT4) exhibited the lowest P_g/P ratio. PB3, RT4-PB3, PB3-RT4 P_g/P ratios showed a slight fall for low Q_g/ND^3 values, but the difference in power drawn between the ungassed and the gassed states was much lower than the one with single and dual Rushton configurations.

Figure 3.6 shows the plot of power ratio against the gas flow number Fl. Again, the single and dual Rushton turbines showed the lowest P_g/P ratio. In fact, it has been reported that the Rushton turbines show a large fall in the power drawn by the impeller when gassed, which can result up to 50 % of the ungassed power at moderate gassing rates. The power drop is due to the formation of gas filled cavities behind the impeller blades (Arjunwadkar et al., 1998a; Hari-Prajitno et al, 1998; Bouaifi and Roustan, 2001). Van't Riet (1975) stated that the formation of large cavities in Rushton turbines produces stepwise decreases in power consumption: each successive large cavity corresponding to a certain drop in power demand. A flat gassed power curve is desirable because it ensures that the energy input to the fluid remains constant whilst aerated, with no loss of gas handling or dispersing ability through a power reduction (Benz, 2003). In this case, PB3-RT4, RT4-PB3 and PB3 combination showed flatter gassed power curves.

Arjunwadkar et al (1998a) in a similar study found that the impeller combination that provided higher gas hold-up was a radial flow impeller mounted below the axial flow impeller. The radial flow impellers breaks up the gas bubbles effectively while the upper impeller ensures circulation and bulk mixing of the vessel contents. This impeller configuration works especially well for non-coalescing system, resulting in uniform dissolved oxygen concentration.

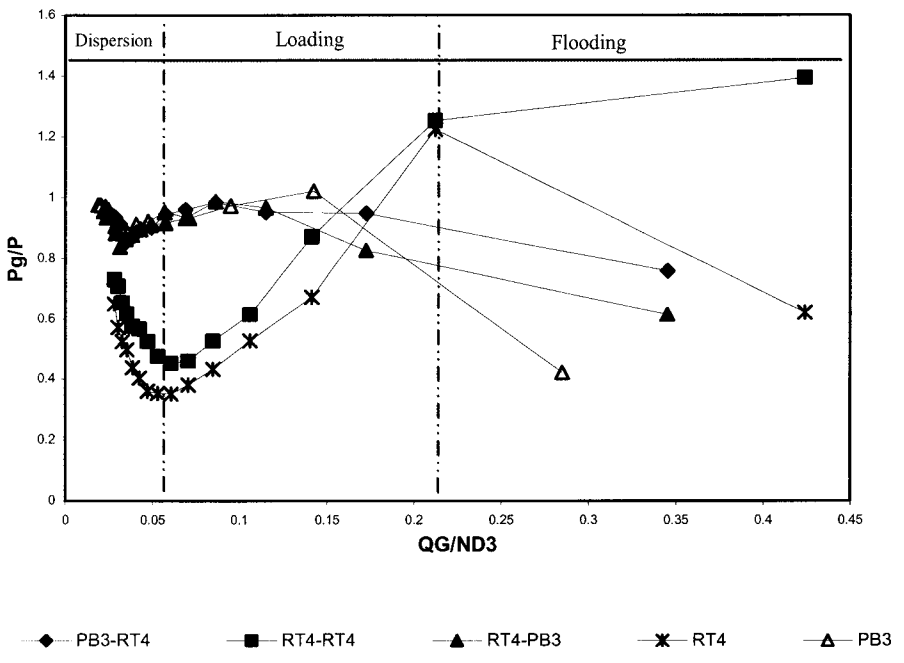

Figure 3.5 Relative power input against gas flow number for different impellers combinations, for air-water system, at 3 vvm and variable N.

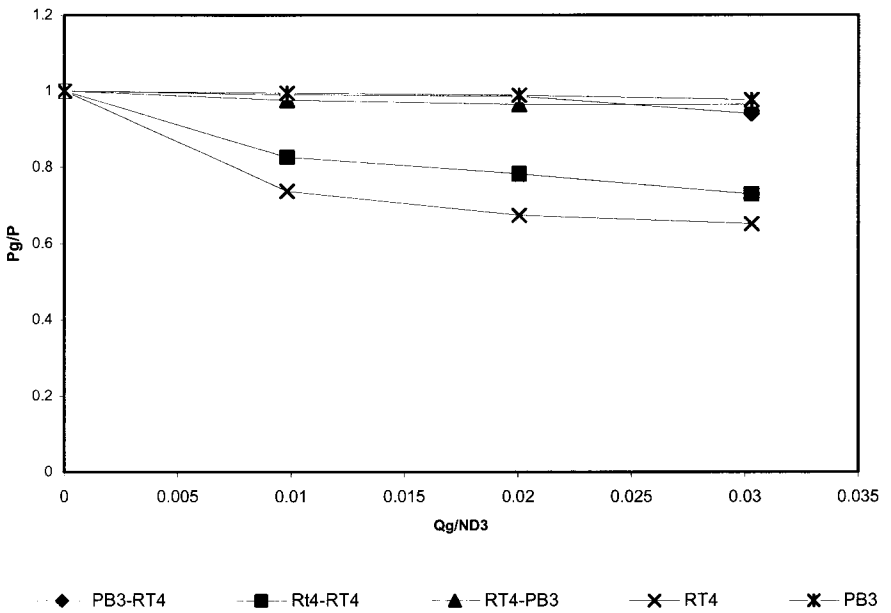

Figure 3.6 Relative power input against gas flow number for different impellers combinations, for air-water system, at constant rpm (N=1450 rpm) and variable Q_G.

3.3.3 k_La measurements

In mechanically agitated continuously stirred tank reactors, the impeller is the main dispersing device and will naturally have a profound effect on the mass transfer characteristics of the system. Figure 3.7 shows the effect of the speed rate, gas flow rate and impeller configuration on the k_La at different temperatures.

Panja and Phaneswara Rao (1991) studied the effect of temperature on k_La at temperatures of 18 and 45 °C at constant gas flow rate and various stirring rates and

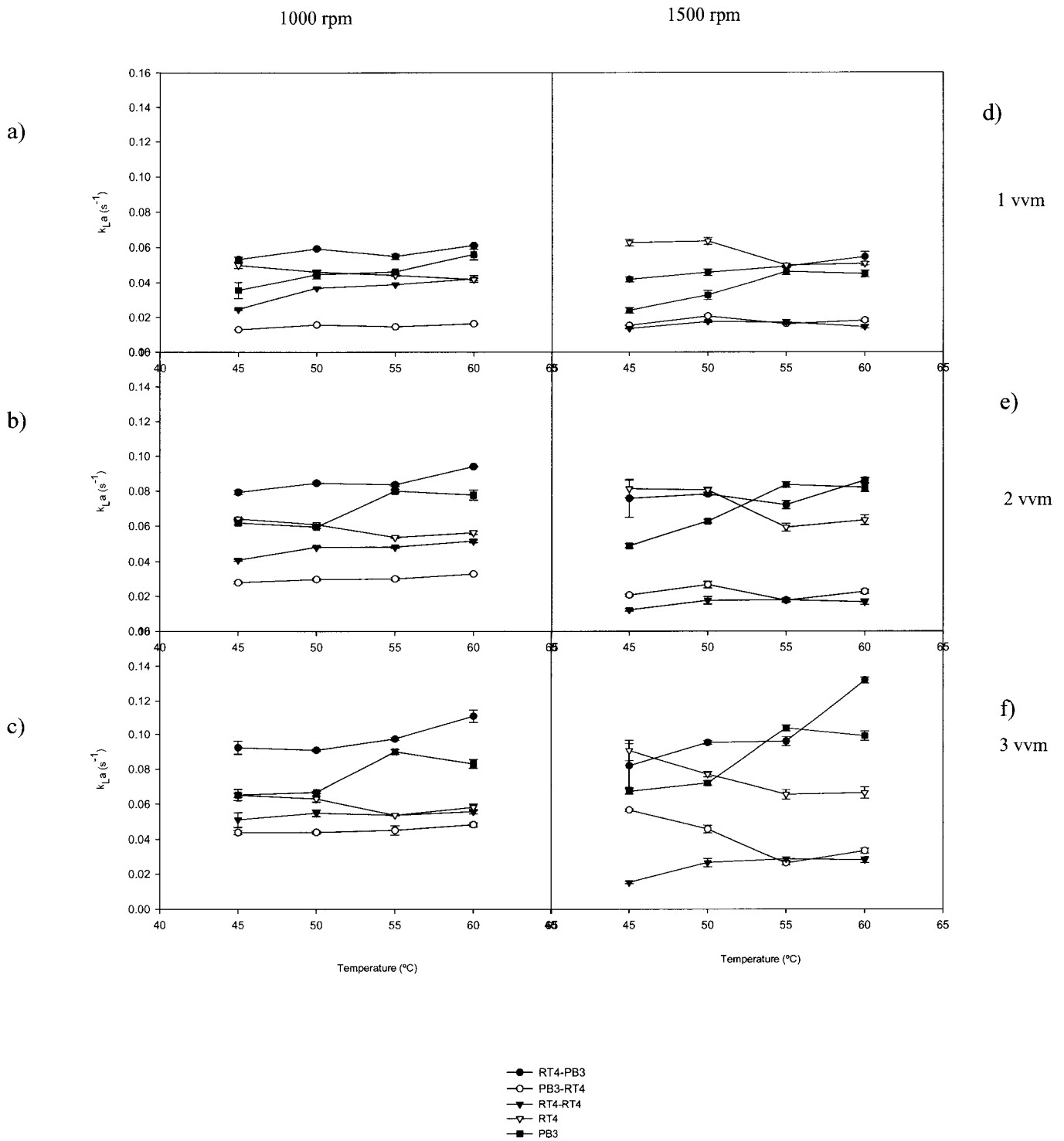

Figure 3.7 Effect of the temperature, gas flow rate and speed rate on the gas-liquid mass transfer coefficient, k_La for different single and dual impeller configurations.

(a) 1000 rpm, 1 vvm; (b) 1000 rpm, 2 vvm; (c) 1000 rpm, 3 vvm;

(d) 1500 rpm, 1 vvm; (e) 1500 rpm, 2 vvm; (f) 1500 rpm, 3 vvm.

stated that k_La increased by about 17-21 % for every 10 °C rise in temperature. Yonggang Zhu and Jie Wu (2002) reported an increase of k_La with the temperature between 20 °C and 60 °C, but the k_La increase rate was dependent on the air flow rate. In this case, for each set of k_La values obtained at fixed conditions (speed rate and gas flow rate), the k_La seemed not to have changed with the temperature increase.

The maximum k_La value was obtained for the RT4-PB3 configuration, at 60 °C, 1500 rpm, 3 vvm (0.14 s^{-1}). RT4-PB3 combination showed the best performance at 1000 rpm, 1 vvm, 2 vvm and 3 vvm and at 1500 rpm, 1 vvm at 60 °C, and 3 vvm at 50 °C and 60 °C. This combination also displayed the highest specific power input for 1000 and 1500 rpm (Table 3.1), indicating that the system was dispersing effectively the gas in the liquid. Single RT4 followed the RT4-PB3 in mass transfer efficiency, showing the highest k_La values at 1500 rpm, 1 and 2 vvm (45 °C and 50 °C) and at 1500 rpm, 3 vvm, (45 °C) associated with the lowest specific power input (Table 3.1). Conversely, the single PB3 combination showed less mass transfer efficiency by displaying lower k_La values when compared with RT4 and RT4-PB3 configurations. RT4-RT4 and PB3-RT4 combinations exhibited the lowest k_La values for the studied conditions. Between them, RT4-RT4 combination displayed higher *kLa* values at 1000 rpm for lower specific power input.

Arjunwadkar et al (1998b) studied the effect of impellers configuration on the k_La and also found that the best combination among dual disc turbine-pitched blade turbine upflow and downflow combinations that exhibited highest k_La values for the same power input, was the disc turbine-pitched blade configuration.

The highest k_La value obtained at 45 °C, 1500 rpm and 3 vvm (the working conditions used in the further experiments) was obtained with the RT4 impeller (0.096 s^{-1}) followed

by the RT4-PB3 combination (0.084 s^{-1}). However, single-impeller stirred tanks are criticized for the uneven distribution of shear and energy dissipation, which are known to affect microbial cultures. The highest k_La values displayed in most of the experiments by RT4-PB3 configuration, associated with the flatness of its gassed power curve, made this combination the most appropriate for microbial aerobic processes. Therefore this configuration was used in further continuous cultures experiments carried out in this fermenter.

Table 3.1 – Specific power input for the studied impeller configurations.

Speed rate (rpm)	Flow rate (vvm)	P/V (KWm^{-3})				
		RT4-PB3	PB3-RT4	RT4-RT4	RT4	PB3
1000	1	10.18	6.45	3.79	2.14	8.80
	2	9.41	6.43	3.49	1.93	8.52
	3	9.00	6.36	3.27	1.74	8.31
1500	1	20.73	13.01	11.28	7.12	17.94
	2	20.62	12.92	10.69	6.51	17.84
	3	19.69	12.95	10.00	6.27	17.64

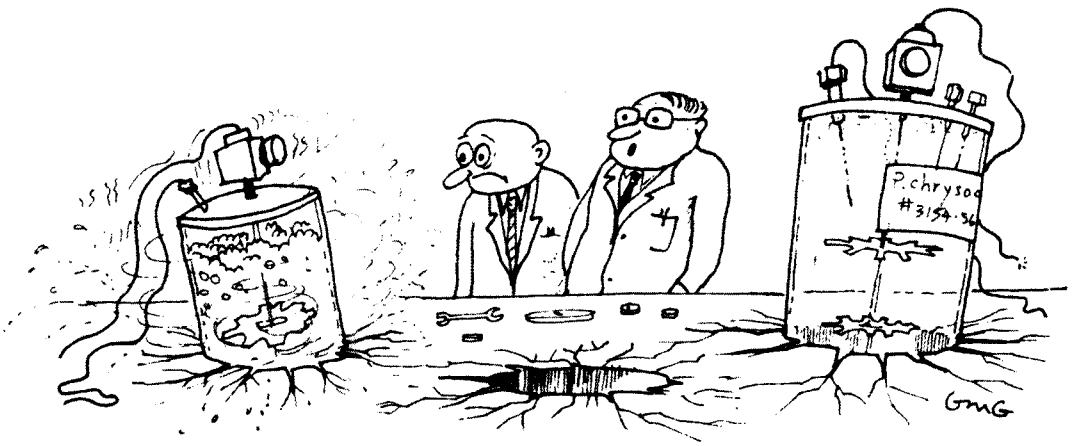

"Are you sure the blades are fitted correctly, Wilkins? That's the third fermenter you've drilled into the bench in a month!"

Nienow, A.W. 1990. Agitators for mycelial fermentations. TIBTECH 8, 224-283

3.4 References

Arjunwadkar, S.J., Saravann, K., Pandit, A.B. and Kulkarni, P.R. 1998a. Optimizing the impeller combination for maximum hold-up with minimum power consumption. Biochem. Eng. J. 1, 25-30.

Arjunwadkar, S.J., Saravann, K., Pandit, A.B. and Kulkarni, P.R. 1998b. Gas-liquid mass transfer in dual impeller bioreactor. Biochem. Eng. J. 1, 99-100.

Benz, G. 2003. Optimizing power consumption in aerobic fermenters. www.cepmagazine.org.

Bouaifi, M. and Roustan, M. 2001. Power consumption, mixing time and homogenization energy in dual-impeller agitated gas-liquid reactors. Chem. Eng. Proc. 40, 87-95.

Doran, P. 1999. Bioprocess Engineering Principles. Academic Press, London pp.155-156.

Gogate, P.R., Beenackers, A.C.M. and Pandit, A.B. 2000. Multiple-impellers systems with a special emphasis on bioreactors: a critical review. Biochem. Eng. J. 6, 109-144.

Hari-Prajitno, D., Mishra, V.P., Takenaja, K., Bujalski, W., Nienow, A.W. and McKemmie, J. 1998. Gas-liquid mixing studies with multiple up- and down-pumping hydrofoil impellers: power characteristics and mixing time. Can. J. Chem. Eng. 76, 1056-1068.

Higbie, R. 1935. The rate of absorption of pure gas into still liquid during short periods of exposure. Trans. Al. Chem. Eng. 31, 365-389.

Krahe M., Antranikian, G. and Märkl, H. 1996. Fermentation of extremophilic micro-organisms. FEMS Microbiol. Rev. 18, 271-285.

Lee, J.H. and Foster, N.R. 1990. Measurements of gas-liquid mass transfer in multi-phase reactors. Appl. Catalysis 63, 1-26.

Markopoulos, J., Paras, S.V. and Babalona, E. 2002. Dispersion characteristics of gas-liquid contactors agitated by single and double-stage Rushton turbines. Chem. Eng. Technol. 25, 163-166.

Nienow, A.W. 1990. Agitators for mycelial fermentations. TIBTECH 8, 224-283.

Nienow, A.W. 2003. Biotechnology. In: Kirk-Othmer Encyclopedia of Chemical Technology, 5th Ed, John Wiley & Sons, Inc., New York, NY.

Panja, N.C. and Phaneswara Rao, D. 1991. Experimental studies on k_La in a mechanically agitator contactor from transient electrical conductivity response data. Trans. I. Chem. E. 69 (partA), 302-307.

Perry and Green. 1984. Perry's Chemical Engineers' Handbook, Mc Graw-Hill, New york, pp(3-101)-(3-103).

Sobotka, M., Prokop, A., Dunn, I.J. and Einsele, A. 1982. Review of methods for the measurement of oxygen transfer in microbial systems. Annual reports on fermentation processes. Academic Press , London, 5 pp. 127-210.

Suresh, A.K., Sridhar, T. and Potter, O.E. 1988. Mass-transfer and solubility in autocatalytic oxidation of cyclohexane. AICHE J. 34, 55-68.

Sverak, S. and Hrubý, M. 1981. Gas entrainment from the liquid surface of vessels with mechanical agitators. Int. Chem. Eng. 21, 519-526.

Van't Riet, K. 1975. Turbine agitator hydrodynamics and dispersion performance", PhD thesis, Delf University of Technology, The Netherlands.

Vasconcelos, J.M.T. 1993. Estudos de fenómenos de transferência em tanques arejados com agitação por andares. PhD thesis, Instituto Superior Técnico, Universidade Técnica de Lisboa.

Zhu, Y and Wu, Jie. 2002. Gas-liquid mass transfer in hot sparged systems. 9th APCChE Congress and 30th Chemeca Conference, New Zeeland.

CHAPTER 4

Stress-induced physiological responses to carbon source pulses in *Bacillus licheniformis* CCMI 1034

4.1. Introduction

Many commercially important bio-processes (product formation or biodegradation) use complex ill-defined culture media, where both simultaneous and polyauxic utilization of multiple substrates highlight the problems associated with sequential growth (Baloo and Ramkrishna, 1991; Venkatesh et al., 1997; Doshi et al, 1997; Doshi and Venkatesh, 1998). In most waste treatment systems, microbial growth occurs in a multisubstrate environment, exhibiting a variety of behavior ranging from simultaneous to sequential utilization of substrates. The diauxic substrate removal by activated sludge has been described in literature (Gaudy, 1962; Kompala et al, 1984). Detailed information on bacterial population dynamics within such systems becomes of particular importance since a high number of dead or dormant cells present during any part of a process will have an obvious detrimental effect on the synthesis of a desired product or on biodegradation process efficiency. Thus, feeds can be optimized, so that process efficiency is improved.

Bacillus spp. are the dominant organisms present in thermophilic aerobic organic waste treatment reactors (LaPara, 1999). Kosseva et al (2003) reported a two-stage strategy for the bioremediation of cheese whey using a thermophilic mixed population of *Bacillus* spp. that was able to degrade lactose, organic acids and ethanol in the second stage, producing CO_2 and biomass.

The present chapter describes the physiological response of a *Bacillus* strain isolated from Lammas bioreactors maintained in a glucose limited steady-state, which was perturbed by glucose and lactose pulses (carbon sources frequently found in industrial growth media and food waste streams). The strain *Bacillus licheniformis* CCMI 1034 was selected among the seven *Bacillus licheniformis* strains isolated from the Lammas bioreactors which showed positive reactions to β-galactosidase (Table 2.3), an enzyme required for lactose consumption. Among these seven strains, *Bacillus licheniformis* CCMI 1034 displayed the highest lactose uptake volumetric rate in a preliminary lactose degradation screening test (Appendix 3).

The effect of each carbon source pulse on the physiology of the individual micro-organism was monitored by multi-parameter flow cytometry and comparison made. The starvation period that followed the carbon pulse exhaustion was also monitored, in order to evaluate the physiological response of the micro-organism to carbon starvation.

4.2 Materials and methods

4.2.1 Organism

Bacillus licheniformis CCMI 1034 was maintained in glass beads using glycerol as cryoprotectant at -72 °C.

4.2.2. Bioreactor Experiments

Six nutrient agar plates grown for 24 hours at 45°C were transferred to the growth medium (GM) which was made up as follows: glucose 2.00 gl^{-1}; KH_2PO_4 1.00 gl^{-1}; $(NH_4)_2SO_4$ 1.50 gl^{-1}; yeast extract 0.10 gl^{-1}; $CaCl_2.2H_2O$ 0.10 gl^{-1}; $MgCl_2.7H_2O$ 0.25 gl^{-1} and supplemented with 2 ml of trace elements solution (Vishniac and Santer, 1957), to inoculate the fermenter. After a period of batch culture, a pump was used to feed sterile medium into the fermenter at a dilution rate of 0.27 h^{-1} with the GM. Glucose-limited steady-state parameters were determined by periodic analysis of optical density, residual glucose concentration and off-gas analysis (CO_2 produced and O_2 consumed).

All experiments were carried out in the cylindro-conical 2L continuously stirred-tank bioreactor described in section 3.2.1. The working volume was kept constant by using a levelled tube linked to a variable speed peristaltic pump. Culture agitation was set at 1500 rpm and the aeration rate at 3.0 vvm. Such a high agitation rate was used to ensure oxygen-sufficient conditions because DO measurements were impossible as the

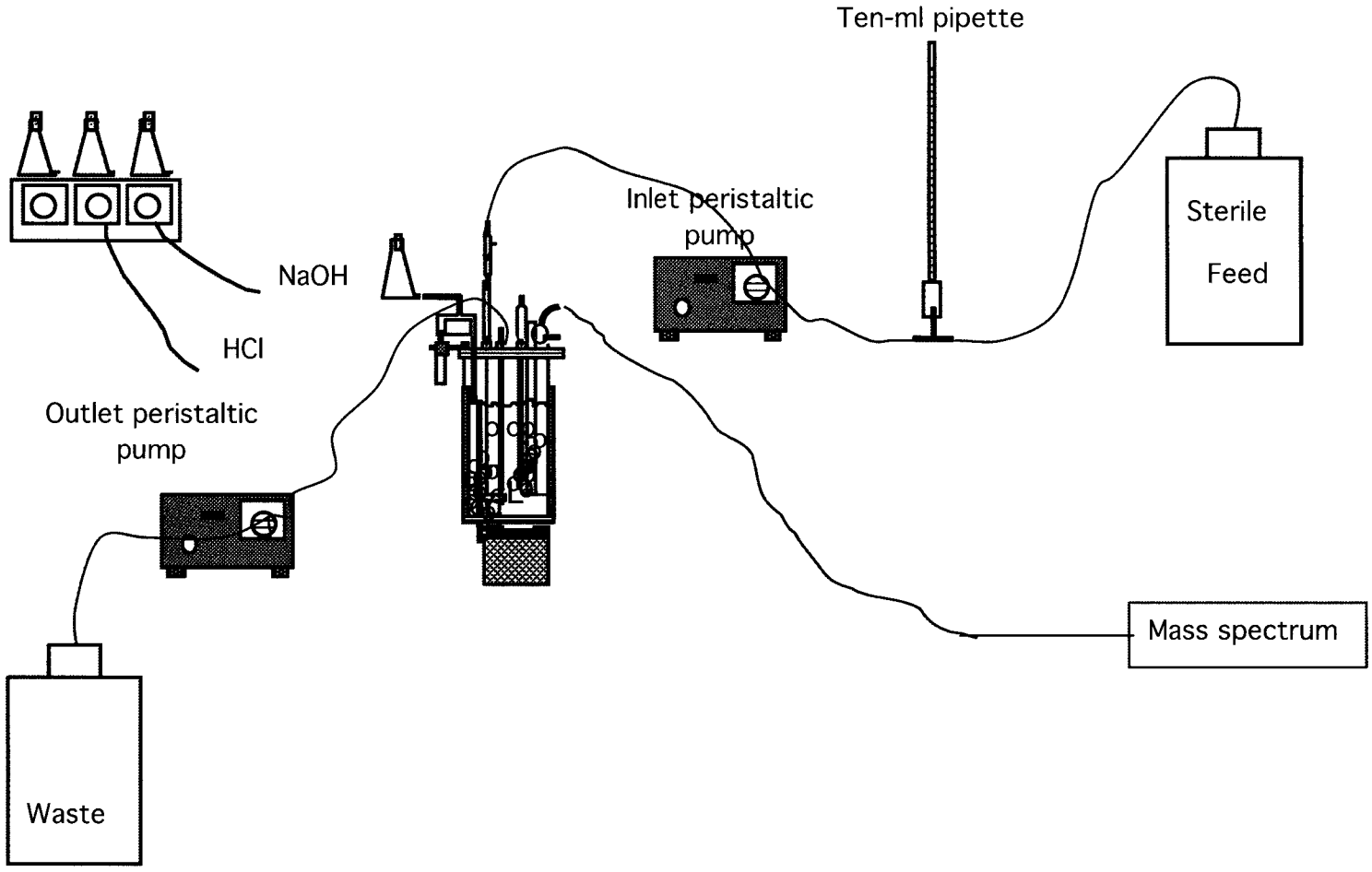

Figure 4.1 Continuous cultivation system of *Bacillus licheniformis* CCMI 1034. Readings of flow were taken regularly in order to adjust the dilution rate.

polarographic dissolved oxygen probe (Broadley James, USA) used in this work rapidly became coated with a biofilm. The aeration rate was set at such a high level to ensure sufficient outlet gas flow to the mass spectrometer, which was located at some distance from the fermenter. Temperature was controlled at 45 °C using the water-jacket of the bioreactor and pH was measured using a steam sterilizable electrode (Broadley James, USA) being controlled automatically through the addition of 2 M NaOH and 2 M HCl on demand to 6.8±0.1. The inlet and exit gas analysis were conducted by means of an online mass spectrometer (VG gas analyser, Fissons Instruments Ltd, UK).

4.2.3 Carbon pulses

Once the steady-state was reached (D=0.27 h^{-1}), the medium feed pump was switched-off, and glucose and lactose pulses containing the other GM nutrients (at the same proportion to the feed) were added to allow a period of batch growth and carbon source exhaustion to occur. The final broth concentrations for each pulse were as follows: glucose, 2.5 g l^{-1} and lactose, 2.37 g l^{-1} (molar equivalence with respect to carbon). The restart of the feeding was followed. Samples were withdrawn from the bioreactor at regular time intervals for biomass and glucose concentration measurements as well as for analysis by multi-parameter flow cytometry.

4.2.4 Starvation period

Once the steady-state was reached, the nutrient feed and outlet culture pumps were switched-off so no liquid medium was added or culture broth removed. This allowed a 4.5 h period of nutrient starvation to occur after which the nutrient feed and outlet culture pumps were switched back on. The dilution rate before conditions were altered (0.27 h^{-1}) was kept the same for each experiment in order to try and ensure comparable physiological starting conditions in all cases (glucose, lactose pulses and starvation period). Once the steady-state was reached, the nutrient feed-line and the outlet culture pumps were switched-off to allow a period of nutrient starvation to occur. Samples were withdrawn from the fermenter at regular time intervals for biomass and glucose assays as well as for analysis by multi-parameter flow cytometry.

4.2.5 Biomass and glucose concentrations

Biomass was measured turbidimetrically by optical density at 600 nm in a double beam spectrophotometer (Uvikon 922, Konton Instruments, England), calibrated against dry cell weight (DCW) at 100°C to constant weight, over 18 hours. Residual glucose concentration was measured by HPLC with an Aminex HPX-87P carbohydrate analysis column (Bio-rad, UK).

4.2.6 Flow cytometry

Propidium iodide (PI, Molecular Probes, P-1304) and 3,3'-Dihexylocarbocyanine iodide ($DiOC_6(3)$, Molecular Probes, D-273) were used in combination in this study. Flow cytometry measurements were made using a Coulter EPICS ELITE flow cytometer with 488 nm excitation from an argon-ion laser at 15 mW. Samples taken from the culture were immediately diluted (at least 1:2000 v/v) with phosphate buffer solution (PBS, pH 7.0) and stained with a mixture of the two fluorescent dyes, PI and $DIOC_6(3)$. Samples were kept in a sonication bath for 10 s just prior to analysis, in order to avoid problems associated with cell aggregation. Sonication for such a short of time has been shown to have no effect on cell physiological state (Nebe-von-Caron and Bedley, 1995). Stock solutions of each dye were prepared as follows: $DIOC_6(3)$ was made up at 10 $\mu g\ ml^{-1}$ in dimethyl sulphoxide (DMSO) and PI was made up at 2 $mg\ ml^{-1}$ in distilled water. The working concentrations of $DIOC_6(3)$ and PI were 5 $ng\ ml^{-1}$ and 1 $\mu g\ ml^{-1}$, respectively. All working solutions were made up freshly each day and passed through a 0.2 μm filter prior to use. In this way problems with microbial contamination and precipitation over long-term storage can be avoid. In addition, software discrimination was set on both the light scattering properties in the forward angle direction (FALS) signal and the right angle direction (RALS) signal. The optical filters were set up so that PI fluorescence was measured at 630 nm and $DIOC_6(3)$ fluorescence was measured at 525 nm. Since there is a spectral overlap between $DIOC_6(3)$ and PI-emitted fluorescence, the systems software

compensation was set up in such a way that $DIOC_6(3)$-emitted fluorescence was eliminated from the PI-emitted fluorescence detector and *vice versa.*

4.2.7 Transmission Electron Microscopy (TEM)

A 1ml culture sample was centrifuged at 9000 rpm, in a laboratory scale centrifuge (MSE Ltd., UK), for 10 minutes and resuspended in 2.5 % v/v glutaraldehyde in 0.1 M cocodylate buffer (pH 7.2) for 1 h. The sample was then spun down (9000 rpm), for 10 min and resuspended in 1% v/v osmium tetroxide in 0.1 M phosphate buffer (pH 7.2) for 1 h. The fixed cells were dehydrated sequentially in graded aliquots (70%, 90%, 100%, dried 100%) of ethanol and embedded in a 1:1 mixture of propylene oxide/Araldite resin. The resin was de-gassed and allowed to polymerise at 60°C for 16 h. Ultra-thin sections (70 nm) were cut using a Reichart-Jung Ultracut E microtome and stained with uranyl acetate and Reynolds lead citrate. The samples were then examined using a Jeol 1200 EX transmission electron microscope with an accelerating voltage of 80 kV.

4.2.8 *Bacillus licheniformis* morphology

Cells from cultures collected during the steady-states and glucose pulse/starvation period experiments were observed under an optical microscope Olympus BX50 (Tokyo, Japan).

4.3 Results and Discussion

4.3.1 Flow cytometry controls

In order to demonstrate that it is possible, using multi-parameter flow cytometry (mix of $DIOC_6(3)$ and PI), to characterize the physiological state of individual cells of the Gram positive bacterium *Bacillus licheniformis* CCMI 1034, it was essential to carry out a number of positively stained controls. These were then used for further comparison with data obtained from the *B. licheniformis* batch periods (glucose pulse and starvation period) and continuous cultivations.

To show that positive $DiOC_6(3)$ staining reflects cytoplasmic membrane potential, cells were incubated in the presence of 15 $\mu g\ ml^{-1}$ (for 10 minutes) of carbonyl cyanide m-chlorophenylhydrazone (CCCP), a known proton protonophore used to collapse cytoplasmic membrane potential (Wu et al. 1995, Lambert and Le Pecq 1984) (Appendix 1), and stained with $DiOC_6(3)$ (Figure 4.2). Under these conditions, mean $DiOC_6(3)$ fluorescence intensity was greatly reduced (mean = 4) when compared with the mean $DiOC_6(3)$ fluorescence intensity (mean = 100) of untreated steady-state cells.

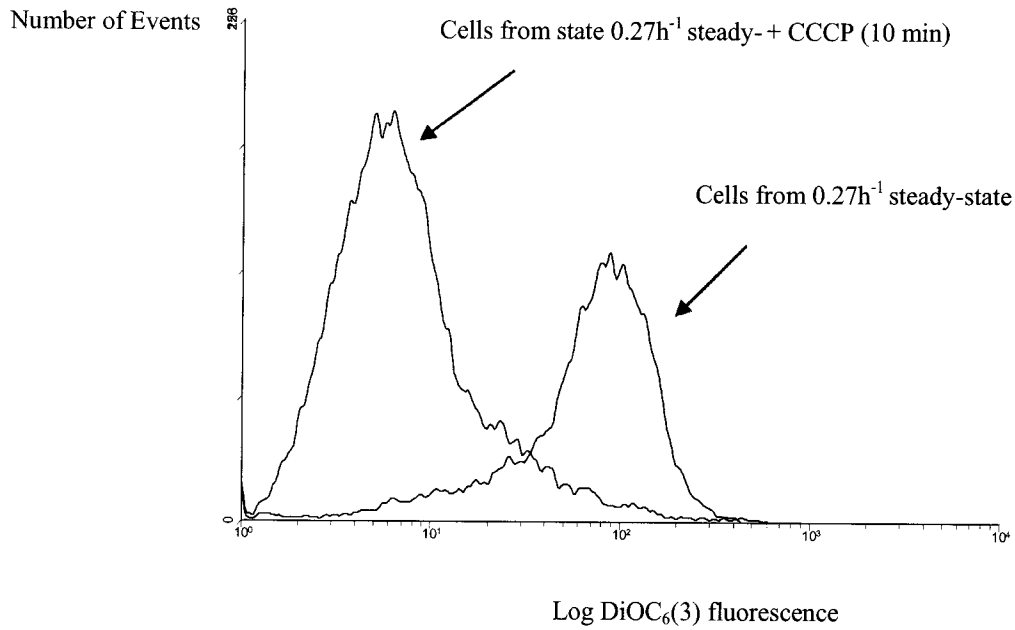

Figure 4.2 Effect of 15 µg ml^{-1} of carbonyl cyanide m-chlorophenylhydrazone (CCCP) on membrane potential of *Bacillus licheniformis* CCMI 1034.

Similar behaviour was observed when *Staphylococcus aureus* was treated with a well known ionophore, gramicidin S, and stained with $DiOC_6(3)$ (Diaper et al 1992) as well as *S. aureus* treated with the same ionophore (CCCP) as used in the present study, but stained with another cytoplasmic membrane potential reflective cationic carbocyanine fluorophore, $DiOC_2(3)$ (Novo et al 1999). As already mentioned, the use of fluorescent probes like $DiOC_6(3)$ are preferential for reflecting cytoplasmic membrane potential in Gram positive cells as those cells only generate a sufficiently large membrane potential to exclude anionic fluorescent stains such as oxonol (Bis-oxonol, $DiBAC_4$, BOX) when metabolising rapidly during exponential growth (Hewitt and Nebe-von-Caron 2004).

The identification of cells possessing depolarised permeabilised cytoplasmic membranes, took place after cells were treated at 100°C for 10 minutes, in a water bath, and then stained with a $DiOC_6(3)$ and PI mixture. Within the treated culture, two sub-populations could be readily identified, corresponding to non stained depolarized cytoplasmic membrane cells (B) and cells stained with both $DiOC_6(3)$ and PI, (D) (Figure 4.3-a). Paradoxically this would mean that these cells had polarised but permeabilised cytoplasmic membranes. A similar observation was described by Mason et al 1995 and Monfort et al 1996. The latter reported that heat killed *Escherichia coli* cells (in a 100°C water bath), was stained with $DiOC_6(3)$, with a mean fluorescence higher than that for healthy cells (those known should be very low or absent, since such cells do not generate a proton motive force across the membrane. However, they postulate that carbocyanine (lipohilic) dyes could bind to the hydrophobic regions of the cytoplasmic membrane of heat-treated cells because such harsh treatment may disrupt the phospholipid bilayer, therefore making the hydrophobic regions more accessible to this lipohilic dye. Similar results were obtained here suggesting the occurrence of non-specific energy-independent binding. Similarly, when cells collected from the steady-state of a continuous culture fermentation ($D=0.27h^{-1}$) were stained with a mixture of $DiOC_6(3)$ and PI (Figure 4.3-b), four sub-populations were readily identified. It is purpose that these correspond to healthy cells (A), stained with $DiOC_6(3)$; cells with a depolarised cytoplasmic membrane (B), no

(a)

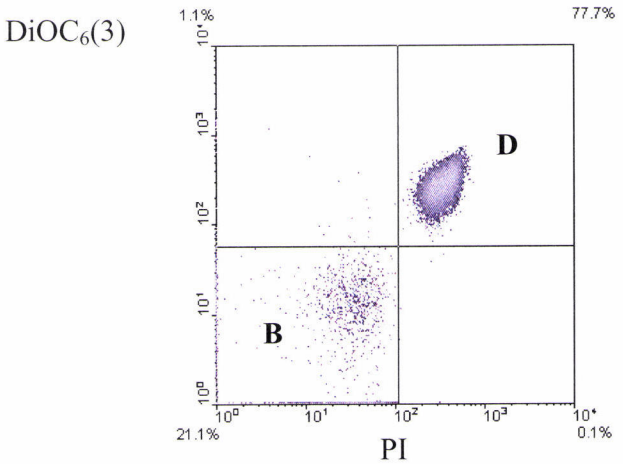

(b)

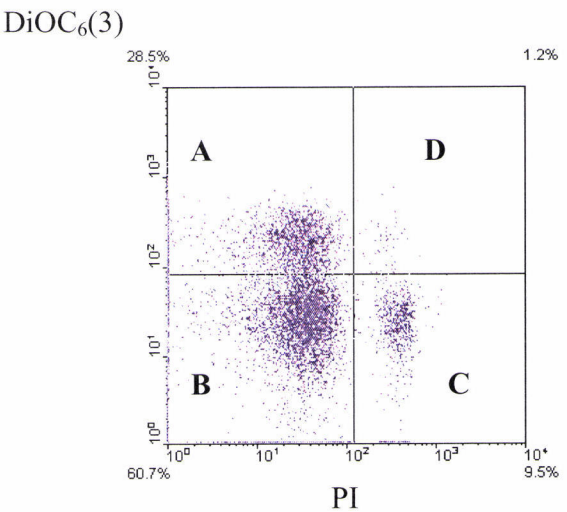

Figure 4.3 (a) Heat-killed *Bacillus licheniformis* CCMI 1034 cells, in a water bath at 100 ºC for 10 minutes. Two main sub-populations were found. These correspond to cells or spores with a depolarised cytoplasmic membrane (B) no staining; and permeabilised cells with a disrupted cytoplasmic membrane 'ghost cells' (D) stained with both $DiOC_6(3)$ and PI.

(b) Steady-state *Bacillus licheniformis* cells CCMI 1034 stained with a mixture of $DiOC_6$ (3) and PI. Four main sub-populations of cells could be identified. These correspond to healthy cells (A), stained with $DiOC_6(3)$; cells or spores with a depolarised cytoplasmic membrane (B), no staining; cells with a permeabilised depolarised cytoplasmic membrane (C), PI staining; and permeabilised cells with a disrupted cytoplasmic membrane 'ghost cells' (D), stained with both $DiOC_6(3)$ and PI.

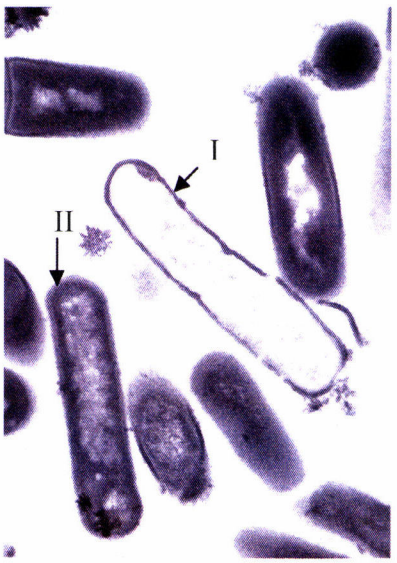

Figure 4.4 Transmission electron micrograph (× 25000) of *Bacillus licheniformis* CCMI 1034 cells starved of nutrients for 3 hours. Electron light 'ghost cell type' (I) structures exist, that had little or no cytoplasmic material inside the cell envelope, when compared to the more usual electron dense 'normal type'cells (II).

staining; cells with a permeabilised depolarised cytoplasmic membrane (C), PI staining; and permeabilised cells with a disrupted cytoplasmic membrane 'ghost cells' (D), stained with both $DiOC_6(3)$ and PI.

The presence of 'ghost cells' was further supported by analyzing starved cells (without nutrient availability for a period of time) using transmission electron microscopy (TEM). Figure 4.4 shows various cell sections. It is possible to identify two distinct cell types. Electron light 'ghost cell type' structures had little or no cytoplasmic material inside the cell envelope, when compared to the more usual electron dense 'normal type' cells. It is purpose that these structures, where the contents of the cell have leaked out, were in an

advanced state of lysis and as such may show enhanced $DiOC_6(3)$ staining as well as PI staining that was shown previously (population D) only for heat treated cells. Therefore it is proposed that when a healthy cell (sub-population A) is stressed, the transport systems cease and the cytoplasmic membrane depolarises (sub-population B), eventually permeabilising (sub-population C) indicating cell death, and then starts to lyse (sub-population D).

4.3.2. Physiological studies: spore germination

When nutrients are scarce *Bacillus licheniformis* cells undergo a two-cell differentiation where the initial prespore develops *via* a series of intermediate morphologically distinct stages into a very resistant, metabolically inactive and highly refractive endospore. It should therefore be possible to follow spore germination by measuring changes in the intrinsic light scattering properties alone (FALS and RALS) and by differential physiological staining. From a sample taken during the initial exponential phase of the starting batch culture, vegetative cells (95% as confirmed by light microscopy) could readily be distinguished from the background, using light scattering alone and the bimodal distribution with respect to RALS that is known to be characteristic for rod shaped organisms (Hewitt et al 1999b) could easily be identified (Figure 4.5-a). Indeed when the

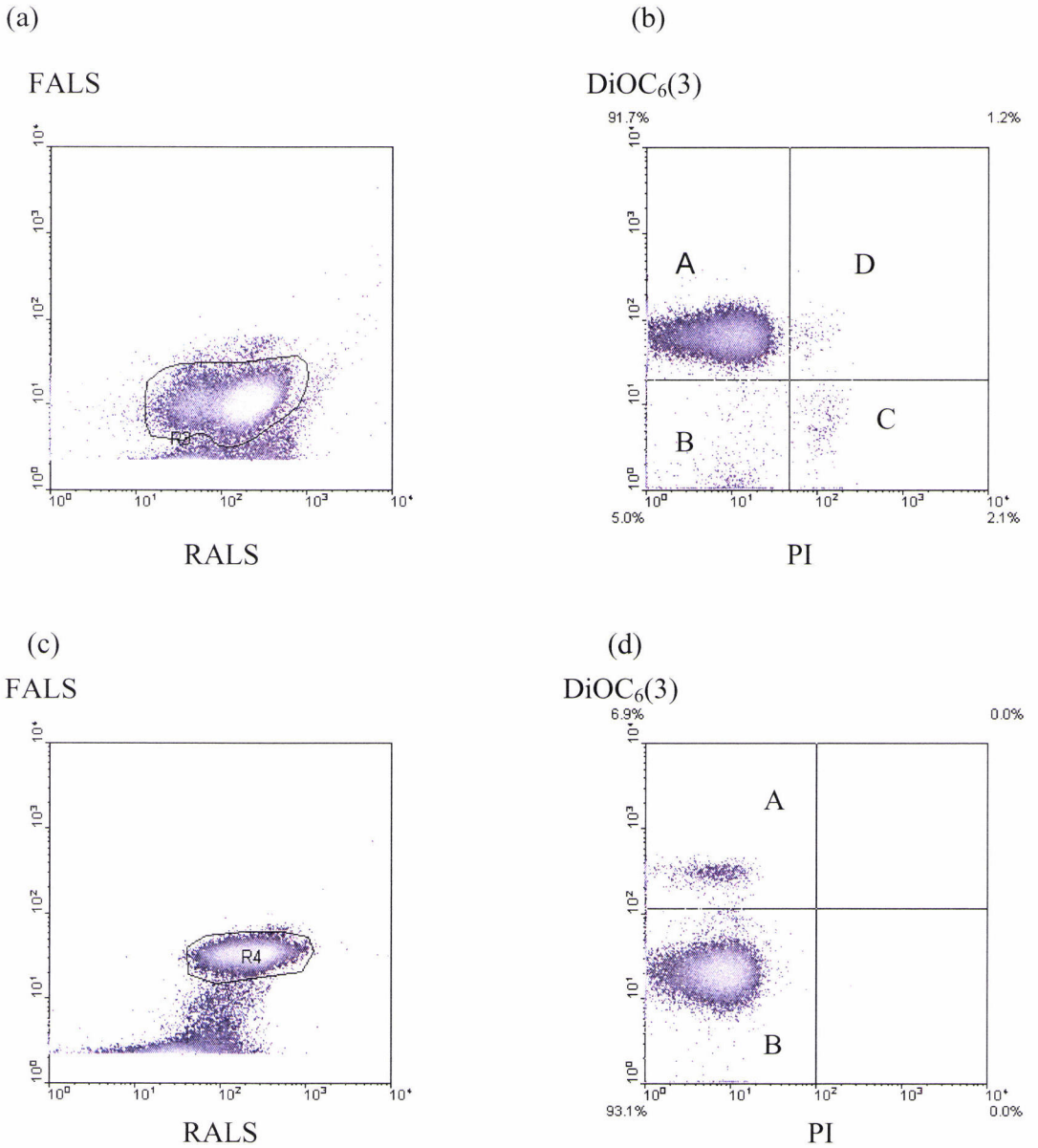

Figure 4.5 (a) FALS versus RALS for *Bacillus licheniformis* CCMI 1034 initial exponential phase growing cells (from the starting batch), illustrating the characteristic diffuse bimodal clustering that is thought to be characteristic for rod-shaped cells. (b) Initial exponential phase growing cells stained with $DiOC_6(3)$ and PI mixture. When compared with the control (Figure 4.3 a and b), all four sub-populations can be identified. (c) FALS versus RALS for *Bacillus licheniformis* CCMI 1034 spores, obtained from a nutrient agar plate incubated for 24 hours. A tighter unimodal distribution with a higher FALS signal could be identified thought to be characteristic for the highly refractive endospores. (d) *Bacillus licheniformis* CCMI 1034 spores stained with a mixture of $DiOC_6(3)$ and PI. When compared with the control (Figure 4.3 a and b), only two sub-populations (A and B) of cells can be distinguished.

same sample was stained with the mixture $DiOC_6(3)$ and PI, most of the cells were identified as being in sub-population A, not surprisingly having intact polarised cytoplasmic membranes (Figure 4.5-b). From a sample taken from a nutrient agar plate (95% spores as confirmed by light microscopy) used for the fermentation inoculum, the bimodal distribution with respect to RALS associated with the vegetative cells could no longer be resolved and a tighter unimodal distribution with a higher FALS signal was identified thought to be characteristic for the highly refractive endospores (Figure 4.5-c) (Comas-Riu and Vives Rego, 2002).

When the same sample was stained with a mixture of $DiOC_6(3)$ and PI, the majority of the events could be identified as sub-population B, having intact depolarised cytoplasmic membranes (Figure 4.5-d). This happens since spores remain metabolically inactive until ready to germinate. Therefore sub-population B (Figure 4.3), may be made up of a mix of cells with depolarised but intact cytoplasmic membranes and spores. Some events in Figure 4.5-d are identifiable as being in sub-population A, these could be made up of healthy vegetative cells or spores in the process of germination since the generation of a cytoplasmic membrane potential must be an early landmark event for the return of a fully metabolically active vegetative cell.

4.3.3. Starvation period

Figures 4.6-a and 4.9-a show the biomass and physiological profiles of a *Bacillus licheniformis* culture when submitted to a starvation period (nutrient feed shut-off) of ~4.5 h. Before and after the interruption of the nutrient feed no glucose was

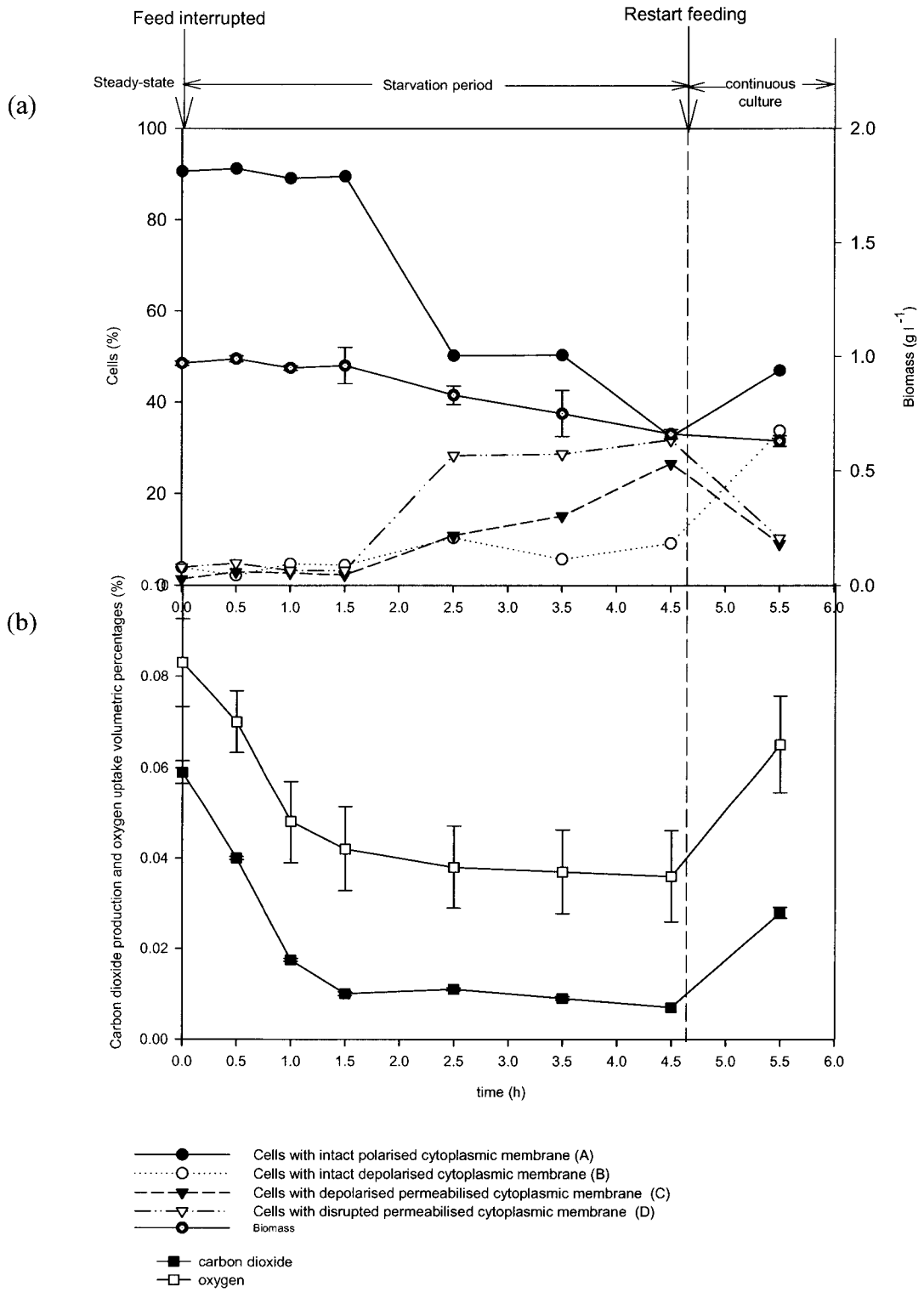

Figure 4.6 Fermentation profiles for a glucose limited continuous culture where the steady state was perturbed by a starvation period.

detected in the growth medium. For up to 1.5 h after the interruption of the feed, biomass concentration remained virtually unchanged (0.95 g l^{-1}), as did the proportions of cells with intact polarised (A), intact depolarised (B), depolarised permeabilised (C) and permeabilised disrupted (D) cytoplasmic membranes. This could be due to the oxidation of storage materials synthesised during the glucose limited steady-state, supplying the energy necessary for maintaining metabolic activity and other cell functions. However, 2.5 hours after the starvation period onset, biomass concentration started decreasing and eventually attained a minimum of 0.62 g l^{-1} in the end of the starvation period. At the same time, the ratio of cells with intact polarised cytoplasmic membranes (A) decreased, reaching a minimum of 32.4 % just before feeding was restarted. The opposite was true for the proportion of cells with intact but depolarised cytoplasmic membranes (B), cells with depolarised permeabilised cytoplasmic membranes (C) and cells with disrupted permeabilised cytoplasmic membranes (D). The proportion in each case increased until the restart of feeding but by varying amounts (Figures 4.6-a and 4.9-a). The presence of a large number of cells with either depolarised permeabilised cytoplasmic membranes or disrupted cyotplasmic membranes (63% in total) suggests that it is a high level of cell death and lysis in the culture in response to carbon starvation that is responsible for the measured substantial drop in biomass concentration. This hypothesis is supported by off-gas analysis (Figure 4.6-b). Immediately after the feed interruption, both carbon dioxide production and oxygen uptake steadily decreased reaching a minimum after 1.5 hours. This remained stable until feeding was restarted. However, oxygen uptake was always higher than carbon dioxide production (RQ <1), indicating that endogenous substrate oxidation might be occurring.

The fact that the ratio of cells with intact but depolarised cytoplasmic membranes (B) did not exceed 10.4 % during the starvation period is surprising since energy required to maintain cytoplasmic membrane potential is scarce. It is thought that sub-population B is in a state of constant flux with cells either progressing rapidly towards spore formation or membrane permeabilisation (death and lysis) or being capable of re-polarising in the presence of a fresh energy source (Hewitt et al, 1999a). The possibility that endospores were being produced as a response to carbon starvation was eliminated because examination of samples collected during this period, using traditional optical light microscopy, did not reveal changes in the proportion of endospores when compared to the steady-state. After feeding was restarted all measurements showed that the culture started to recover from the stress associated with the starvation.

4.3.4 Glucose pulse

Figures 4.7-a and 4.9-b show the biomass and physiological profiles of *Bacillus licheniformis* culture when submitted to a glucose pulse, after continuous feeding was terminated and the following 4.5 h period before continuous feeding was started again. Immediately after the glucose pulse, the biomass concentration began to rise reaching a maximum of 1.6 g l^{-1} 1.25 h later at which time the additional glucose had been

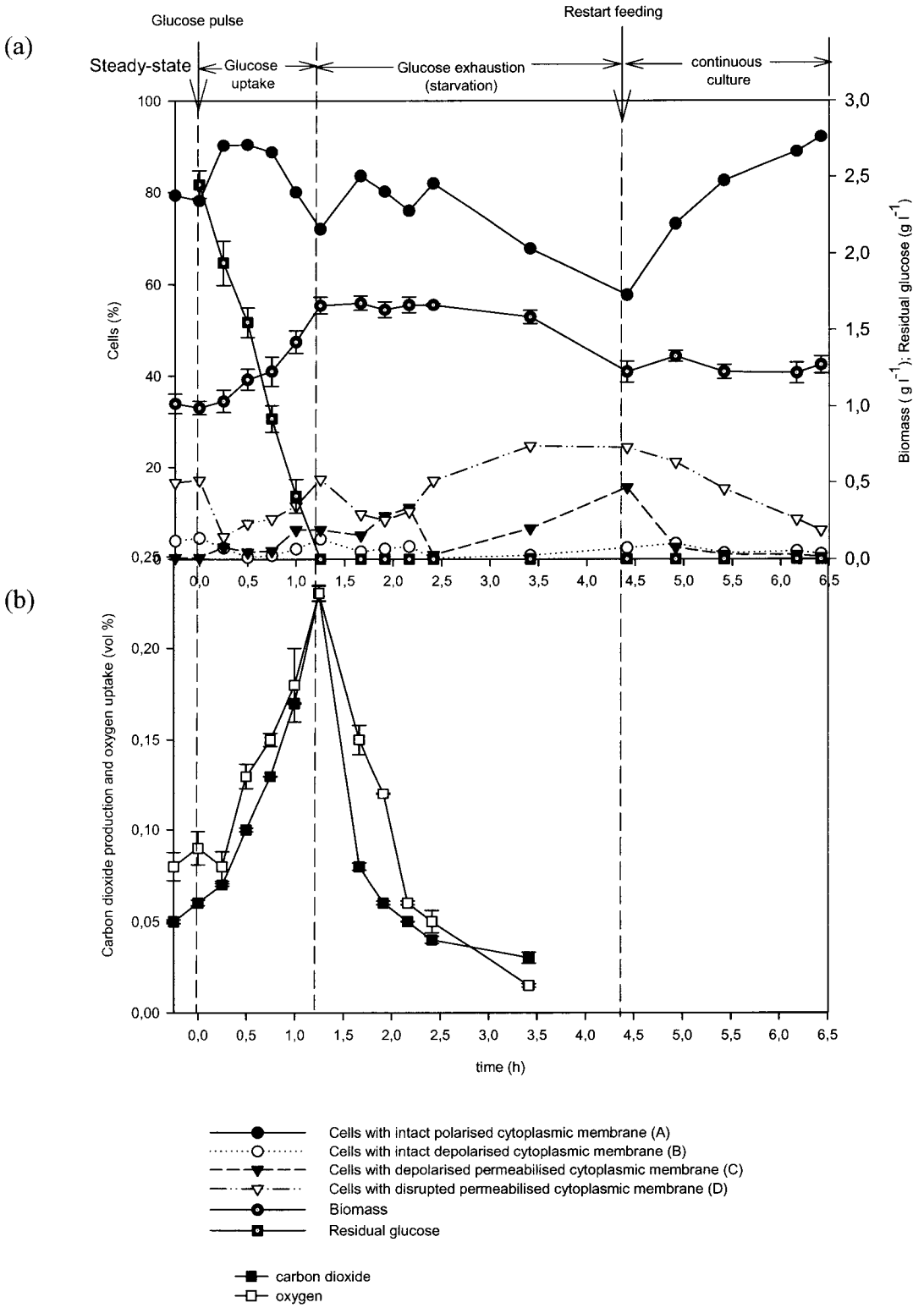

Figure 4.7 Fermentation profiles for a glucose limited continuous culture where the steady state was perturbed by a 2.5 g l^{-1}glucose pulse followed by a starvation period.

exhausted. Thereafter the biomass concentration began to fall until the restart of continuous feeding at which point steady-state conditions were resumed. During this period the number of polarised cytoplasmic membrane cells (A) also increased, reaching a maximum proportion of 90%. This proportion was maintained for a short period (~ 0.75 h) but began to fall before the additional glucose had been exhausted reaching a minimum of 72% when glucose was exhausted (1.25 h). Immediately after glucose exhaustion, the number of cells with polarised cytoplasmic membranes (A) began to increase before falling until the continuous feed was restarted whereupon the proportion began to rise again until the end of the experiment. Exactly the opposite behavior was observed for the proportion of cells with intact but depolarised (B), depolarised permeabilised (C) and permeabilised disrupted (D) cytoplasmic membranes but by varying amounts (Figures 4.7-a and 4.9-b). The initial increase in the proportion of cells with intact polarised cytoplasmic membranes (A) after glucose had been exhausted is rather surprising indicating that an alternative energy source was being used to maintain cell function and viability. This could have come from the oxidation of storage materials built-up during the glucose sufficient period or from nutrients released from lysed cells. The mechanism, where dead cells provide nutrients for the maintenance of the remaining surviving cells is well established and is termed cryptic growth (Watson et al., 1998).

The carbon dioxide produced and oxygen uptake increased immediately after the glucose pulse (Figure 4.7-b) reaching a maximum before decreasing sharply once glucose was exhausted. During the following 1.25 hours the rate of decrease of oxygen uptake and carbon dioxide production was less pronounced, suggesting that although cell growth had

stopped, endogenous metabolism was occurring accounting for the high proportion of cells with intact polarised cytoplasmic membranes (A) and the maintenance of the biomass concentration. 3.5 h after the glucose pulse, oxygen uptake was less than carbon dioxide production, (RQ >1) suggesting the end of endogenous material oxidation. In fact, at that time the proportion of cells with depolarised permeabilised (C) and disrupted permeabilised cytoplasmic membranes (D) increased indicating cell death and lysis.

4.3.5 Lactose pulse

Figures 4.8-a and 4.9-c show the biomass and physiological profiles of a *Bacillus licheniformis* culture when submitted to a lactose pulse after continuous feeding was terminated and the following 20 h period before continuous feeding was started again. Immediately after the lactose pulse there was a 2-3 h period where no lactose was consumed whilst biomass concentration and the proportion of cells with intact polarised cytoplasmic membranes (A) decreased. During this period there was a concomitant increase in the proportion of cells with permeabilised depolarised (C) and disrupted permeabilised cytoplasmic membranes (D) whilst the proportion of cells with intact depolarised cytoplasmic membranes (B) remained unchanged. A similar physiological response was noted after the onset of the starvation period discussed before, which would suggest that during this period (2-3 h after the lactose pulse addition) no readily assimilable carbon source was available. After this period, lactose started to be consumed and was exhausted 11 h after the lactose pulse addition.

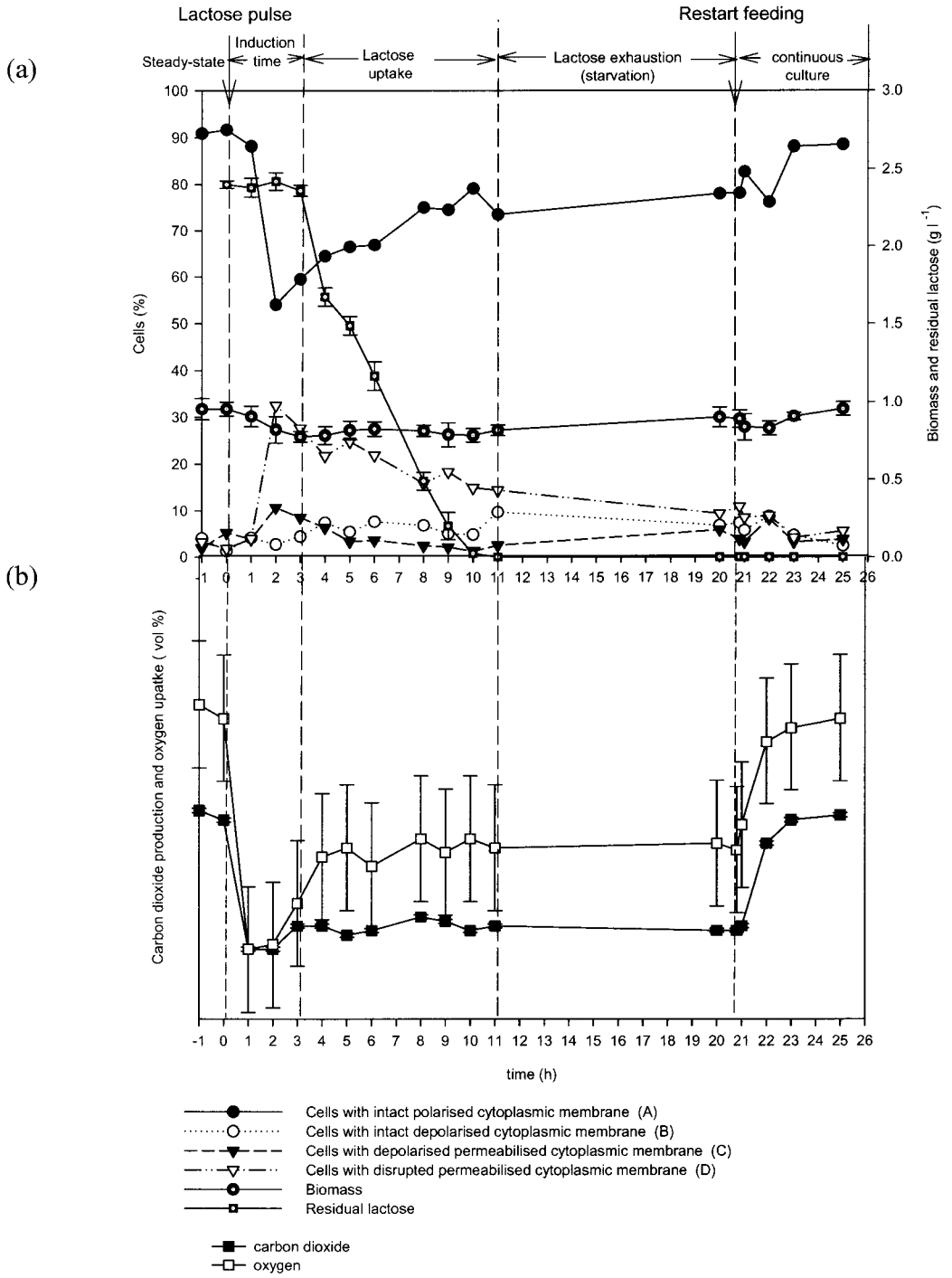

Figure 4.8 Fermentation profiles for a glucose limited continuous culture where the steady state was perturbed by a 2.37 g l^{-1} lactose pulse followed by a starvation period.

It is known that cells of *Bacillus* spp. when previously grown on a glucose based medium are not able to use lactose immediately (Stülke and Hillen, 1999). To do so, several additional enzymes are required, and their synthesis takes some time and only after cells become exposed to lactose as the sole carbon source. In this case, the time taken for enzyme synthesis would appear to be approximately 2-3 h. During the period where lactose was consumed (2 – 11 h after the lactose pulse) the proportion of cells with intact polarised cytoplasmic membranes (A) increased until the end of the experiment even when lactose was exhausted and when the continuous feed was restarted. The biomass concentration remained relatively constant whilst the proportion of cells with intact but depolarised (B), depolarised permeabilised (C) and disrupted permeabilised (D) cytoplasmic membranes fell but by varying amounts (Figures 4.8-a and 4.9-c) until the restart of feeding. The fact that there was no increase in the number of stressed cells after lactose exhaustion (Figures 4.8-a and 4.9-c) is not surprising since it is known that during carbon starvation, the micro-organism diverts resources towards the induction of a number of survival strategies. One of these, the accumulation of intracellular storage materials, namely polyhydroxyalcanoates (PHAs), during lactose uptake, has been reported for *Bacillus* spp. (Povolo and Casella, 2003). In this case, the biomass yield and the specific growth rate were low ($Y^{lactose}_{x/s}$ = 0.05 g biomass (g lactose)$^{-1}$, $\mu^{lactose}$ = 0.009 h^{-1}, Table 4.1) when compared with the glucose pulse biomass yield and specific growth rate ($Y^{glucose}_{x/s}$ = 0.26 g biomass (g glucose)$^{-1}$, $\mu^{glucose}$= 0.47 h^{-1}, Table 4.1), suggesting that the micro-organism was using lactose mainly for the production of storage materials rather than for cell growth.

Table 4.1 Kinetic parameters for the glucose and lactose pulse studies.

	Glucose limited steady-state just prior to the carbon source pulses		Batch growth after substrate pulses addition		
	D=μ (h^{-1})	$Y_{x/s}$ ($g\ g^{-1}$)	μ (h^{-1})	$Y_{x/s}$ $g\ g^{-1}$	Lag phase (h)
Glucose	0,27	0,55	0.45	0.26	0
Lactose	0,27	0,55	0.009	0.05	2-3

The above hypotheses were confirmed by off-gas analysis (Figure 4.8-b). Immediately after the lactose pulse, both oxygen uptake and carbon dioxide production decreased. The same was observed immediatelly after the feed interruption during the starvation period indicating a lack of readily assimilable carbon (Figure 4.6-b). 2-3 h after the lactose pulse both oxygen uptake and carbon dioxide production increased. This coincided with the increase in proportion of cells with intact polarised cytoplasmic membranes (A) indicating an increase in cell metabolic activity. During the period where lactose was consumed, oxygen uptake and carbon dioxide production were lower than during the glucose-limited steady state and after the glucose pulse (Figure 4.7-b). After lactose was exhausted, oxygen uptake and carbon dioxide produced remained constant until the continuous glucose feed was re-started whereupon both increased sharply. Examination of samples using a traditional optical microscope did not reveal any increase in endospore numbers when compared to the steady state.

It is known that *Bacillus* spp. produce a robust resting cell state, the endospore, as a response to nutritional limitation, which can remain dormant for many years. Endospore

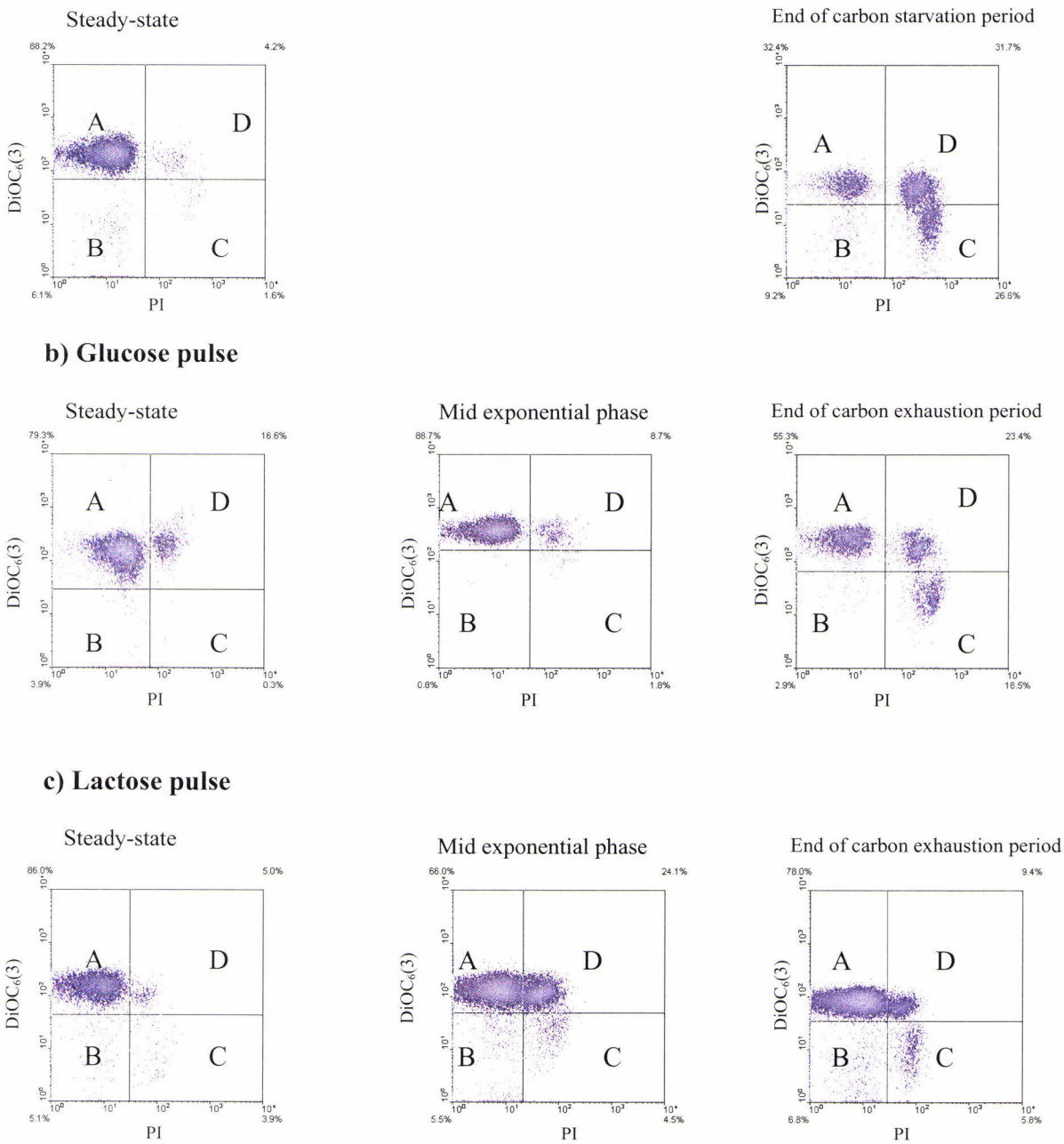

Figure 4.9 Cell samples taken at various times during a glucose limited continuous culture periodically perturbed by glucose/lactose pulses and starvation periods stained with a mixture of PI and $DiOC_6(3)$. When compared with the control data (Figure 4.3 a and b) up to four main sub-populations of cells can be distinguished, corresponding to healthy cells (A), stained with $DiOC_6(3)$; cells with a depolarised cytoplasmic membrane (B), no staining; cells with a depolarised permeabilised membrane (C), PI staining; and permeabilised depolarised cells with a disrupted cytoplasmic membrane 'ghost cells' (D), stained with both $DiOC_6(3)$ and PI.

formation is an elaborate and energy intensive process that requires several hours to complete. If during this period nutrients become available, cells in the process of sporulation would be at a competitive disadvantage in relation to those cells not envolved in sporulation and hence able to resume growth rapidly. Therefore, cells delay sporulation until forced to do so by prolonged depletion of nutrients (González-Pastor et al, 2003). In all the cases studied here during carbon starvation (starvation period, glucose and lactose exhaustion periods) there was no increase in endospore numbers when compared with the steady state. It is known that spore production in response to unfavorable conditions in *Bacillus* spp. can take up to 8 hours (Driks, 2002). The starvation period, as well as the glucose exhaustion period lasted less than 8 hours, so any endospores, if sporulation had been induced, would not have had time to reach full maturity. However, the lactose exhaustion period lasted 9.8 h, but no endospores were formed. In this case it was probable that other survival mechanisms such as the use of storage materials or criptic growth may have delayed the onset of sporulation.

It is clear that the physiological responses of *Bacillus licheniformis* CCMI 1034 steady state continuous cultures perturbed by lactose/glucose pulses or a starvation period were very different and these responses could be followed by multi-parameter flow cytometry.

4.4 References

Baloo, S. and Ramkrishna, D. 1991. Metabolic regulation in bacterial continuous cultures:I. Biotechnol. Bioeng. 38, 1337-1352.

Comas-Riu, J. and Vives-Rego, J. 2002. Cytometric monitoring of growth, sporogenesis and spore cell sortying in *Paenibacillus polymyxa* (formerly *Bacillus polymyxa*). J. Appl. Microbiol. 92, 475-481.

Diaper, J.P., Tither, K. and Edwards, C. 1992. Rapid assessment of bacterial viability by flow cytometry. Appl. Microbiol. Biotechnol. 38, 268-272.

Doshi, P., Rengaswamy, R. and Venkatesh, K.V. 1997. Modelling of microbial growth for sequential utilization in a multisubstrate environment. Proc. Biochem. 8, 643-650.

Doshi, P. and Venkatesh, K.V. 1998. An optimal model for microbial growth in a multiple subtrate environment: simultaneous and sequential utilization. Proc. Biochem. 33, 663-670.

Driks, A. 2002. Overview: development in bacteria: spores in *Bacillus subtilis*. Cellular Mol. Life Sc. 59, 3, 389-391.

Gaudy, A.F. 1962. Studies on induction and repression in activated sludge systems. Appl. Microbiol. 10, 263- 271.

Gonçalez-Pastor, J.E., Hobbs, E.C. and Losick, R. 2003. Cannibalism by sporulating bacteria. Science 301, 510-513.

Haughland, R.P. 2002. Handbook of Fluoresecent Probes and Research Products, Molecular Probes, ninth edition.

Hewitt, C.J., Nebe-Von Caron, G., Nienow, A.W. and McFarlane, C.M. 1999a. Use of multi-staining flow cytometry to characterize the physiological state of *Escherichia coli* W3110 in high cell density fed-batch cultures. Biotechnol. Bioeng. 63, 705-711.

Hewitt C. J., Nebe-von Caron G., Nienow A. W. and McFarlane C. M. 1999b. The use of multi-parameter flow cytometry to compare the physiological response of *Escherichia coli* W3110 to glucose limitation during batch, fed-batch and continuous culture cultivation. J. Biotechnol. 75, 251-254.

Hewitt C. J. and Nebe-von-Caron G. 2004. The application of multi-parameter flow cytometry to monitor individual microbial cell physiological state. In: Advances in Biochemical Engineering/Biotechnology, 'Physiological Stress Responses in Bioprocesses'. Ed Enfors S. O., Springer. Special volume 89, pp 197 – 223

Kosseva, M.R., Kent, C.A. and Lloyd, D.R. 2003. Thermophilic bioremediation strategies for a dairy waste. Biochem. Eng. J. 15, 125-130.

Kompala, D.S., Ramkrishna, D. and Tsao, G. 1984. Biotechnol. Bioeng. 26, 1272-1281.

Lapara T.M. and Alleman, J.E. 1999. Thermophilic aerobic biological wastewater treatment. Water. Res. 33, 895-908.

Lambert, B., LePecq, J.-B. 1984. Effect of mutation, electric membrane potential and metabolic inhibitors on the accessibility of nucleic acids to ethidium bromide in *E. coli* cells. Biochemistry 23, 166-179.

Mason, D.J., Lopéz-Amorós, R., Allman, R., Stark, J.M. and Lloyd, D. 1995. The ability of membrane potential dyes and calcafluor white to distinguish between viable and non-viable bacteria. J. Appl. Bacteriol. 78, 309 – 315.

Monfort, P. and Baleux, B.1996. Cell cycle characteristics and changes in membrane potential during growth of *Escherichia coli* as determined by cyanine fluorescent dye and flow cytometry. J. Microbiol. Meth. 25,79-86.

Nebe-von Caron and Badley, R.A. 1995. Viability assessment of bacteria in mixed populations using flow cytometry. J. Microsc. 179, 55-66.

Nikolajsen, K., Nielsen, J. and Villadsen, J. 1991. Structured modelling of a microbial system: III. Growth on mixed substrates. Biotechnol. Bioeng. 38, 24-29.

Novo, D., Perlmutter, N.G., Hunt, R.H. and Shapiro, H.M. 1999. Accurate rate flow cytometry membrane potential measurement in bacteria using diethyloxacarbocyanine and a ratiometric technique. Cytometry 35, 55-63.

Povolo, S. and Casella, S. 2003. Bacterial production of PHA from lactose and cheese whey permeate. Macromol. Symp. 197, 1-9.

Stülke, J. and Hillen, W.1999. Carbon catabolite repression in bacteria. Curr. Opin. Microbiol. 2, 195-201.

Venkatesh, K.V., Doshi, P. and Rengaswamy, R. 1997. An optimal strategy to model microbial growth in a multiple substrate environment. Biotechnol Bioeng. 56, 635- 644.

Vishniac, W. and Santer, M. 1957. The Thiobacilli. Bacteriol. Rev. 21, 95-213.

Watson, S.P., Clements, M.O. and Foster, S.J. 1998. Characterization of starvation-survival response of *Staphylococcus aureus*. J. Biotechnol. 180, 1750-1758.

Wu, Q., Knowles, R., Niven, D.F. 1995. Effects of ionophores on denitrification in *Flexibacter Canadensis*. Can. J. Microbiol. 41, 227-234.

CHAPTER 5

Impact of growth conditions on *Bacillus licheniformis* CCMI 1034 morphology and physiology

5.1 Introduction

Generally, thermophilic aerobic treatments provide poor bacterial settling resulting from dispersed growing micro-organisms. As a result, biomass separation becomes difficult and often limits the overall treatment efficiency. An alternative may be the use of immobilized micro-organisms. Pertulla et al (1991) effectively utilized a packet bed reactor to treat sulphite mill condensate at 65 °C. Biofilms, the attachment of micro-organisms to surfaces or to one another (flocculation), are defined as microbial communities immobilised in a microbial extracellular polymeric matrix which provides the organism with ecological advantage as a mode for adhesion to surfaces and protection of pathogenic bacteria against phagocytosis (Mulder, 1989; Tijhuis et al, 1996). In many places, this biofilm is unwanted, e. g., fouling of heat exchangers or membranes. In aquatic environments, the attachment of bacteria to submerged solid surfaces such as ships, oil drilling rigs, pipelines and heat exchangers contribute for the deterioration of such structures through corrosion or clogging (Pringle, 1983). Biofilms may have also a significant detrimental effect on the synthesis of desired products as the cells inside the biofilm become starved due to nutrient diffusional limitations, and

eventually die, therefore do not contribute for the product formation, leading to the product yield decrease. In physiological studies, the attachment of micro-organisms to fermenter walls or flocculation often leads to a misinterpretation of the kinetic parameters.

However, biofilm formation is a natural immobilization process and can be exploited to human advantage. It may have advantages in some biotechnological processes such as whole-cell immobilization technology, a process with many industrial applications. For instance, the vinegar, the citric acid production (Boletti, 1921; Sakurai at al., 1997) and metal extraction (Rawlings, 2002) use biofilms. One of the most important biotechnological applications of biofilm formation is the activated sludge process used in wastewater treatment. The success of biological wastewater treatment is to a large extent governed by the micro-organisms attachment ability, thereby facilitating the separation of particles from treated water.

The morphological characteristics of the biofilm (biofilm thickness, density and surface shape) are very important for the bioprocess efficiency and separation of biofilm particles from the treated stream. For high process efficiency, a relatively small thickness and a high amount of biofilm area are needed, so that nutrients are able to diffuse through the biofilm thus becoming available to all cells. On the other hand, fluffy biofilms lead to instabilities with respect to separation of biofilm particles from the treated wastewater (Villaseñor et al, 2000).

Therefore, the control of the operational conditions that leads to these two opposite situations – cell attachment or dispersed growth - is of crucial importance, for the knowledge of the industrial use of the micro-organisms. In particular, the control of

growth conditions that leads to thin and smooth biofilms is determinant for the enhancement of the biodegradation process (Loosdrecht, 1995).

It has been reported that the main components of the extracellular polymers (ECP) found in biofilms are carbohydrates, proteins, lipids and nucleic acids due to the excretion of intracellular polymers or as result of cell lysis. The ECP quantity and composition play an important role in the micro-organism attachment properties. Different nutrient limitations during the micro-organisms growth may induce different ECP compositions which may change the cell surface characteristics therefore the attachment properties and the morphology (Brown et al, 1977; Dignac et al, 1998; Durmaz and Sanin, 2001; Sanin et al, 2003). In mixed and single culture studies when carbon is found in excess relative to nitrogen or *vice versa*, the composition of extracellular polymeric substances changes markedly. When nitrogen is in excess more proteinaceous polymeric polymers are produced, whereas when carbon is in excess more carbonaceous (polysaccharide) polymers are produced. Under these conditions, it has been demonstrated that the surface hydrophobicities of the two systems change significantly (Sanin et al, 2003). Therefore the limiting nutrient can modulate the cell surface hydrophobicity, thus the morphology.

Considering the importance of different morphologies on the fermentation performance, and reports that changes in the morphology of filamentous micro-organism can be caused by mechanical forces, the effect of agitation on morphology in submerged fermentations requires attention. Agitation is considered one of the most important factors influencing mycelial morphology, as well as the total power input (Amanullah at al, 1999).

In continuous cultures the mycelial morphology is influenced by the nature of the limiting nutrient, by shear stress and dilution rate (Wiebe et and Trinci, 1991).

The present chapter aimed at the achievement of growth conditions that led to *Bacillus licheniformis* CCMI 1034 dispersed growth or biofilm formation. For this purpose, *Bacillus licheniformis* CCMI 1034 carbon-limited and nitrogen-limited steady-state continuous cultures were carried out at different stirring rates and dilution rates, in order to evaluate the effect of the limiting nutrient, the agitation and the dilution rate on the morphology, therefore on the microbial attachment ability of the micro-organism. The cell physiological response at the individual cell level was evaluated by multi-parameter flow cytometry.

5.2 Materials and Methods

5.2.1 Micro-organism

Bacillus licheniformis CCMI 1034 strain was maintained in glass beads, using glycerol as cryoprotectant, at – 72 °C.

5.2.2 Bioreactor Experiments

The medium designed for the glucose-limited growth, contained: Glucose, 2.00 gl^{-1}, KH_2PO_4, 1.00 gl^{-1}, $(NH_4)_2SO_4$, 1.50 gl^{-1}, yeast extract, 0.10 gl^{-1}, $CaCl_2.2H_2O$, 0.10 gl^{-1},

$MgCl_2.7H_2O$, 0.25 gl^{-1} and 2 ml l^{-1} trace elements solution (Vishniac and Santer, 1957). The medium designed for the nitrogen-limited growth contained: Glucose, 2.00 gl^{-1}, KH_2PO_4, 1.00 gl^{-1}, $(NH_4)_2SO_4$, 0.25 gl^{-1}, yeast extract, 0.10 gl^{-1}, $CaCl_2.2H_2O$, 0.10 gl^{-1}, $MgCl_2.7H_2O$, 0.25 gl^{-1} and 2 ml l^{-1} trace elements solution (Vishniac and Santer, 1975). Six nutrient agar plates grown for 24 hours at 45°C were transferred to the growth medium, to inoculate the bioreactor. After a period of batch cultivation, a variable speed peristaltic pump was used to feed sterile medium into the fermenter vessel at adequate dilutions rates. Glucose-limited and nitrogen-limited steady-state conditions were determined by periodic analysis of biomass, residual glucose and ammonium concentrations, and off-gas analysis.

In this work it was not possible to use the bioreactor used in the previous chapter. The experiments were carried out in an Infors ISF-1000 2 L benchtop-fermenter (UK) with a 1300, 1240 or 1140 ml working volume (depending on the stirring rate, 500, 1000 and 1750 rpm, respectively), equipped with two six-blade Rushton impellers (D = 4.8 cm). The vessel was fitted with three equally spaced baffles, width 15.41 mm (Figure 5.1). The torque exerted by the impellers was measured using a VISCO-MIX (Coesfeld Messtechnik GmbH, Dortmund, Germany). The gas-liquid mass transfer coefficient, k_La, was calculated by measuring the rate of oxygen transfer in nitrogen purged tap water (Sobotka et al, 1982). The working volume was kept constant by using a levelled tube linked to a variable speed peristaltic pump.

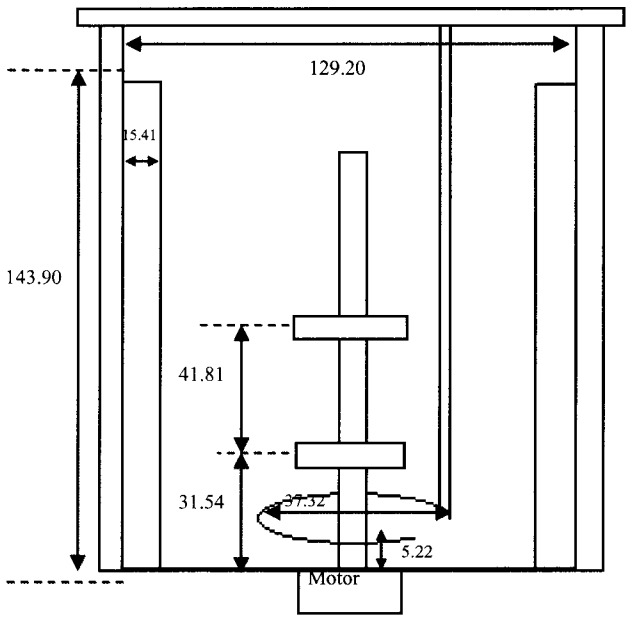

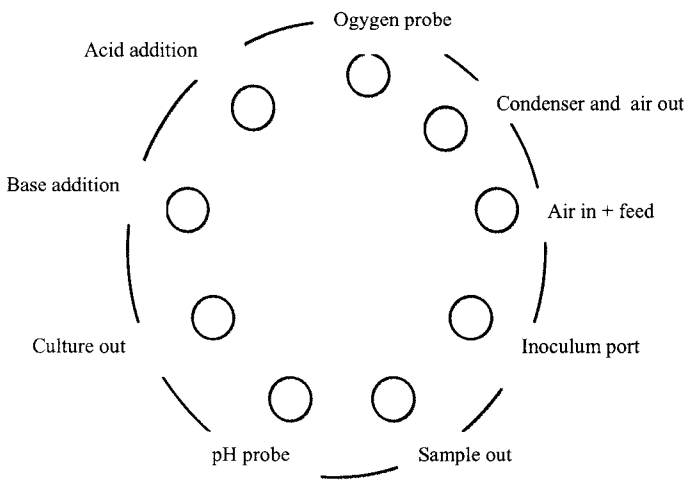

Figure 5.1 The Infors 2L vessel (dimensions in mm) and its top plate with the probe insertions points.

The aeration rate was 2 vvm. The DO measurements were impossible as the polarographic dissolved oxygen probe used in this work became rapidly coated with biofilm. Temperature was controlled at 45 °C using the vessel water-jacket, and pH was measured using a steam sterilizable electrode and was controlled automatically through the addition of 2 M NaOH solution and 2 M HCl on demand to 6.8±0.1. The inlet and exit gas analysis were conducted by means of an on-line mass spectrometer (VG gas analyser, Fissons Instruments Lda, UK).

5.2.3 Growth measurement

Biomass, expressed as dry cell mass, was measured gravimetrically on 5 ml culture samples, from which cells were harvested, washed and dried for 18 h at 100°C.

5.2.4 Residual glucose, organic acids and ammonium concentrations measurements

The residual glucose and organic acids in filtered samples were determined in a Gilson HPLC system with an Aminex HPX-87P carbohydrate analysis column (Bio-rad, UK). Residual ammonium concentrations in filtered samples were assayed using the Merck ref 1.00683 ammonium assay kit.

5.2.5 Microbial adhesion to hydrocarbons test

Changes in the biofilm cells surface hydrophobicity were determined by measuring the attachment of bacteria to hydrocarbons, using the method developed by Rosemberg et al, (1980) and adapted by Sanin et al, (2003). 1.2 ml of cell suspension were transferred to a 10 ml round bottom tube. After the initial optical density ($OD_{initial}$) was measured, 0.2 ml of n-hexadecane was added. Following 10 min of preincubation at 45 °C, the mixture was agitated uniformly for 120 s. After allowing 15 min for the n-hexadecane to rise completely, the aqueous phase was carefully removed with a Pasteur pipette and transferred to a 1 ml cuvette. Optical density (OD_{final}) was determined at 400 nm. Results are given in percentages from the following relation:

$$\text{Hydrophobicity} = 100 \cdot \left(1 - \frac{OD_{final}}{OD_{initial}}\right)$$

5.2.6 Calculation of metabolic rates

Metabolic rates (substrate consumption, product formation, carbon dioxide production and oxygen utilization, carbon recovery, carbon conversion efficiency and molar growth yields) were calculated according to Roseiro et al (1999):

The specific rate of glucose consumption

$$q_s = \frac{D(S - S_R)}{X} \qquad (1)$$

where D is the dilution rate, S the input glucose concentration, S_R the glucose residual concentration and X the steady-state bacterial dry weight;

The specific rate of product formation

$$q_p = \frac{D \cdot P}{X} \qquad (2)$$

where P is the product concentration;

The specific rate of carbon dioxide

$$q_{CO_2} = \frac{41.3 \cdot F \cdot \%CO_2}{V \cdot X} \qquad (3)$$

where F is the airflow, V the culture volume, % CO_2 is the percentage of carbon dioxide production from the measurements in the effluent gas in the on line mass spectrometer;

The specific rate of oxygen utilization

$$q_{O_2} = \frac{41.3 \cdot F \cdot \%O_2}{V \cdot X} \qquad (4)$$

where % O_2 is the percentage of oxygen uptake from the measurements in the effluent gas in the on line mass spectrometer;

Carbon recovery

$$CR = \frac{(41.7 \cdot D) + q_{CO_2} + q_p}{6.q_{glucose}} \qquad (5)$$

Carbon conversion efficiency

$$CCE = \frac{(41.7 \cdot D) \cdot 100}{6 \cdot q_{glucose}} \qquad (6)$$

The maintenance coefficient m and the theoretical growth yield Y^{max} were calculated according the Pirt equation (Roseiro et al, 1999)

$$q_s = \frac{\mu}{Y^{max}} + m \qquad (7)$$

5.2.7 Flow cytometry

Flow cytometry measurements were carried out as described in section 4.2.6. Different sonication periods were applied to *Bacillus licheniformis* samples, in order to determine the operation period that allowed the complete dispersion of the biomass clumps. The treated samples were observed under an optical microscope, to evaluate the effect of the sonication on the cell clumps. It was found that 10 s of ultrasonic treatment just prior to the analysis ensured cell detachment. Sonication for such a short of time has been shown to have no effect on cell physiological state as already mentioned (Nebe-von-Caron and Bedley, 1995).

5.2.8 *Bacillus licheniformis* CCMI 1034 morphology

Cells from cultures collected during the *B. licheniformis* continuous cultures were observed under an optical microscope Olympus BX50 (Tokio, Japan)

5.3 Results and Discussion

5.3.1 Effect of stirring rate on *Bacillus licheniformis* CCMI 1034 morphology and physiology

Agitation experiments were conducted in order to evaluate the effect of stirring on the morphology and physiology of *Bacillus licheniformis* CCMI 1034. Figure 5.2 shows the biomass and residual glucose concentrations, oxygen uptake and carbon dioxide production volumetric percentages, k_La and power specific input profiles for three stirring rates (500, 1000 and 1750 rpm) at a fixed dilution rate (D=0.87 h^{-1}, glucose-limited growth). Figure 5.2 also displays the density plots of $DiOC_6(3)$ fluorescence versus PI fluorescence for the selected stirring rates (I, II and III) as well *B. licheniformis* morphology observed under the optical microscope (1, 2 and 3).

At 500 rpm *Bacillus licheniformis* grew as long filamentous rod chains which attached to the fermenter wall surface forming a thick biofilm. The biomass concentration was 0.62 g l^{-1} and residual glucose concentration was below the detection level. The culture exhibited a high level of heterogeneity due to large fragments of biomass that detached from the biofilm. Flow cytometric analysis showed that at this stirring rate three main subpopulations could be distinguished. When compared with the control (Figure 4.3), those subpopulations correspond to healthy cells with polarised cytoplasmic membrane (A) (80.3 %), cells with depolarised cytoplasmic membrane cells (B) (9.3 %) and cells with disrupted permeabilised cytoplasmic membrane (D) (10.2 %) (Figure 5.2-I).

The increase of stirring rate (1000 rpm) increased the k_La 1.5 fold (Figure 5.2. The long rod chains broke, and the biofilm was partially removed.

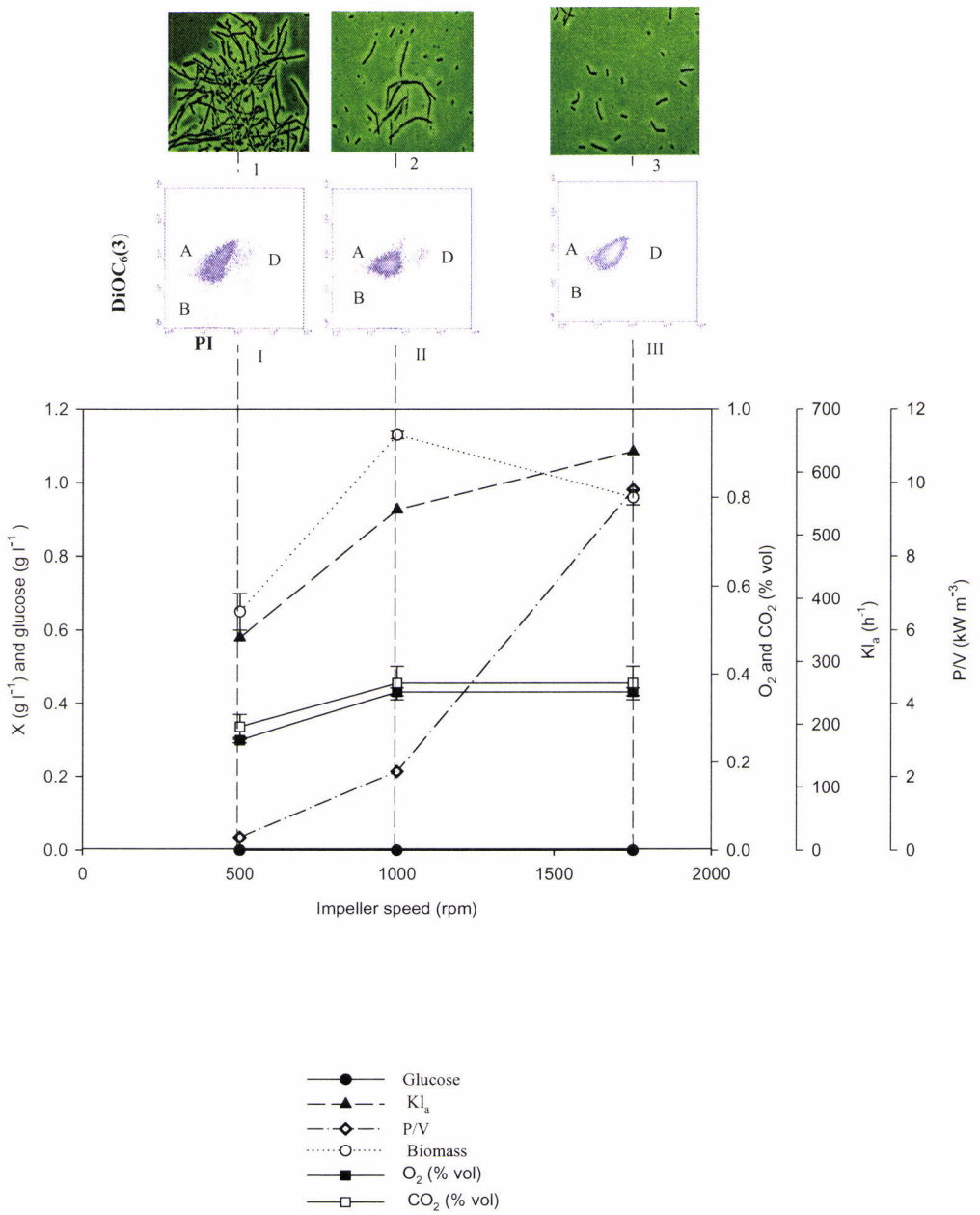

Figure 5.2 Influence of the stirring rate on biomass and residual glucose concentrations, oxygen uptake and carbon dioxide production volumetric percentages, k_La and specific power input when *B. licheniformis* CCMI 1034 grew under carbon limitation, at 0.87 h^{-1} at 45°C, pH 7 and glucose feed concentration 2 g l^{-1}. Pictures 1, 2 and 3 correspond to the optical microscope observations (magnification 1000) for 500, 1000 and 1750 rpm, respectively. Pictures I, II and III correspond to $DiOC_6(3)$ and PI fluorescence density plots at 500, 1000 and 1750 rpm, respectively. Three sub-populations could be distinguished. When compared with the controls (Figure 4.3), these sub-populations correspond to healthy cells (A) stained with $DiOC_6(3)$; depolarised cytoplasmic membrane cells (B) no staining; and disrupted permeabilised cytoplasmic membrane cells (D) stained with $DiOC_6(3)$ and PI. Subpopulation proportions: 500 rpm: (A) 80.3 %; (B) 9.3; (D) 10.2 %; 1000 rpm: (A) 89.2%; (B) 3.3 %; (D) 7.5 %; 1750 rpm: (A) 97.3 %); (B) 0.85 %; (D) 1.9 %.

As a result, the biomass concentration inside the vessel increased (1.12 g l^{-1}) leading to the increase of oxygen uptake and carbon dioxide production volumetric rates. The culture became progressively more homogeneous. At this stirring rate, flow cytometric analysis showed that the number of polarised cytoplasmic membrane cells (A) increased (89.2 %), whilst the depolarised cytoplasmic membrane cells (B) and disrupted permeabilised cytoplasmic membrane cells (D) decreased (3.3 % and 7.5 % respectively) (Figure 5.2-II) compared with the subpopulations found at 500 rpm.

At 1750 rpm the micro-organism grew as a cell suspension and no biofilm was formed. This type of morphology allowed homogeneous and stable cultures. The biomass concentration was 0.96 g l^{-1} and the residual glucose concentration remained below the detection level. Flow cytometric analysis revealed an increase of cytoplasmic membrane polarised cells (A) (97.3%) and a marked decrease of stressed cells (depolarised cytoplasmic membrane cells (B) 0.85 %, disrupted permeabilised cells (D) 1.9 %, (Figure 5.2-III). The increase of the shear stress by means of the increase of stirring rate hindered the cell attachment and dispersed the biomass allowing the nutrient diffusion throughout the culture to individual cells, which was reflected in the high proportion of polarised (healthy) cells. Moreover, the oxygen availability increased at higher stirring rates (the k_La increased 1.1 fold at 1750 rpm), which could contribute for the reestablishment of the cytoplasmic membrane potential, thus decreasing the number of depolarised cytoplasmic membrane cells, as oxygen is the final electron receptor at the respiratory chain, therefore responsible for the membrane potential maintenance.

The power input increased six fold when the stirring rate increased from 500 to 1000 rpm. When the stirring rate increased to 1750 rpm, the corresponding power input increased five fold.

5.3.2 Carbon limited fermentations

The previous experiments showed the formation of a thick biofilm when *B. licheniformis* CCMI 1034 was growing at 0.87 h^{-1} under glucose limitation, at a stirring rate of 500 rpm, due to its filamentous morphology. The thick biofilm induced a highly heterogeneous stressed culture. In fact, Villaseñor et al (2000) stated that thick biofilms have not a suitable performance during the bioprocesses as the nutrient diffusion through is hindered by the cell layers thickness. Therefore the biofilm inner layers cells became starved and eventually metabolically inactive. By increasing the agitation, the culture became progressively more homogeneous as the rod chains were broken, and the stressed cell subpopulations decreased.

Carbon limited steady-state continuous cultures fermentations at the stirring rate of 1000 and 1750 rpm, at different dilution rates, were conducted in order to evaluate the effect of the stirring rate and the dilution rate on the attachment ability, culture stability and physiology of this micro-organism.

5.3.2.1 Carbon limited growth at 1000 rpm

Figure 5.3 shows the influence of dilution rate on biomass and residual glucose concentration, at 1000 rpm. The optical microscope observations (1, 2 and 3), as well as the $DiOC_6(3)$ and PI fluorescence density plots (I, I and III) are depicted in the same plot.

Three regions were defined based on different *Bacillus licheniformis* CCMI 1034 morphologies. From 0.1 h^{-1} to 0.64 h^{-1} *Bacillus licheniformis* grew as a homogenous cell suspension, which was reflected in the small biomass concentration standard deviations (STD<0.06 g l^{-1}). At 0.27 h^{-1}, the biomass concentration reached 1.1 g l^{-1} and remained stable up to 0.64 h^{-1}. The flow cytometric analysis at D=0.1h^{-1} revealed that the proportion of polarised cytoplasmic membrane cells (A) was 92.3%, whilst the proportion of depolarised cytoplasmic membrane cells (B) was 0.4% and disrupted permeabilised depolarised cytoplasmic membranes (D) was 7.3% (Table 5.1).

Between 0.64 h^{-1} and 0.87 h^{-1} *B. licheniformis* CCMI 1034 cells formed chains which aggregated and attached to the fermenter wall surface forming a thin and smooth biofilm. Smooth biofilms are considered strong biofilms[1], whilst rough biofilms with protrusions are considered weak and less efficient (Tijhuis et al, 1994, 1996). Biomass concentration in the bulk decreased from 1.12 g l^{-1} (D=0.64 h^{-1}) to 0.59 g l^{-1} (D=0.87 h^{-1}). Flow cytometric analysis at 0.87 h^{-1} showed that the polarised cytoplasmic membrane cells (A) slightly decreased (93.2% at 0.1 h^{-1} and 90.4% at 0.87 h^{-1}) whilst the depolarised cytoplasmic membrane (B) cells increased (0.4 % at 0.1 h^{-1} and 5.5% at

[1] The definition of weak and strong biofilm is related to the biofilm resistance to detachment (the transport of biomass from an attached microbial film to the bulk liquid phase) (Tijhuis et al, 1996).

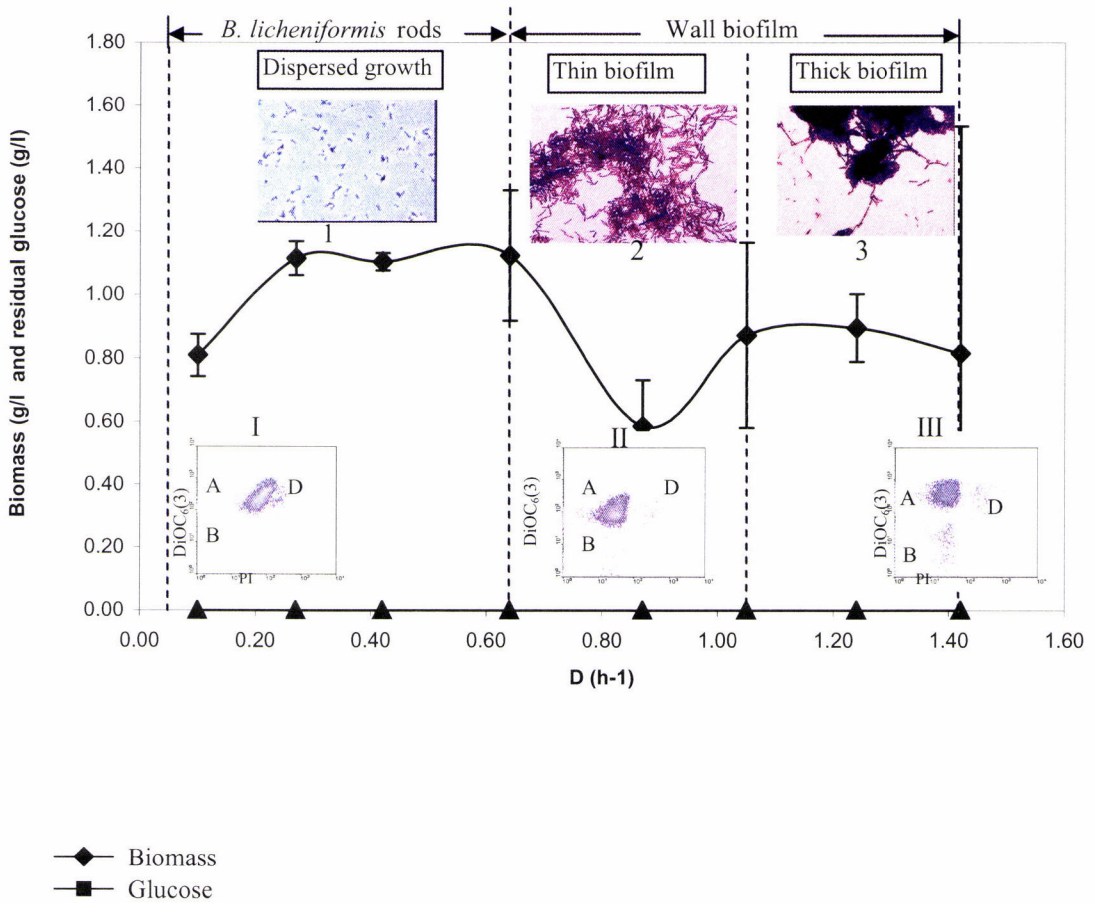

Figure 5.3 Influence of dilution rate on biomass and residual glucose concentrations, *Bacillus licheniformis* sub-populations profiles and morphology when the micro-organism grew under carbon limitation at 45 °C, pH 7, 1000 rpm and glucose feed concentration 2 g l^{-1}. The biomass concentration bars correspond to the standard deviation. Pictures 1, 2 and 3 correspond to the optical microscope observations at 0.1 h^{-1}, 0.87 h^{-1} and 1.44 h^{-1} respectively (picture 1 was taken to a fresh sample and pictures 2 and 3 were taken to gram staining samples; magnification 1000). Pictures I, II and III correspond to the $DiOC_6(3)$ and PI fluorescence density plots, at 0.1 h^{-1}, 0.87 h^{-1} and 1.44 h^{-1} respectively. Three sub-populations could be distinguished. When compared with the controls (Figure 4.3) the sub-populations correspond to polarised cytoplasmic membrane cells (A) stained with $DiOC_6(3)$; depolarised cytoplasmic membrane cells (B) no staining; and disrupted permeabilised cytoplasmic membrane cells (D) stained with $DiOC_6(3)$ and PI.

0.87 h^{-1}) although the disrupted permeabilised cytoplasmic membrane cells slightly decreased (7.3 % at 0.1 h^{-1} and 5.5 % at 0.87 h^{-1}) (Figure 5.3). This result suggested that although the cells attached in long chains forming a thin biofilm, the nutrients could still diffuse through the cell layers thus becoming available to a high number of cells, as the proportion of polarised cytoplasmic membrane cells remained high, as compared with the suspended cell growth observed at 0.1 h^{-1}. In fact, it has been reported that thin biofilms allow an efficient diffusion of substrate through which ensures the metabolic activity of the biofilm cells (Vilaseñor, 2000).

Above 1.05 h^{-1} *B. licheniformis* CCMI 1034 cell chains formed a thicker and rough wall biofilm, which is considered weak biofilm. This observation is in agreement with Tijhuis (1994) who reported that the biofilm thickness increase with the substrate load, thus the dilution rate. The thick biofilm formation led to unstable and heterogeneous cultures. This was reflected in the biomass concentration standard deviations, which considerably increased with the dilution rate (at D=1.4 h^{-1}, STD=0.7 g l^{-1}). Because there was biomass retention (due to wall biofilm growth and cell detachment), the wash-out did not occur in the dilution rates range between 0.1 h^{-1} - 1.42 h^{-1}. Residual glucose concentration was always below the detection level.

The hydrophobicity measurements indicate that the cell surface was not hydrophobic up to 1.05 h^{-1}. However, above this dilution rate the cell surface hydrophobicity attained 17%. Loodsrecht et al (1987) stated that the cell attachment ability increase with the cell surface hydrophobicity. In this case the increase of the cell surface hydrophobicity at higher dilutions rates could explain the strong cell attachment ability, which led to the thick biofilm formation.

Table 5.1 Influence of the nutrient limitation, stirring rate, and dilution rate on the morphology and cell sub-populations proportions of *Bacillus licheniformis* CCMI 1034.

	Limiting nutrient							
	Carbon				Nitrogen			
Stirring rate (rpm)	1000		1750		1000		1750	
Dilution rate (h^{-1})	0.1	1.44	0.1	1.24	0.1	1.6	0.1	1.6
Morphology	Dispersed growth	Thick and rough biofilm	Dispersed growth	Dispersed growth	Flocs	Fluffy flocs	Compact flocs	Compact flocs
Polarised cytoplasmic membrane cells (A) (%)	92.3	70	94.2	95.0	96.9	90.5	-	-
Depolarised cytoplasmic membrane cells (B) (%)	0.4	22.4	1.2	2.9	0.3	4.7	-	-
Disrupted permeabilised cytopaslmic membrane cells (C) (%)	7.3	7.5	3.9	1.0	2.6	4.2	-	-

Flow cytometric analysis revealed a marked increase of depolarised cytoplasmic membrane cells (B) (22.4%) at 1.44 h^{-1} (Table 5.1) whilst the proportion of polarised cytoplasmic membrane cells subpopulation (A) decreased (70%), and the disrupted permeabilised cells subpopulation (D) remained unchanged, when compared with the dilution rate of 0.1 h^{-1} (7.5 %) (Figure 5.3, Table 5.1). This stress response was different from the one observed when cells were carbon starved 4.5 h after the feed interruption, as described in section 4.3.3, where an increase of depolarised permeabilised cytoplasmic membrane cells (subpopulation C) and disrupted permeabilised cytoplasmic membrane cells (subpopulation D) was observed. In the present case, as the morphology of the micro-organism became more filamentous and the culture became progressively more heterogeneous at high dilution rates, the broth viscosity increased, leading to the formation of stagnant, non-mixed zones. Hence, nutrient gradients might have established within the vessel. In aerobic viscous

fermentations such as this, oxygen depletion became an important problem as its availability in the growth medium is low. On the other hand, the diffusion of oxygen through aerobic biofilms is usually the limiting step of the process (Tijhuis et al, 1994; Gibbs et al, 2000) so in this case the depletion of this nutrient in the thick biofilm inner cells was likely. Therefore, the increase of depolarised cytoplasmic membrane cells could be due to oxygen depletion in the biofilm inner cells, which could contribute for the cytoplasmic membrane potential collapse. The lack of this nutrient could decreased the ATP synthesis which could affect the active transport therefore the electrochemical gradient (Appendix 1).

5.3.2.2 Carbon limited growth at 1750 rpm

Figure 5.4 shows the influence of the dilution rate on the biomass, residual glucose concentrations, morphology and sub-population profiles when *Bacillus licheniformis* CCMI 1034 grew under carbon limitation, at 1750 rpm. The optical microscope observations (picture 1), as well as the $DiOC_6(3)$ and PI fluorescence density plots (I and II) are depicted in the same plot. The culture remained homogeneous and stable throughout the dilution rate range (0.1-1.24 h^{-1}), as judged by the low biomass concentration standard deviations, even at high dilution rates (at D=1.24 h^{-1}, STD=0.02

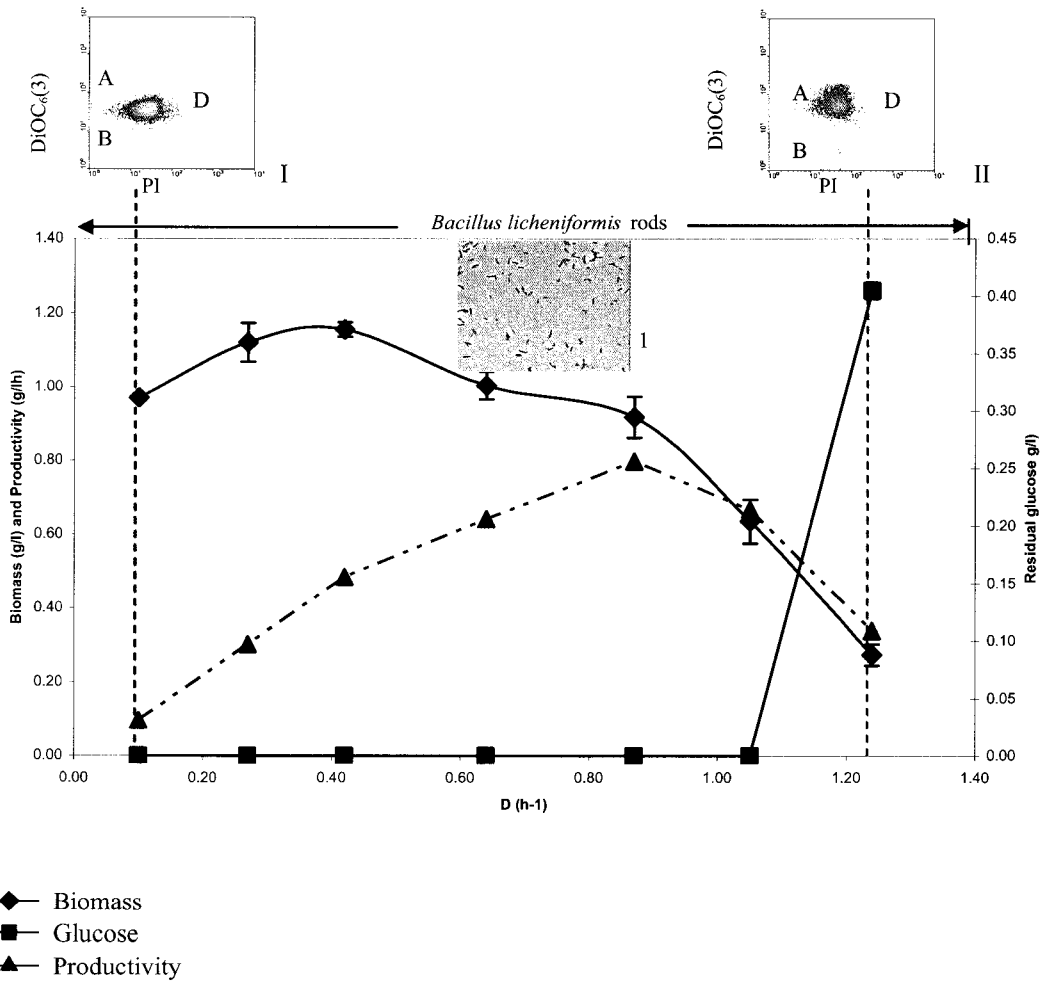

Figure 5.4 Influence of the dilution rate on biomass and residual glucose concentrations, *B. licheniformis* sub-populations profiles and morphology when the micro-organism grew under carbon limitation at 45°C, pH 7, 1750 rpm and glucose feed concentration 2 g l^{-1}. The cell productivity (DX) curve against the dilution rate is also depicted. The biomass concentration bars correspond to the standard deviations. Picture 1 corresponds to the optical microscope observation at 1.24 h^{-1} (fresh sample, magnification 1000), but there were no morphological changes throughout the dilution rate range. Pictures I and II correspond to the $DiOC_6(3)$ and PI fluorescence density plots, at 0.1h^{-1} and 1.24 h^{-1} respectively. Three sub-populations could be distinguished. When compared with the control (Figure 4.3), these sub-populations correspond polarised cytoplasmic membrane cells (A) stained with $DiOC_6(3)$, depolarised cytoplasmic membrane cells (B) no staining; and disrupted permeabilised cytoplasmic membrane cells (D) stained with $DiOC_6(3)$ and PI.

gl^{-1}). Moreover, the optical microscope observations only revealed individual cell rods, over the dilution rate range. The biomass concentration slightly increased from 0.98 gl^{-1} ($D=0.1h^{-1}$) to 1.16 g^{-1} ($D=0.44h^{-1}$), and then decreased as D was moving to 1.24 h^{-1}. However, even at these high dilution rates, there was no biofilm below the liquid level. The increase of the shear stress by means of the impeller speed hindered *B. licheniformis* cells attachment, allowing stable and homogeneous cultures. These results are in accordance with Lohr et al. (1989) who stated that homogeneous cultures of filamentous organisms are only possible if mycelia is disrupted by high shear forces. Flow cytometric analysis from samples taken at 0.1 h^{-1} revealed the presence of three sub-populations, corresponding to polarised cytoplasmic membrane cells (A) (94.2%), depolarised cytoplasmic membrane cells (B) (1.2%) and disrupted permeabilised cytoplasmic membrane cells (D) (3.9%). In this case, the increase of the dilution rate to 1.24 h^{-1} did not change significantly the initial cell subpopulations proportions (Table 5.1). This result was expected since the increase of shear stress hindered the cell attachment. Therefore biomass clumps, source of stressed cells, were not formed.

5.3.2.2.1. Efficiency of carbon conversion in glucose limited culture at 1750 rpm

The increase of stirring led to homogenous cultures which allowed stable cultures. Therefore the efficiency of carbon conversion by *Bacillus licheniformis* CCMI 1034 was studied (Figure 5.5, Table 5.2).

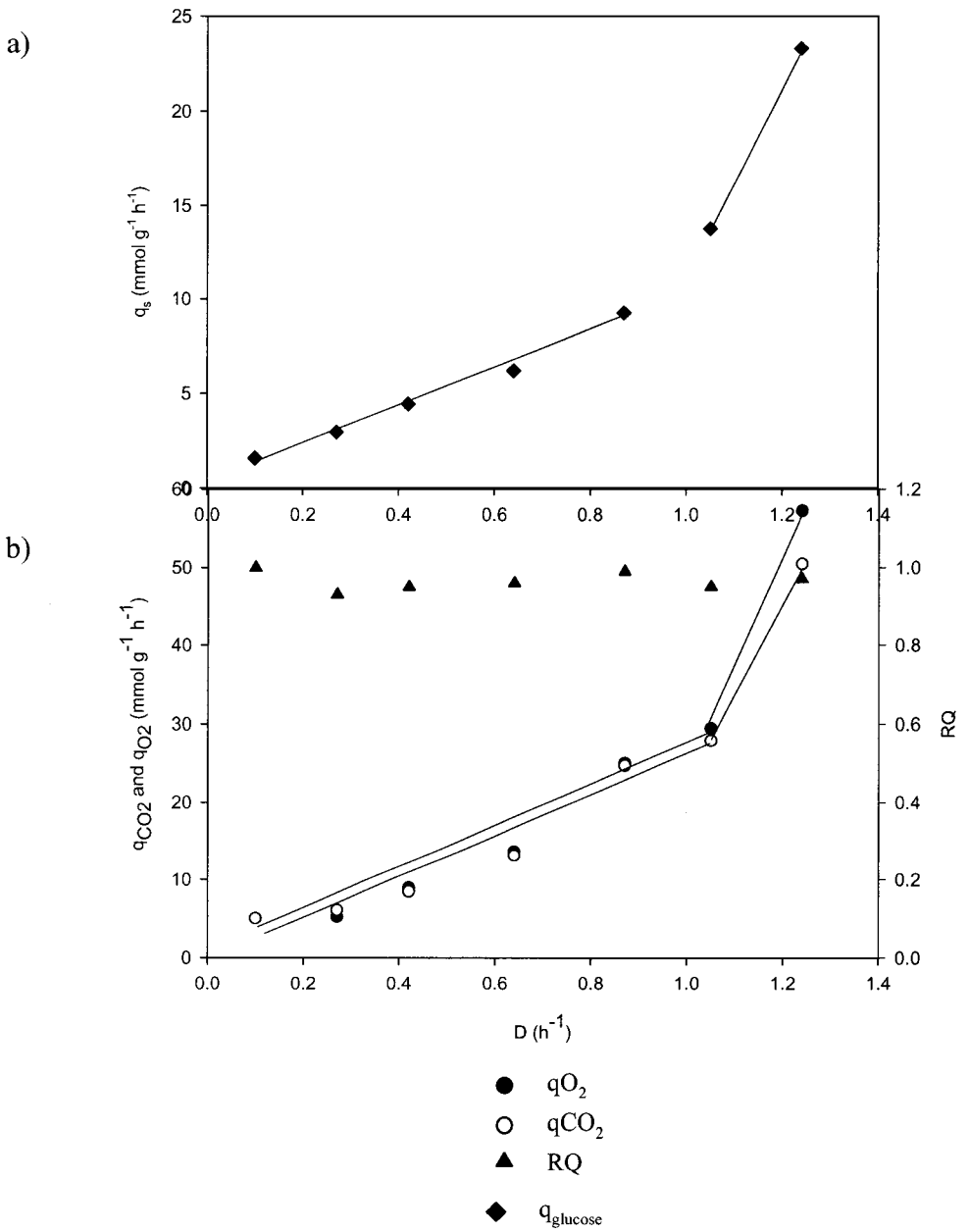

Figure 5.5 (a). Influence of the dilution rate on carbon source consumption by *Bacillus licheniformis* growing at 45 °C, pH 7, 1750 rpm and glucose feed concentration 2 g l^{-1}. (b) Influence of the dilution rate on the specific rates of O_2 consumption and CO_2 production in *Bacillus licheniformis* CCMI.

conversion of the carbon into cell mass was 65.52 % (Table 5.2). The maximum glucose consumption was 8.43 mM h^{-1} at D=0.87 h^{-1}.

The carbon-limited metabolic rates were used to calculate the maintenance coefficient (m) i.e., the growth-independent carbon fraction used for purposes like maintenance transmembrane ion gradients, turnover of cell walls and macromolecules, etc., all referred to as maintenance processes. The study of energetics of growth has been carried out under constant limiting conditions using "Pirt-type" equations as an approach to assess the effect of dilution rate on limiting substrates [*Bacillus licheniformis* (Frankena et al, 1985; Bulthuis et al, 1989), *Methylophilus methylotrophus* and *Methylobacterium* sp. (Roseiro et al, 1999)].

In the present work, the y-intercept and slope obtained from the q_s versus D plot (Figure 5.5) a maintenance coefficient m of 0.43 mmol glucose h^{-1} (g cells)$^{-1}$ and a theoretical maximum biomass yield $Y_{X/S}$ of 108.9 g cells (mol glucose)$^{-1}$ were determined for *Bacillus licheniformis* CCMI 1034. Frankena et al (1985) reported a maximum growth yield of 90.9 g cells (mol glucose)$^{-1}$ and a maintenance coefficient of 0.14 mmol glucose (g cells)$^{-1}$ of non protease production *Bacillus licheniformis* growth in the chemostat with glucose as carbon and energy source, at 37 °C. In fact, pure cultures of fast growing thermophilic aerobes have showed high maintenance requirements due to high turnover of cell material (Kuhn at al, 1980; Cometta et al, 1982).

The rate of glucose consumption ($q_{glucose}$) evolved linearly up to 0.87 h^{-1}. Above this dilution rate the $q_{glucose}$ deviated from the original straight line (Figure 5.5-a).

The distribution of the carbon source in *Bacillus licheniformis* CCMI 1034 was studied. The flux of carbon from glucose toward cell and product synthesis as well as carbon

dioxide production is depicted in Table 5.2. High values of CR indicate that the cell is not excreting products but directing most of the carbon source to growth purposes. Therefore, CR levels of approximately 100% are typical in glucose-limited cultures. The production of unknown metabolites or a shift towards a different growth-limitation produces a

Table 5.2 Influence of the dilution rate on carbon utilization of *Bacillus licheniformis* CCMI 1034 cells growing at 45 °C, pH 7, 1750 rpm and glucose feed concentration 2 g l^{-1}. Carbon recovery close to 100% is an indication of carbon limitation (CR above this limit is due to error accumulation in the calculation of $q_{glucose}$ and q_{CO2}) and carbon efficiency (CCE) indicates the amount of carbon used for growth purposes. The calculation of CR did not take into account the acetate production specific rate; CR corrected took into account the acetate production specific rate.

D (h^{-1})	$Y_{x/s}$ g biomass. (mol glucose)$^{-1}$	CR (%)	Corrected CR (%)	CCE (%)
0.1	63.00	122.34	122.34	50.61
0.27	91.72	98.58	98.58	63.74
0.42	94.58	97.73	97.73	65.14
0.64	103.17	107.33	107.33	71.10
0.87	94.75	110.18	110.18	65.52
1.05	76.26	86.79	86.79	53.00
1.24	53.19	73.05	77.31	36.97

decrease in the value of CR. The culture shows values of CR around 100% up to 0.87 h^{-1}, indicating that *Bacillus licheniformis* continuous culture occurred under carbon limitation. The carbon conversion efficiency (CCE), expressing the quantity of carbon used for cell growth, steadily increased up to 0.64 h^{-1} (Table 5.2).

The influence of the dilution rate on the metabolic rates (q_{O2} and q_{CO2}) is shown in Figure 5.5-b. Carbon dioxide production and oxygen uptake metabolic rates exhibit the same profile, evolving linearly up to 1.05 h^{-1}, then rising sharply in that region to values of 50.5 and 52.3 mmol g^{-1} h^{-1} respectively. The specific glucose uptake rate follows the same profile. This shift was in agreement with the decrease of CR, above 0.87 h^{-1} (Table 5.2), indicating that products could be synthesized at this high dilution rate. In fact, the detection of 0,45 g l^{-1} of acetate allowed the carbon recovery to attain 77.3 %. The remaining carbon percentage to 100%, at 1.05 h^{-1} and 1.24 h^{-1} was probably due to an glucose-limited fermentation at lower stirring rate (1000 rpm), specially at high dilutions rates. In this case, the higher stirring rate (1750 rpm) hindered the biofilm formation, although extracellular polymers could be present mainly at high dilutions rates (1.05 h^{-1} and 1.24 h^{-1}).

Respiratory quotient remained constant at values around 1 throughout the range of dilution rates indicating that the metabolism stayed in an oxidative status.

5.3.3 Nitrogen limited fermentations

5.3.3.1 Nitrogen limited growth at 1000 rpm

Figure 5.6 shows the changes of biomass and residual ammonium concentrations versus the dilution rate, at 1000 rpm. The optical microscope observations (1 and 2) , as well as the $DiOC_6(3)$ and PI fluorescence density plots (I and II) are depicted in the same plot. The biomass concentration decreased from 0.63 g l^{-1} at 0.1 h^{-1} to 0.50 g l^{-1} at 0.87 h^{-1} and then increased to 0.56 g l^{-1}, remaining stable up to 1.6 h^{-1}. The standard deviations were less than 0.12 g l^{-1}. The residual ammonium concentration was below the detection level up to 1.2 h^{-1}, but above this value it increased (17.6 mg l^{-1} at 1.4 h^{-1}) and then decreased (7.8 mg l^{-1} at 1.6 h^{-1}) . However, the wash-out did not occur in the dilution rates range studied (0.1 h^{-1} – 1.6 h^{-1}). Optical microscope observations revealed that the rod cells attached to each other (two or three) and formed fluffy flocs. With the increase of the dilution rate (thus the substrate load), the flocs increased in size and their surface became rough and with protrusions. In general, rough and fluffy biofilms lead to instabilities with respect to the separation of biofilm particles from the treated water (Tijhuis et al 1996). This type of morphology led to biomass retention inside the vessel particularly at high dilution rates as the larger flocs settled at the vessel bottom thus generating a biomass gradient. The cell surface hydrophobicity did not change throughout the dilution rate range, indicating a lower cell attachment ability comparing with *B. licheniformis* growth under carbon limitation at 1000 rpm, where an increase of the

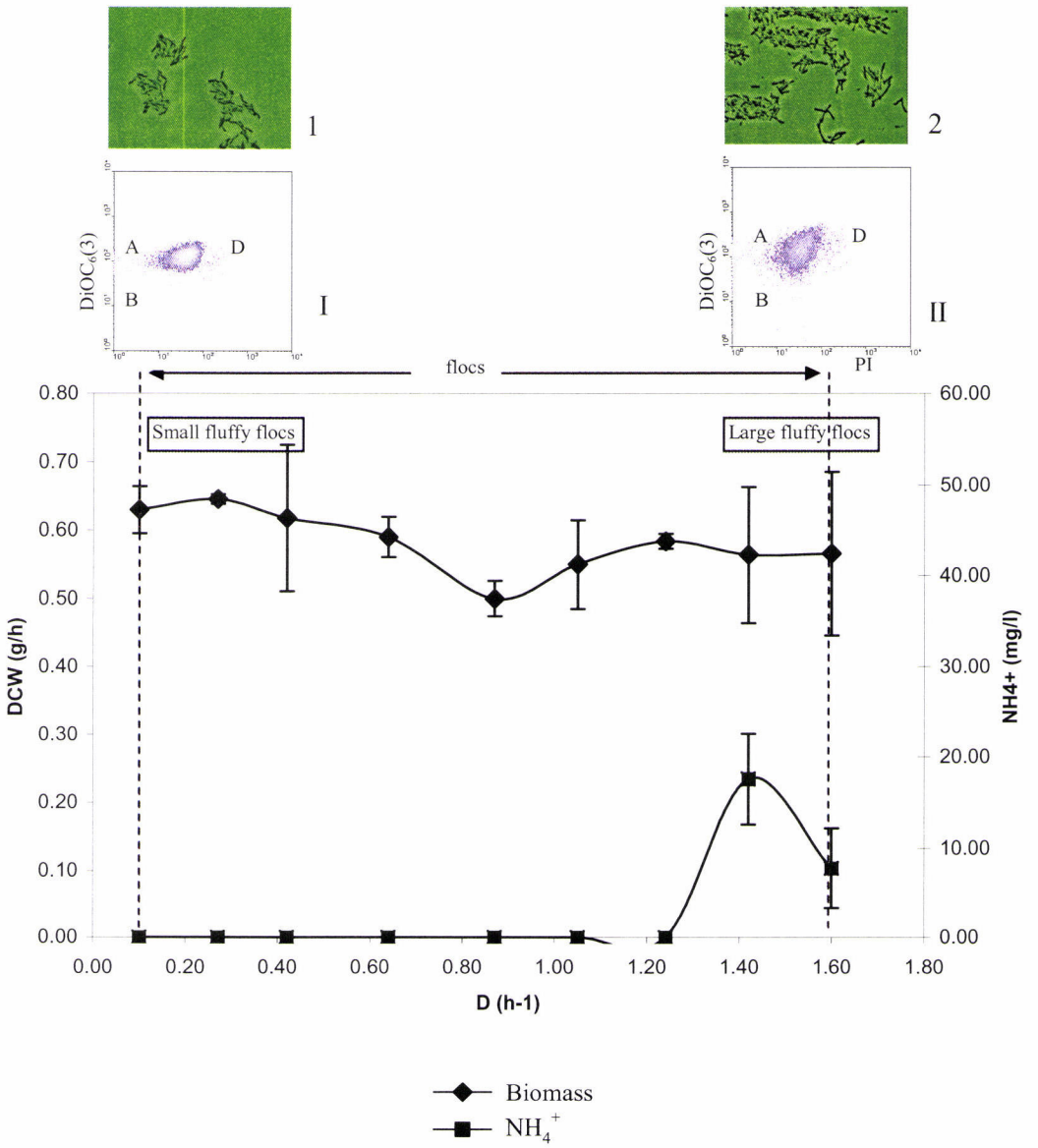

Figure 5.6 Influence of the dilutin rate on the biomass and residual ammonium concentrations, *Bacillus licheniformis* sub-populations profile and morphology. The micro-organism was growing under nitrogen limitation at 45 °C, pH 7, 1000 rpm and ammonium sulphate feed concentration 0.25 g l^{-1}. The biomass concentration bars correspond to the standard deviation. Pictures 1 and 2 correspond to the optical microscope observations (fresh samples, magnification 1000) at 0.10 h^{-1} and 1.60 h^{-1}. Pictures I and II correspond to the $DiOC_6(3)$ and fluorescence density plots, at 0.10 h^{-1} and 1.60 h^{-1} respectively. Three sub-populations could be distinguished. When compared with the controls (Figure 4.3), the sub-populations correspond to healthy cells (A) stained with $DiOC_6(3)$; depolarised cytoplasmic membrane cells (B) no staining; and disrupted permeabilised cytoplasmic membrane cells (C) stained with $DiOC_6(3)$ and PI.

hydrophobicity was observed at D≥1.24 h^{-1} (section 5.3.2.1). In fact, in this case there was no wall biofilm formation although the cells attached to one another forming flocs. Flow cytometric analysis of samples taken at 0.1 h^{-1} revealed three sub-populations corresponding to polarised cytoplasmic membrane cells (A) (96.9 %), depolarised cytoplasmic membrane cells (B) (0.3%) and cells with disrupted permeabilised depolarised cytoplasmic membranes (D) (2.6 %) (Table 5.1). The increase of the dilution rate to 1.6 h^{-1} slightly decreased the polarised cytoplasmic membrane cells (A) (90.5 %) which was followed by an increased of depolarised cytoplasmic membrane cells (B) (4.7 %) and a slightly increase of disrupted permeabilised cytoplasmic membrane cells (4.2 %) (Table 5.1). The high proportion of polarised cytoplasmic membrane cells at this dilution rate indicated that nutrients could diffuse throughout the floc biomass layers allowing a high proportion of metabolically active cells. These results supported the idea that the cell attachment ability was lower under nitrogen limitation than under carbon limitation. As the hydrophobicity increased, the cells growing under carbon limitation became stronger attached to one another thus the nutrient diffusion was hindered by the dense and thick biofilm cell layers, which increased the number of stressed cells due to starvation. These findings are in accordance with Sanin et al (2003) who found that when micro-organisms are carbon starved (nitrogen excess conditions) the overall hydrophobicity of the microbial surfaces and their attachment abilities increased. The authors claimed that when micro-organisms are growing under carbon limitation, excess of nitrogen is channelled into protein formation and some of this excess ends up on the extracellular polymer matrix. As proteins and aminoacids are the hydrophobic components of the ECP, the increase of proteins and aminoacids in ECP causes an

increase of the cell surface hydrophobicity, which strongly influences the cell attachment ability (Loodsrecht et al, 1987). On the contrary, when the micro-organisms are growing under nitrogen limitation, there is excess carbon in the medium and some of it is channeled into extracellular carbohydrate production which promotes an increase of more hydrophilic components (polysaccharides) of the ECP (Sanin et al, 2003). Therefore although flocs were formed, the cell attachment ability decreased.

5.3.4.2 Nitrogen limited growth at 1750 rpm

The effect of increasing stirring rate (1750 rpm) on the biomass and residual ammonium concentrations is shown in Figure 5.7. The optical microscope observations are depicted in the same plot (1 and 2) and showed that the flocs were denser and their surfaces were smoother than those found in nitrogen-limited fermentation, at 1000 rpm. With the increase of the dilution rate, the compacted flocs became denser and larger and seemed like beads. At this stirring rate, the biomass concentration remained approximately constant from 0.1 h^{-1} to 1.24 h^{-1}, and the residual ammonium concentration was below the detection level. Above this dilution rate, the biomass concentration started decreasing and the residual ammonium concentration sharply increased, reaching 36 mgl^{-1} at 1.6 h^{-1}. In this case, although the culture was heterogeneous due to the biomass beads, the increase of stirring rate decreased the biomass standard deviations (< 0.07 g l^{-1}) and allowed the decrease of the biomass concentration inside the vessel at high dilution rates, unlike the cultures at the 1000 rpm nitrogen-limited fermentation, where the biomass

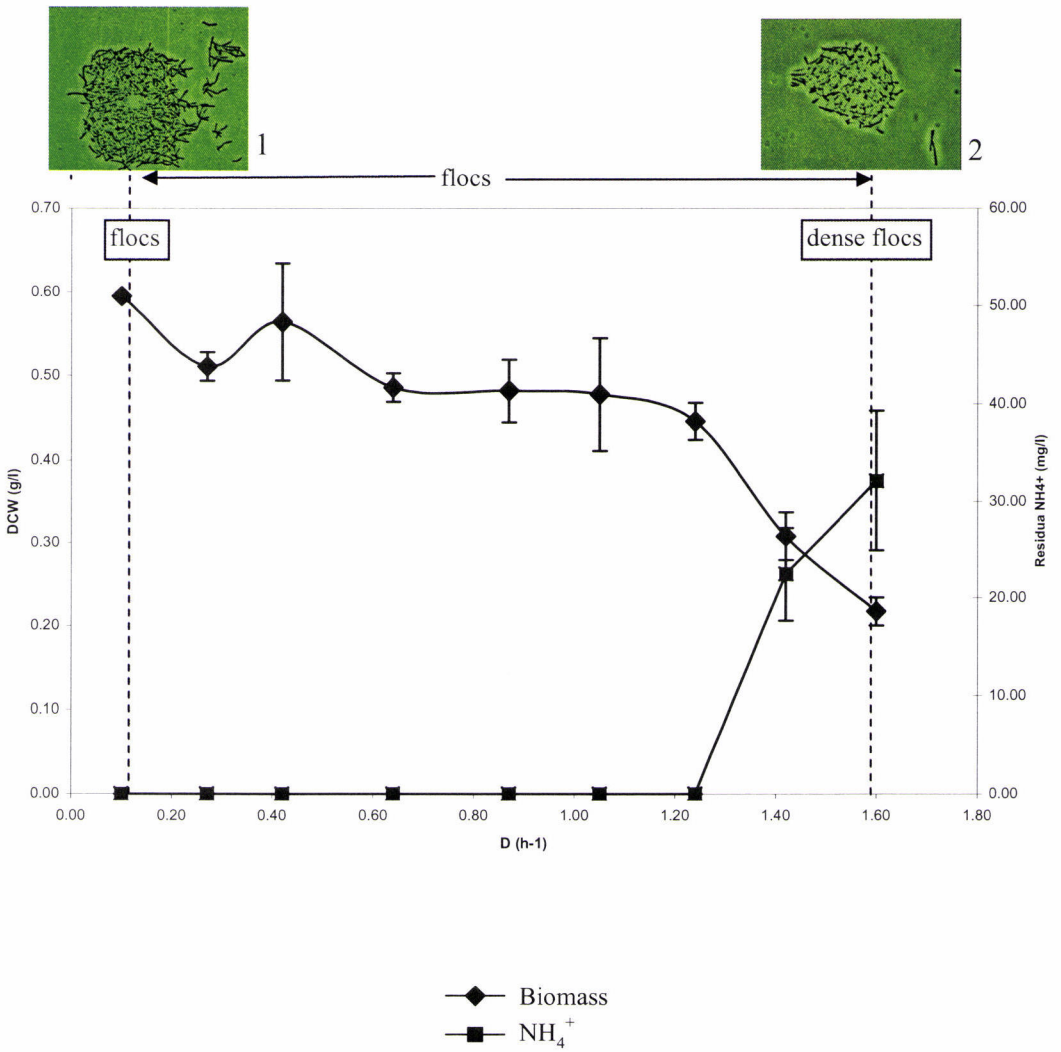

Figure 5.7 Influence of the dilution rate on the biomass and residual ammonium concentrations, *Bacillus licheniformis* sub-populations profile and morphology when the micro-organism grew under nitrogen limitation, at 45 °C, pH 7, 1750 rpm and ammonium sulphate feed concentration 0.25 g l^{-1}. Pictures 1 and 2 correspond to the optical microscope observations (fresh samples; magnification 1000) at 0.1 h^{-1} and 1.60 h^{-1} respectively. Flow cytometric analysis was not possible due to the compaction of the flocs.

concentration did not decrease throughout the dilution rate range.

This morphology did not allow cell surface hydrophobicity measurements neither flow cytometry analysis, because the compact flocs were not destroyed by the ultra-sonic pre-treatment and could obstruct the flow cytometric equipment. Therefore, it was not possible to evaluate the physiological state of the floc inner cells.

Usually, thermophilic aerobic treatment processes have poor bacterial settling characteristics resulting from the dispersed growing micro-organisms, which make difficult the biomass separation from the treated wastewater, thus limiting the overall bioprocess efficiency. In this work, the control of *B. licheniformis* CCMI 1034 morphology was achieved through the limiting nutrient, dilution rate and stirring rate, and it was possible to define growth conditions conducive to a thin and smooth biofilm composed by metabolically active cells (carbon limiting growth, at a dilution rate between 0.64 and 0.87 h^{-1}). Therefore the attachment ability of this micro-organism when growing under defined growth conditions may facilitate the biomass separation from the treated food waste, thus increasing the overall biodegradation process efficiency.

5.4 References

Amanullah, A., Blair, R., Nienow, A.W., and Thomas, C.R. 1999. Effects of agitation intensity on mycelial morphology and protein production in chemostat cultures of recombinant *Aspergillus oryzae*. Biothecnol. Bioeng. 62, 434-446.

Boletti, F.T. 1921. Manufactor of vinegar. Microbiology; a textbook on micro-organisms general and applied. C.E. Marshall. London, Churchill, 636-648.

Brown, C.M., Ellwood, D.C. and Hunter, J.R. 1977. Growth of bacteria at surfaces: influence of nutrient limitation. FEMS Microbol. Lett. 1, 163-166.

Bulthuis, B.A., Koningstein, G.M., Stouthamer, A., van Verseveld, H. 1989. A comparision between aerobic growth of *Bacillus licheniformis* in continuous culture and partial-recycling fermentor, with contributions to the discussion on maintenance energy demand. Arch. Microbiol. 152, 499-507.

Cometta, S., Sonnleitner, B., and Fiechter, A. 1982. The growth behaviour of *Thermus aquaticus* in continuous cultivation. Eur. J. Appl. Microbiol. Biotechnol. 15, 69-74.

Dignac, M.-F., Urbain, V., Rybacki, D., Bruchet, A., Snidaro, D. and Scribe, P. 1998. Chemical description of extracellular polymers: implication on activated sludge floc structure. Wat. Sci. Technol. 38, 45-53.

Durmaz, B. and Sanin, F.D. 2001. Effect of carbon to nitrogen ratio on the composition of microbial extracellular polymers in activated sludge. Wat. Sci. Technol. 44, 221-229.

Frankena, J., van Verseveld, H., Stouthamer, A. 1985. A continuous culture study of bioenergetic aspects of growth and production of exocellular protease in *Bacillus licheniformis*. Appl. Microbiol. Biotechnol. 22, 169-176.

Gibbs, P.A., Seviour, R.J. and Schmid, F. 2000. Growth of filamentous fungi in submersed culture: problems and possible solutions. Crit. Rev. Biotechnol. 20, 17-48.

Kuhn, H.J., Cometta, S. and Fiechter, A. 1980. Effects of growth temperature on maximal specific growth rate, yield, maintenance and death rate in glucose-limited continuous culture of the thermophilic *Bacillus caldotenax*.

Lhor, D., Buschulte, T., and Gilles, E.-D. 1989. Continuous cultivation of *Streptomyces tendae* in different media. Appl. Microbiol. Biotechnol. 32, 274-279.

Loosdrecht, M.C., Lyklema, J., Norde, W., Schraa, G. and Zehnder, A. 1987. The role of bacterial cell wall hydrophobicity in adhesion. Appl. Environ. Microbiol. 53, 1893-1897.

Loosdrecht, M.C.H., Eikelboom, D., Gjaltema, A., Mulder, A., Tijhuis, L., and Heijnen, J.J. (1995). Biofilm structures. Wat. Sci. Technol. 32, 35-43.

Mulder, R., Teixeira de Mattos, M.J. and Neijssel, O.M. 1989. The mechanism of aggregate formation by *Selemonas ruminantum*. Appl. Microbiol. Biotechnol. 32, 350-355.

Nebe-von Caron and Badley, R.A. 1995. Viability assessment of bacteria in mixed populations using flow cytometry. J. Microsc. 179, 55-66.

Pertulla M., Konrádsdóttir, M., Pere, J., Kirstjánsson, J.K. and Viikari, L. 1991. Removal of acetate from NSSC sulphite pulp mill condensates using thermophilic bacteria. Wat. Res. 25, 599-604.

Pringle, J.H. and Fletcher, M. 1983. Influence of substrate wettability on attachment of freshwater bacteria to solid surfaces. Appl. Environ. Microbiol. 45, 811-817.

Rawlings, D.E. 2002. Heavy metal mining microbes. Ann. Rev. Microbiol. 56, 65-91.

Roseiro, J.C., Partidário, P.J. and Marçal, M.J. 1999. Physiology and kinetics of trimethylamine conversion by two methylotrophic strains in continuous cultivation systems. Appl. Microbiol. Biotechnol. 52, 546-552.

Rosemberg, M. Gutnick, D. and Rosemberg, E. 1980. Adherence of bacteria to hydrocarbons: a simple method for measuring cell-surface hydrophobicity. FEMS Microbiol. Lett. 9, 29-33

Sakurai, A., H., Imai, Y., Takenaka and Sakakibara, M. 1997. Simulation of citric acid production by rotating disk contactor. Biotechnol. Bioeng. 56, 689-696.

Sanin, S.L., Sanin, F. D. and Bryers, J.D. 2003. Effect of starvation on the adhesive properties of xenobiotic degrading bacteria. Proc. Biochem 38, 909-914.

Sobotka, M., Prokop, A., Dunn, I.J. and Einsele, A. 1982. Review of methods for the measurement of oxygen transfer in microbial systems. Annual reports on fermentation processes. Academic Press , London, 5 pp. 127-210.

Tijhuis, L., van Loosdrecht, M. and Heijnen, J.J. 1994. Formation and growth of heterotrophic aerobic biofilms on small suspended particles in airlift reactors. Biotechnol. Bioeng. 44, 595-608.

Tijhuis, L., Hijman, B., Van Loosdrecht, M.C.H. and Heijnen, J.J. 1996. Influence of detachment, substrate loading and reactor scale on the formation of biofilms in airlift reactors. Appl. Microbiol. Biotechnol. 45, 7-17.

Villaseñor, J.C., Van Loosdrecht, M.C.M., Picioreanu, C. and Heijnen, J.J. 2000. Influence of different substrates on the formation of biofilms in a biofilm airlift suspension reactor. Wat. Sci. Technol. 41, 323-330.

Vishniac, W. and Santer, M. 1957. The Thiobacilli. Bacteriol. Rev. 21, 95-213.

Wiebe, M. and Trinci, A. 1991. Dilution rate as a determinant of mycelial morphology in continuous culture. Biotechnol. Bioeng. 38, 75-81.

Zoutberg, G.R., Willemsberg, R., Smit, G., Teixeira de Mattos, M.J. and Neijssel, O.M. 1989. Solvent production by an aggregate-forming variant of *Clostridium butyricum*. Appl. Microbiol. Biotechnol. 32, 22-26.

CHAPTER 6

Final conclusions and suggestions for further work

The three *Bacillus* species isolated from the Lammas Bioreactors (*B. licheniformis*, *B. subtilis* and *B. pumilus*) could be characterized and differentiated through their fatty acid and enzymatic activities profiles. *B. licheniformis* strains exhibited the most significant enzymatic production. Numerical analyses (PCA and HAC) showed that *B. licheniformis* strains were the most homogeneous regarding their fatty acid profiles. All the *Bacillus* species displayed a higher level of homogeneity between strains concerning their enzymatic activities profiles than their fatty acids.

Previous bioreactor characterization experiments suggested that a Rushton turbine mounted below a Pitched-blade would be the most suitable configuration for microbial fermentations. This combination was used in the further bioreactor experiments.

The addition of glucose and lactose pulses to *B. licheniformis* CCMI 1034 glucose-limited steady-states led to different physiological responses. Kinetic data together with the cell physiological state information suggested that *B. licheniformis* CCMI 1034 growth on lactose induced storage materials synthesis which allowed the presence of a high proportion of polarised cytoplasmic membrane cells nine hours after the lactose exhaustion. This response was not observed during the glucose pulse, where the number

of polarised cytoplasmic membrane cells began to decrease 1.25 hours after the glucose exhaustion. When the culture was submitted to stress conditions (starvation, glucose and lactose exhaustion periods) always recovered after the addition of fresh medium and eventually attained the steady-state conditions.

The control of the growth conditions induced different types of *B. licheniformis* CCMI 1034 morphologies. A thin and smooth biofilm composed by a high proportion of metabolic active cells was achieved when the micro-organism was growing under carbon limitation, at 1000 rpm, and a dilution rate between 0.64 and 0.87 h^{-1}. This type of biofilm (strong) allowed the diffusion of nutrients through, thus a high number of cells could contribute for the biodegradation process efficiency. The increase of the stirring rate to 1750 rpm resulted in dispersed growth.

The micro-organism growth under nitrogen limitation induced floc formation. At lower stirring rate (1000 rpm) the flocs were fluffy and their surface was rough which make the biomass separation from the treated stream ineffective. The increase of the stirring rate to 1750 rpm brought about denser flocs which surface was smooth, thus making easy the biomass separation from the treated stream. However, it was not possible to know the physiological state of the floc cells.

The different bioreactors used in Chapters 4 and Chapter 5 induced different glucose limited steady-state subpopulations (Figure 4.10 and Figure 5.2 I, D=0.27 h^{-1}). Moreover, the permeabilised cytoplasmic membrane cells (C) subpopulation was almost absent

during the experiments carried out in the Infors HT bioreactor (Chapter 5). Whilst the LSL bioreactor (Chapter 4) was equipped with a RT4-PB3 impellers combination, the Infors bioreactor (Chapter 5) was equipped with a RT6-RT6 impellers combination. These results might suggest that different impeller combination induced different stress levels in the microbial culture, leading to different physiological responses of the culture. Therefore detailed studies of the impact of different impeller combinations on the culture at the single cell level are recommended.

B. licheniformis CCMI 1034 when grown under carbon limitation, at 1000 rpm between 0.64 h^{-1} and 0.87 h^{-1} formed long chains which aggregated and attached to the fermenter wall surface forming a thin wall biofilm composed by a high proportion of metabolically active cells. It is known that for good process efficiency, a relatively small thickness and a high amount of biofilm area per unit volume is needed. Therefore food waste biodegradation proceses efficiency under these conditions could be improved using small suspended particles as carrier material for the biofilms, in airlift bioreactors. In this way, larger carrier surface area could be achieved allowing a higher biofilm area per unit volume.

APPENDIX 1

The cytoplasmic membrane

1. Structure

The cytoplasmic membrane, also called the cell membrane or plasma membrane is about 7 nanometers and lies internal to the cell wall and encloses the cytoplasm of the bacterium. Like all biological membranes in nature, the bacterial cytoplasmic membrane is composed by phospholipid and protein molecules. The phospholipid bilayer is arranged so that the polar ends of the molecules (the phosphate and glycerol portion of the phospholipid that is soluble in water) form the outermost and innermost surface of the membrane while the nonpolar ends (the fatty acid proportions of the phospholipids that are insoluble in water) form the center of the membrane (Figure A1-1). This overall structure of the cytoplasmic membrane is stabilized by interaction of the hydrophobic "tails" and by hydrogen bonding between the hydrophilic "heads" of the phospholipids. In addition, cations such as Mg^{2+} and Ca^{2+} also help to stabilize the membrane by combining ionically negative charges of the phospholipids (Gootschalk, 1985).

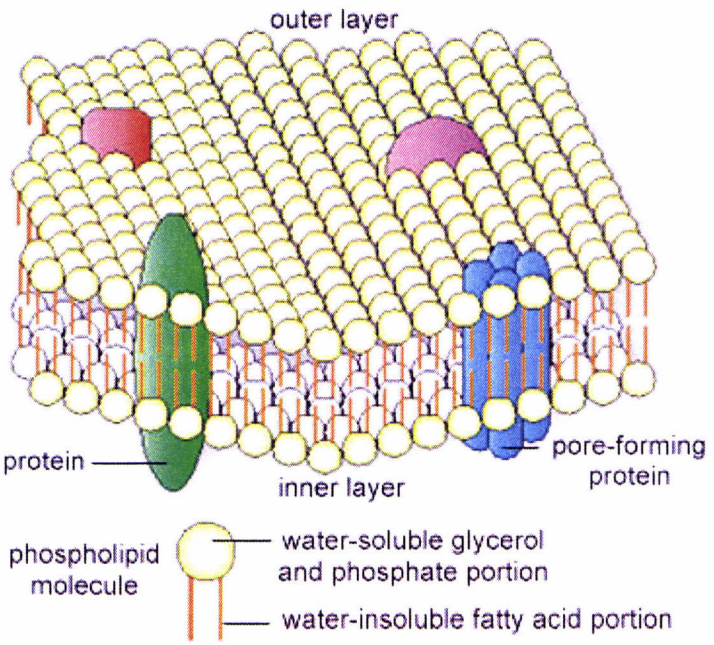

Figure A1-1 A schematic diagram of the cytoplasmic membrane.

2. Function

The cytoplasmic membrane is a thin structure that completely surrounds the cell. This structure plays several critical roles in cell function. First and foremost, the membrane functions as permeability barrier, preventing the passive leakage of cytoplasmic constituents into or out of the cell [Figure A1-2 (a)]. In addition, the membrane is a site of many proteins, many of which are involved in one way or another in the transport of substances into and out of the cell [Figure A1-2 (b)]. The cytoplasmic membrane is also a device for energy conservation in the cell. The membrane can exist in an energetically "charged" form in which a separation of protons (H^+) from hydroxyl ions (OH^-) occurs across its surface [Figure A1-2 (c)] (Brock, 2000).

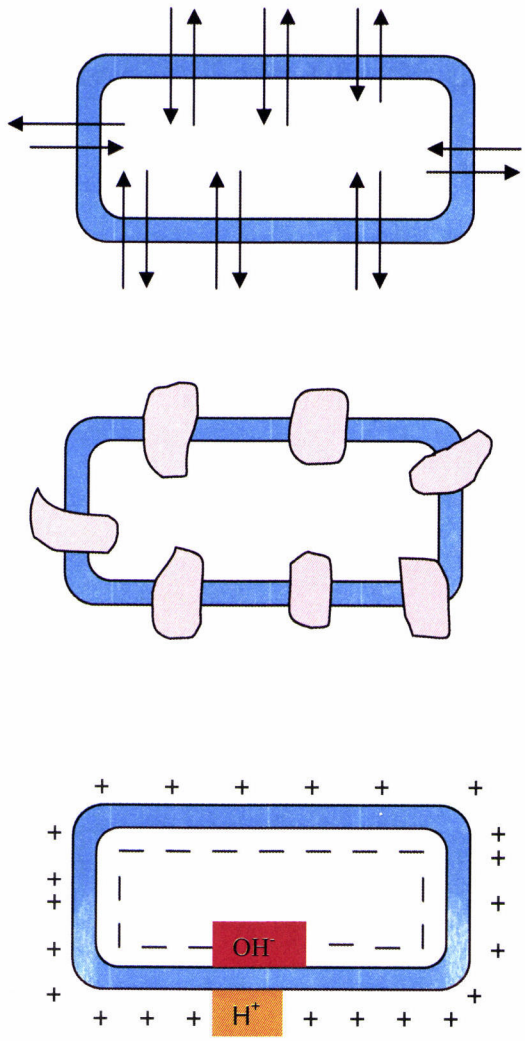

(a) Permeability barrier – prevents leakage and functions as the gateway for transport of nutrients into and out of the cell.

(b) Protein anchor – site of many proteins involved in transport and bioenergetics.

(c) Energy conservation – Site of generation and use of the proton motive force.

Figure A1-2 The major functions of the cytoplasmic membrane.

In aerobic respiration, substrates molecules are oxidized completely to CO_2 and ATP, being the molecular oxygen the external electron acceptor. Therefore electrons are transferred from organic compounds to the terminal electron acceptor, driving ATP synthesis at the expense of the proton motive force. In prokaryotic cells, the protons are transported from the cytoplasm of the bacterium across the cytoplasmic membrane to the periplasmic space located between the cytoplasmic membrane and the cell wall. The electron transport carriers are oriented in the membrane in such a way that a separation of

protons to electrons occurs across the membrane during the transport process (Figure A1-3).

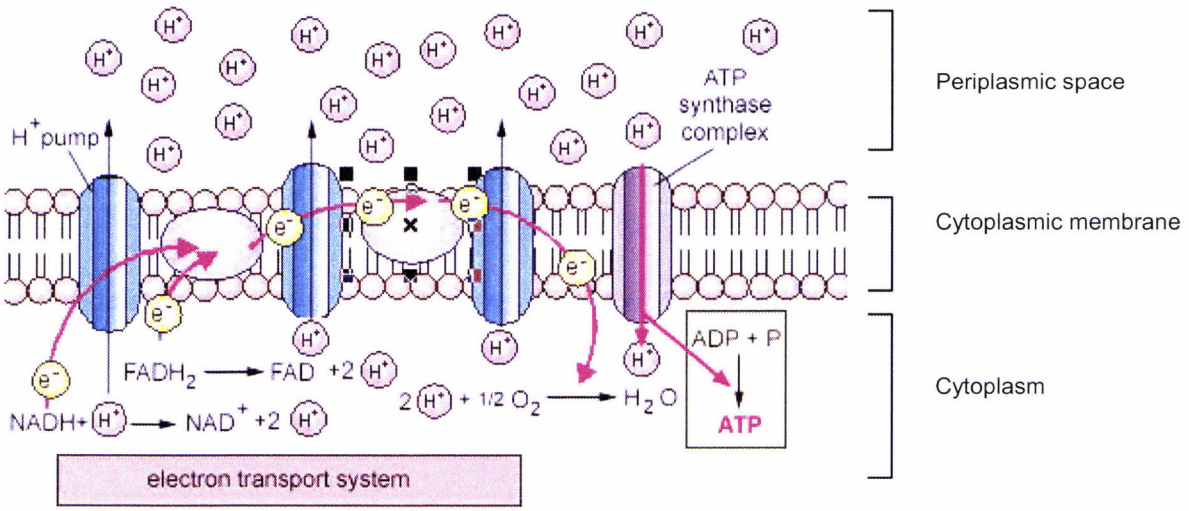

Figure A1-3 ATP Production during aerobic respiration by oxidative phosphorylation involving an electron transport system in prokaryotes.

At the end of the electron transport chain, the electrons are passed to the final electron acceptor, the oxygen, and reduce it. The reduction of oxygen to H_2O requires H^+ from the cytoplasm which, together with the extrusion of H^+, cause a net accumulation of OH^- inside the membrane. This charge separation is a form of metabolic energy, analogous to the potential energy present in a charge battery. The energized state of the membrane, referred as a proton-motive force (ΔP), is responsible for driving many energy-requiring functions in the cell including some form of transport, mobility and the biosynthesis of the cell energy currency, ATP. ΔP consists of two components: (i) the proton gradient (ΔpH) between the membrane outside and inside and (ii) the membrane potential ($\Delta\psi$)

due to the proton extraction, becoming the inner membrane negatively charged. This proton motive force provides the energy necessary for enzymes called ATP synthases, also located in the cytoplasmic membrane, to catalyze the synthesis of ATP from ADP and phosphate. This generation of ATP occurs as the protons cross the membrane through the ATP synthase complexes and re-enter either the bacterial cytoplasm.

At the end of the electron transport chain involved in aerobic respiration, the last electron carrier in the membrane transfers 2 electrons to half an oxygen molecule (an oxygen atom) that simultaneously combines with 2 protons from the surrounding medium to produce water as an end product (Brock, 2000; Voet and Voet, 1995).

3. Uncoupling of oxidative phosphorylation

Electron transport and oxidative phosphorylation (the synthesis of ATP) are normally tightly coupled. Compounds such as 2,4-dinitrophenol (DN) and carbonyl cyanide m-chlorophenylhydrazone (CCCP) are lipophilic weak acids therefore readily pass through membranes. In the membrane pH gradient, they bind protons on the acidic side of the membrane, diffuse through, and release them on the alkaline side, thereby dissipating the gradient. As a sequence, ΔpH cannot be established, $\Delta\psi$ is reduced to zero and ATP cannot be synthesize by electron transport phosphorylation. Uncoupling therefore prevent ATP synthesis without affecting electron transport. Because their mode of action, uncouplers are also called protonophores. Generally, ionophores are substances that vastly increase the permeability of membranes to particular ions by binding it, diffusing

through the membrane, and releasing the ion on the other side, collapsing the membrane potential by eliminating the gradient concentration of that ion across the membrane (Voet and Voet, 1995).

References

Brock, Thomas D. 2000. Biology of micro-organisms. Ninth ed. Prentice-Hall, Inc., New Jersey pp117-133.

Gottschalk, G. 1995. Bacterial metabolism. Second ed. Springer-Verlag, New York, pp. 27 – 36.

Voet, Donald and Voet, Judith. 1995. Biochemistry. Second ed. John Wiley & Sons, Inc. New York pp582-592.

http://www.cat.cc.md.us/courses/bio141/lecguide/unit1/prostruct/u1fig3.html

APPENDIX 2

Numerical analyses

1. Principal Component Analysis (PCA)

Principal Component Analysis (PCA) aims to reduce the dimensionality of a data set consisting of a large number of interrelated variables, retaining as much as possible of the variation present in the data. This is achieved by transforming to a new set of variables, the principal components, which are uncorrelated, and which are ordered so that the first few retain most of the variation present in all of the variables (Jolliffe, 2002). The principal component analysis calculates orthogonal linear combinations, T, of the auto scaled variables, X, based on the maximum variance criterion. Such linear combinations are called loadings. The coefficients, L, of the linear combinations are called loading. These three quantities are related as fellows:

$$T=X.L$$

or

$$t_{im}=\sum_j x_{ij}.l_{jm}$$

Since $L^{-1}=L^t$, the original variables can be written as linear combinations of the components:

$$X=T.L^t$$

or

$$x_{ij}==\sum_m t_{im}.l_{mj}$$

The sum of the variances of all components equals the sum of the variance of the original p variables. Principal components can be calculated from the covariance matrix, S. Let $\lambda_1 \leq \lambda_2 \leq .. \leq \lambda_p$ be the eigenvalues of S, and v_1, v_2, ..v_p the corresponding eigenvectors. Then the i^{th} vector of loadings, l_i, (i.e., the ith column of L) is v_i and the variance of the i^{th} principal component score, t_i, (i.e, the i^{th} column of T) is λ_i.

There are several methods to calculate the eigenvectors of a covariance matrix. In the present work, the singular value method was used (SVD). It has two steps: first the symmetric matrix is transformed into tridiagonal form, and then the tridigonal matrix is diagonalized by Q-R algorithm. The plot of the projections of the objects (the *Bacillus* strains) onto the first two principal component axes, i.e., t_1 vs t_2 is called the score plot and is a linear projection of objects onto the two-dimensional subspace that conserves most of the variance. The principal component projection that better represents the original configuration gives the relations between the original variables and the objects.

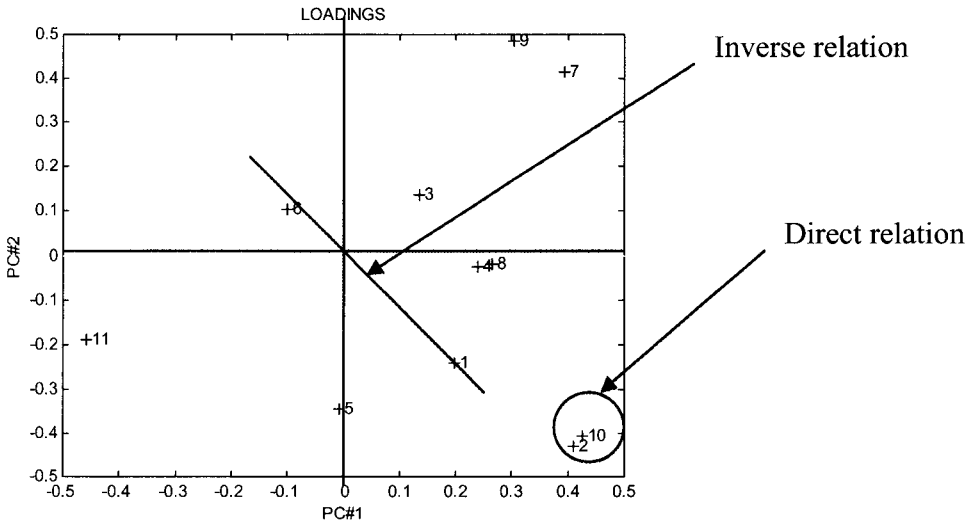

Figure A2 1 PC_1-PC_2 plot showing the direct and inverse relations between objects.

2. Hierarchical clustering

Hierarchical cluster analysis produces a hierarchy of objects such that any cluster of a partition is fully included in one of the clusters of the later partitions. Such partitions are best represented by a dendogram. This strategy is different from nonhierarchical clustering, which outcomes in one single partition. There are two main hierarchical strategies: agglomerative clustering and divisive clustering. Agglomerative clustering was used in this work and starts with n objects in n separate clusters (these are the leaves of the dendogram) and, after n-1 agglomeration steps, ends with all n objects in one single cluster (this is the root of the dendogram). In each step, the number of clusters is decreased by one, merging the two closest clusters. The first step, is to calculate an n×n distance matrix based on one of the following distance metrics:

$$d_{ik} = \sqrt{\sum_j (x_{ij} - x_{kj})^2}$$

For fatty acid profiles, d_{ik} represents the difference between the area percentages x_{ij} and x_{kj} of the j^{th} fatty acid peak for the i^{th} and k^{th} organisms, respectively. For enzymatic profiles, d_{ik} represents the difference between the enzymatic reaction intensities x_{ij} and x_{kj} of the j^{th} enzyme for the i^{th} and k^{th} organisms respectively.

This formula corresponds to the Euclidean distance. At each step of the algorithm, there is a distance matrix. The entry d_{ik} of this matrix is the distance from the cluster i to cluster k. At the beginning, when each cluster contains a single observation, d_{ik} is the distance from observation i to observation k. At each step, this matrix is reduced by one row to one column. The two rows (and two columns) s and t corresponding to the resulting new cluster, are merged and are replaced by a new row (and column) i, corresponding to the resulting new cluster. An updating distance formula defines the elements of this new row (column) d_{ik} from the elements of the two old rows columns d_{sk} and d_{tk}.

References

Jollife, I.T. Principal component analysis. Second ed. Springer, New York, 10-28.

Scan software for chemometric analysis, Reference Manual. 1995. USA.

APPENDIX 3

Preliminary screening tests for the selection of the strain exhibiting the highest lactose consumption percentage

Materials and Methods

All *Bacillus licheniformis* strains which produced β–galactosidase in the apiZYM tests (*B. licheniformis* CCMI 1030, *B. licheniformis* CCMI 1032, *B. licheniformis* CCMI 1033, *B .licheniformis* CCMI 1034, *B. licheniformis* CCMI 1035, *B. licheniformis* CCMI 1036 and *B. licheniformis* CCMI 1037) (Table 2.3) were grown in a lactose liquid medium. *Bacillus* strains slants were obtained by growth on nutrient agar at 45 °C for 24 hours. Two milliliters of cell suspension were transferred into 1litre baffled Erlenmayer flasks containing 100 ml of growth medium (g l^{-1}): lactose 10.00; KH_2PO_4 1.00; $(NH_4)_2SO_4$ 1.50; yeast extract 0.50; $CaCl_2.2H_2O$ 0,10; $MgCl_2.7H_2O$ 0.25, and supplemented with 2 ml of trace elements solution, were incubated in an orbital shaker at 45 °C, 1500 rpm, for 72 h. Biomass was measured by optical density at 600 nm in a double beam spectrometer (Unikon 922, Konton Instruments, England) and calibrated against dry cell weight at 100 °C for 18 h to constant weight. Residual lactose concentration was measured by HPLC with Aminex HPX-87P analysis column (Bio-rad, UK).

Results

Table A4.1 – Dry cell weight (at 0, 24, 48 and 72 h) and lactose uptake volumetric rate during the lactose screening test.

Strains	Dry cell weight ($g\ l^{-1}$)				Lactose uptake volumetric rate ($mg.\ l^{-1}.h^{-1}$)
	0h	24h	48h	72h	
B. licheniformis CCMI 1030	0.02	0.17	0.20	0.14	104.71
B. licheniformis CCMI 1032	0.01	0.03	0.12	-	114.61
B .licheniformis CCMI 1033	0.01	0.09	0.30	0.47	187.20
***B .licheniformis* CCMI 1034**	**0.01**	**0.11**	**0.60**	**0.57**	**254.99**
B. licheniformis CCMI 1035	0.03	0.12	0.25	0.23	87.02
B. licheniformis CCMI 1036	0.01	0.08	0.12	0.10	54.32
B. licheniformis CCMI 1037	0.02	0.14	0.16	0.12	72.09

B. licheniformis CCMI 1034 was the selected strain as it showed the highest lactose uptake volumetric rate.

APPENDIX 4

Chemicals and suppliers

Chapter 2

CHEMICALS	MOLECULAR WEIGHT ($g\ mol^{-1}$)	FORMULA	SUPPLIERS
Glucose monohydrate	198.16	$C_6H_{12}O_6$	José Manuel Vaz Pereira
Potassium hydrogen phosphate	136.09	KH_2PO_4	Riedel-deHäen
Magnesium sulphate heptahydrate	246.47	$MgSO_4.7H_2O$	Merck
Calcium chloride-2-hydrate	147.02	$CaCl_2.2H_2O$	Merck
Ammonium sulphate	132.04	$(NH_4)_2SO_4$	Riedel-deHaën
Yeast extract			Hi Media
Ethylenediaminetetracetic acid (EDTA)	372.2	$C_{10}H_{16}O_8N$	Sigma
Zinc sulphate heptahydrate	287.54	$ZNSO_4.\ 7H_2O$	Merck
Manganese (II) chloride tetrahydrate	197.90	$MnCl_2.4H_2O$	Riedel-deHäen
Cobaltouschloride hexahydrate	237.95	$CoCl_2.6H_2O$	Analar
Sodium molibdate dehydrate	241.96	$NaMoO_4.2H_2O$	BDH
Calcium chloride dehydrate	147.02	$CaCl_2.2H_2O$	Merck
Iron sulphate heptahydrate	278.02	$FeSO_4.7H_2O$	Merck
Boric acid	136.09	H_3BO_3	Merck
Potassium iodide	166.01	KI	Merck

Chapters 3 and 4

CHEMICALS	MOLECULAR WEIGHT ($g\ mol^{-1}$)	FORMULA	SUPPLIERS
D-Glucose anhydrous	180.16	$C_6H_{12}O_6$	Fisher
Potassium hydrogen phosphate	136.09	KH2PO4	Fissons
Magnesium sulphate heptahydrate	246.47	$MgSO_4.7H_2O$	Fisher
Calcium chloride-2-dehydrate	147.02	$CaCl_2.2H_2O$	BDH
Ammonium sulphate	132.04	$(NH_4)_2SO_4$	BDH
Yeast extract			Oxoid
Lactose	342.30	$C_{12}H_{22}O_{11}$	Sigma

Erratum

Currently	Should read
	Page ii, Line 21
(...dilution rate and the stirring rate changed)	(... dilution rate and power input (agitation intensity) changed)
	Page iii, Line 3
... at 1000 rpm...	...at 1000 rpm (specific power input = 2.14 kW m^{-3})
	Page iii, Line 7
... to 1750 rpm...	... to 1750 rpm (specific power input = 9.81 kW m^{-3})
	Page vi, Line 6
... velocidade de agitação...	...potência aplicada (velocidade de agitação)...
	Page vi, Line 9
...à velocidade de agitação de 1000 rpm...	...à velocidade de agitação de 1000 rpm (potência específica aplicada = 2.14 kW m^{-3}
	Page vi, Line 15
...para 1750 rpm...	... para 1750 rpm (potência específica aplicada = 9.81 kW m^{-3})
	Page xi, Line 7
...31th ...	...31st...
	Page xvii, between Line 11 and 12
CCE is missed	CCE carbon conversion efficiency (%)
	Page xvii, between Line 14 and 15
CR is missed	CR carbon recovery (%)
	Page xviii, Line 8 (second column)
g l^{-1}	mmol l^{-1}
	Page xix, Line 17
15-Methy lpentadecanoic	15-Methyl pentadecanoic
	Page 6, Line 11
(...; Sucuru and al, 1975...)	(...;Sucuru et al, 1975...)
	Page 9, Line 13
(Hewitt, et al,...)	(Hewitt et al,...)
	Page 12, Line 22
(Wallner at al, 1995)..	(Wallner et al, 1995).
	Page 28, Line 9
...a ultracentrifuge...	...an ultracentrifuge...
	Page 43, Line 18
... a rapid physiological...	... a rapid phenotypic...
	Page 52, Line 12
RT	RT_4
	Page 55, Line 9
$\ln\left(\frac{C^* - C}{C^* - C_i}\right) = -k_L a \,.\, t$	$\ln\left(\frac{C^* - C_L}{C^* - C_i}\right) = -k_L a \,.\, t$
	Page 57, Line 2
...occurring. Surface aeration...	...occurring. Therefore it was concluded that the Np for RT4 was 4.3 and for PB3 was 5.8. Surface aeration...
	Page 58, Line 6-7
...(at constant Q_g)	... (at constant Q_g, variable N)
	Page 59, Line 5
...gas flow number Fl.	...gas flow number Fl (at constant N, variable Q_g).

Page 79, Line 10

...healthy cells (those known should be very low or absent...)	...healthy cells (those known to have a polarised cytoplasmic membrane). Theoretically $DiOC_6(3)$ positive staining reflects a membrane potential due to metabolic activity, therefore the fluorescence of heat treated cells should be very low or absent...

Page 89, Line 18

...(Watson et al., 1998).	...(Watson et al, 1998).

Page 100, Line 13

...(Mulder, 1989;)	...(Mulder et al, 1989;)

Page 100, Line 17

...(Pringle, 1983)	...(Pringle and Fletcher, 1983)

Page 101, Line 8

... (Boletti, 1921; Sakurai at al., 1997)	... (Boletti, 1921; Sakurai et al, 1997)

Page 102, Line 2

...(Loosdrecht, 1995)	...(Loosdrecht et al, 1995)

Page 103, Line 2

...(Wiebe et and Trinci, 1991)	...(Wiebe and Trinci, 1991)

Page 103, Line 6

...at different stirring rates and dilution rates...	...at different stirring rates (power input) and dilution rates...

Page 105, Figure 5.1, the Infors vessel

Motor	Rotor

Page 111, Figure 5.2, symbol and axis legends

Kl_a	k_La

Page 116, Line 20

...cell surface attachment ability increase...	...cell surface attachment ability increased...

Page 117 , Table 5.1, first column

... Disrupted permeabilised cytopaslmic membrane cells (C)	... Disrupted permeabilised cytoplasmic membrane cells (D)

Page 120 (Line 19) – Page 122 (Line 1)

...was studied (Figure 5.5, Table 5.2). conversion of the carbon into cell mass...	...was studied (Figure 5.5, Table 5.2). The residual glucose concentration was 0 at a $D \leq 1.05\ h^{-1}$, but above this the glucose concentration started to increase, reaching 0.42 g l^{-1} at 1.24 h^{-1}. The maximum cell production rate (0.80 g l^{-1} h^{-1}) was obtained in the region close to D= 0.87 h^{-1}, where the conversion of the carbon into cell mass...

Page 124, Line 12 - 13

...was probably due to an glucose-limited fermentations...	...was probably due to ECP production, associated with biofilm formation, observed in the previous glucose-limited fermentations...

Page 131, Line 10

...comparision between aerobic growth...	...comparison between aerobic growth...

Page 132, Line 10

...of the thermophilic *Bacillus caldotenax*.	...of the thermophilic *Bacillus caldotenax*. European J. Appl. Microbiol. Biotechnol. 19, 303-315.

Page 137, Line 19

... (Figure 4.10 and Figure 5.2 I, D=0.27 h^{-1}).	... (Figure 4.9 and Figure 5.2 I, D=0.27 h^{-1}).

Page 149, Line 13

... of trace elements solution, were incubated...	... of trace elements solution. The Erlenmayers were incubated...